1. INTRODUCTION

All modern systems for retrieving or assimilating information from satellite sounding radiances include schemes for simulating the radiances (or brightness temperatures) corresponding to collocated forecast or radiosonde profiles. These calculations are required either as part of the real-time retrieval/assimilation processes or in off-line monitoring and tuning activities or in both. The radiative transfer models involved are subject to errors. The random components of these errors are usually important, in that they are comparable to or greater than the instrument noise and so are a significant part of the "total system noise". They should therefore be taken into account when determining the appropriate weight to give to the radiance data (see *Eyre*, 1989). Equally if not more important are the systematic errors in the radiative transfer models which arise mainly from errors in the spectroscopic data on which the radiative transfer model are based. Although active research continues in atmospheric spectroscopy in order to reduce these errors, it is clear that, for the foreseeable future, they will continue to be significant, i.e. comparable to or greater than the total system noise. More importantly, they are often comparable to the radiance changes corresponding to typical errors in the atmospheric temperature field in short-range forecasts from a numerical weather prediction (NWP) model. Unless radiative transfer errors are controlled and corrected to below this level, it is difficult to use the measured radiances to positive effect in NWP.

The importance of the radiance bias problem has been recognized for many years and empirical correction schemes have been developed (e.g see *Smith et al.*, 1984; *Chedin and Scott*, 1984; *Susskind et al.*, 1983). Methods have also been proposed for addressing the problem indirectly at the inversion stage (*Fleming et al.*, 1986). Most work to date has used comparisons with radiances computed from collocated radiosonde profiles to study the bias problem, but radiosonde data also contain biases which present significant problems (e.g. see *Uddstrom*, 1988). In addition, it has been demonstrated that a successful bias correction scheme must take into account the spatially varying and air-mass dependent nature of the radiance biases (*Kelly and Flobert*, 1988; *McMillin et al.*, 1989; *Uddstrom*, 1991).

This paper describes a scheme for monitoring the biases between measured TOVS brightness temperatures and those calculated from forecast temperature/humidity profiles, and for generating corrections for the biases for application in the TOVS one-dimensional variational analysis (1DVAR) scheme (see *Eyre et al.*, 1992). This scheme is now used at ECMWF as part of the operational assimilation of TOVS radiance information. The same bias correction method is also applicable to TOVS data used in three-dimensional variational analysis (3DVAR) (see *Pailleux*, 1990; *Pailleux et al.*, 1991).

Section 2 discusses the characteristics of the TOVS bias correction problem. Section 3 describes the data for which the bias correction scheme has been developed. Section 4 describes the theory of the method,

and section 5 its implementation. Section 6 presents results from the application of the scheme and discusses some of their implications.

2. THE BIAS CORRECTION PROBLEM

It is not possible to monitor the bias in a radiative transfer scheme in isolation. We can accumulate statistics of the differences between measured radiances and those calculated from collocated atmospheric profiles (from forecasts, analyses or radiosondes) and study their bias characteristics. These data may contain contributions to the bias from several sources. It is important to recognise these and to consider which we may wish to correct and which we may not (see *Watts*, 1989).

The available "measurements" have undergone calibration and pre-processing. Measured-minus-calculated brightness temperature differences may contain contributions from biases in the measurements, resulting from calibration errors or from biases introduced in the pre-processing of the data (e.g. systematic errors in limb correction or cloud clearing). Ideally these should be identified and corrected at source, but whilst they are present they have the same effect as errors in the radiative transfer calculations; it is the bias in the difference which affects the retrieval/assimilation. The correction should therefore include the effects of measurement bias.

Apart from biases in the radiative transfer model itself, which we intend to correct, there are possible biases in its input data. These include the temperature/humidity profiles — forecast, analysed or sonde. The treatment of the biases in the context of NWP data assimilation is problematic and is discussed below. There are other inputs not derived from the NWP model, such as ozone amount. These may contain biases which should be corrected as though they were radiative transfer model errors, with the additional problem that these biases may vary with time.

Returning to the temperature/humidity profile biases, we have to consider carefully the requirements of our application. Are we seeking to correct the radiances absolutely? Or are we just trying to remove relative biases between two systems? For NWP applications, the primary requirement is that the radiance data do not appear biased relative to the forecast model and relative to other data (e.g. radiosondes). Absolute biases should also be removed if possible, but they are of secondary importance.

One potential problem when correcting biases relative to a NWP model is any tendency of the system to drift: bias in the NWP model would then be interpreted as bias in the radiative transfer model, and correcting for it could lead to positive feedback, reinforcing the drift. Tuning against radiosondes avoids this problem but is affected by others: the biases between different radiosondes, higher levels of noise in

the difference statistics, and problems in constructing sufficiently large and representative samples of collocated data.

We are adopting the following strategy to address these problems:

(a) Biases between measured brightness temperatures and those calculated from forecast profiles are corrected as described in this paper.

(b) Only forecast profiles close to active radiosonde stations are used. Since the forecast/assimilation system will have used radiosonde data from these stations recently, this should prevent significant problems caused by model drift.

(c) Statistics of radiosonde-forecast differences are to be used to remove relative biases between different radiosondes (in a separate system, not described here). Data from radiosonde comparison campaigns will be used to confirm results on relative and absolute radiosonde errors.

In this way it is planned to use the NWP model as a transfer medium to tune radiosondes against each other and against satellite radiance data in a consistent manner. In any operational context, the observing systems and the NWP model are subject to frequent changes, and so the whole bias correction system will require continual monitoring. Moreover, the biases themselves will be specific to the particular NWP system within which they are derived; they will not necessarily be applicable to other NWP systems.

The biases in the radiative transfer model for some channels are found to vary systematically between the equator and the poles, and a successful correction scheme for global data must take account of this. Various schemes have been proposed to apply a correction which is a function of "air-mass", in some sense. In this work, we demonstrate acceptable performance from a simple scheme which uses a sub-set of the measured brightness temperatures as detectors of "air-mass" and hence as predictors in a regression relation which generates a spatially-varying bias. In this context, "air-mass" is rather a loose term but can refer to any aspect of the atmospheric profile which is correlated with the predictors.

Some contributions to the bias may vary with time. It is therefore desirable that the bias be monitored continuously and updated as necessary. Experience so far suggests that updating about once per month is both desirable and practicable.

3. THE DATA

The TOVS brightness temperatures on which the scheme has been developed are global, cloud-cleared data generated by NOAA/NESDIS and available in Europe in near real-time as part of the "120 km BUFR TOVS" data set. These data have already undergone substantial pre-processing at NESDIS (see *Smith et al.*, 1979) followed by cloud-detection and cloud-clearing (*McMillin and Dean*, 1982; *Reale et al.*, 1986). The cloud-clearing route is identified with the data and can be either "clear", "partly cloudy" or "cloudy".

The calculated brightness temperatures are generated within the framework of the PRESAT scheme which has been used operationally at ECMWF for pre-processing 120 km BUFR TOVS data since May 1991. The initial operational use of PRESAT has been to improve the quality control and data selection of TOVS temperature/humidity profiles received from NESDIS. However another important role for PRESAT has been to calculate and store the differences between the clear-column brightness temperatures (which accompany the NESDIS retrievals) and corresponding brightness temperatures computed from short-range (nominally 6-hour) forecast profiles.

NWP model fields at 3-hour intervals are interpolated quadratically in time and bilinearly in space to the location of each TOVS sounding. The temperature and humidity profiles are then interpolated linearly from the NWP model levels to the 40 pressure levels of the TOVS radiative transfer scheme (*Eyre*, 1991). Above the top of the NWP model (i.e. currently for pressures less than 10 hPa), the profile is extrapolated as described by *Eyre* (1989). The radiative transfer scheme then operates on the input atmospheric profile to generate corresponding brightness temperatures for all the TOVS channels required. An important aspect of the radiative transfer model which affects the subsequent bias correction is the use of the so-called γ-correction method (*Smith et al.*, 1984). The computed transmittance from each pressure level to space is raised to the power γ, where γ is a constant for each channel. At present, the values of γ are obtained from NOAA/NESDIS once for each satellite. Since their effect is to raise or lower the whole weighting function, they affect the brightness temperature bias, and so the bias corrections will be specific to the particular value of γ used.

PRESAT computes the measured-minus-forecast brightness temperature differences and stores them along with the measurements themselves. An archive of these data is currently available from mid-April 1991. Up to the time of writing, the information on the instrument scan angle (the so-called NESDIS "mini-box" number) is missing from these data, and so the first part of the bias correction scheme described below cannot be applied. However, PRESAT has also been run on an experimental data set (in February 1989) in which scan angle information is available, and the full bias correction scheme has been developed and tested.

4. THE BIAS CORRECTION METHOD

The correction scheme is in two parts: firstly a correction for the bias in the measurement at each scan angle relative to nadir (if scan angle information is available), followed by a bias correction which varies as a function of "air-mass". The cloud-cleared brightness temperature in channel j measured at scan angle θ (but adjusted to nadir) is $T_j(\theta)$. The datum to be corrected is the departure of this measurement from the corresponding forecast brightness temperate T_j^F calculated at nadir:

$$d_j(\theta) = T_j(\theta) - T_j^F \tag{4.1}$$

4.1 Scan bias correction

The first step is to use the information on the scan angle (if available) to make a correction for the relative mean biases between measurements at different scan angles. The scan bias correction is given by:

$$s_j(\theta) = \overline{d_j(\theta)} - \overline{d_j(\theta=0)} \tag{4.2}$$

where the overbar represents a global mean for data at scan angle θ calculated from a large quantity of data. $s_j(\theta)$ is thus a mean bias relative to scan centre ($\theta = 0$). The scan bias correction is applied as follows to form corrected departures:

$$d_j' = d_j(\theta) - s_j(\theta) \tag{4.3}$$

Since the cause of this relative bias lies in the measurements or their pre-processing, the same correction can also be applied to the measurements themselves:

$$T_j' = T_j(\theta) - s_j(\theta) \tag{4.4}.$$

4.2 Bias correction varying with air-mass

The second step is to correct for biases which are correlated with "air-mass" as sensed by the measurements themselves. A sub-set of channels is selected to represent the air-mass predictors, and any bias in the departures which is correlated with these predictors is removed. The bias correction is given by:

$$b_j = a_{oj} + \sum_{i=1}^{M} a_{ij} T_i^P \tag{4.5}$$

where T_i^P, $i = 1 \rightarrow M$, is a sub-set of the corrected measurements T_j', $j = 1 \rightarrow N$. Using the notation T^P and A_j to represent vectors with elements T_i^P and a_{ij} ($i = 1 \rightarrow M$) respectively, the coefficients A_j are calculated by linear regression as follows:

$$A_j = S\{d_j', T^P\} \cdot [S\{T^P, T^P\}]^{-1} \tag{4.6}$$

where $^{-1}$ represents matrix inverse and $S\{...\}$ represents a covariance matrix calculated from a large

quantity of global data. The offset constant, a_{oj}, is given by:

$$a_{oj} = -\overline{d_j'} - A_j^T \cdot \overline{T^p} \tag{4.7}$$

where ^{T} represents matrix transpose. The bias correction is then applied as follows to form further corrected departures:

$$d_j'' = d_j' - b_j \tag{4.8}$$

5. APPLICATION

This method describes the separate stages through which the bias correction method is applied in practice at ECMWF. The corresponding software is described in Annex A.

5.1 Data selection

Data are extracted from archived files containing all the data output by PRESAT (including measured brightness temperatures and their departures) for each 6-hour NWP assimilation cycle for both NOAA operational satellites (currently NOAA-11 and -12). The first stage is to assemble data from each satellite individually covering an adequate period. 14 days of data has been found more than adequate for calculation of stable coefficients and also sufficient for studying spatial variations in the residual bias fields (see section 6). To produce bias corrections for operational use, our current practice is to take data covering a whole month selecting all assimilation cycles from every other day (i.e. about 60 6-hour cycles).

The next stage is to select the most suitable and reliable data for computing correction coefficients. Data can be selected according to land and/or sea and according to cloud-clearing route. At present only clear soundings over sea are used. Clear soundings are likely to be the highest quality measurements and contain data for all channels. Data over the sea are likely to have the least problems from residual cloud-contamination, because the sea surface temperature is used in one of the cloud detection tests, and also to have the most accurate surface temperature for the forecast brightness temperature calculation. A potential problem with this approach is that the corrections generated are biased towards clear areas. Examination of the corrections applied to data from partly cloudy areas has shown that this does not appear to be a significant problem in practice.

At this stage the data set tends to be dominated by the tropics and southern hemisphere mid-latitudes. In order to create a more balanced distribution between different latitude bands, soundings are selected every nth sample, where n is given (at present) by:

band index	latitude band	n
1	90 - 60 S	1
2	60 - 30 S	3
3	30 S - 30 N	4
4	30 - 60 N	1
5	60 - 90 N	1

5.2 Quality control

Before data are used to calculate coefficients, they are subjected to the following stages of quality control:

a) Gross check. If any brightness temperature for a predictor channel is outside limits (currently 150 K to 350 K) or any brightness temperature departure is outside limits (currently -20 K to +20 K), then the data in all channels are rejected.

b) Window channel check. If the departure in a selected window channel is too great then data in all channels are rejected. Ideally, HIRS channel 8 should be used here. However, at present NESDIS apply a water vapour absorption correction to this channel, and the correction itself has peculiar error characteristics which differ between satellites. HIRS channel 10 is used; it is not such a clean window but is free from these problems. Data are rejected at present if the departure is outside the limits, -4 K to +8 K. The negative side is the most effective quality control and mainly traps residual cloud effects. [This test should be consistent with the corresponding quality control used for processing real-time data, otherwise the data used may be biased with respect to the NWP model.]

A further check, rejecting areas of sea-ice, has also been tried but is not currently used. It was found to lead to coefficients which produced large errors when applied back to data over sea-ice, because the atmospheric profiles there tend to be well outside the range of the profiles used in the generation of coefficients.

The mean and standard deviation of departures are then calculated in all channels for data which pass the above tests. All data are then processed a second time with an additional check.

c) Rogue check. If the departure in any channel differs from the mean departure by more than R times the standard deviation (currently R = 3), then data in all channels are rejected.

At present, bias corrections are only calculated for the following channels: HIRS channels 1-8 and 10-15, and MSU channels 2-4. See Fig. 1 for their weighting functions. Only the departures in these channels determine quality control decisions.

As an option in the quality control, data can be selected inside a "radiosonde mask" which identifies only those areas within a given radius of an active radiosonde station. This is to address the potential problem of model drift discussed in section 2. A radius of 5 degrees (latitude equivalent) is currently used, which causes about 35% of data over sea to be accepted.

5.3 Scan bias correction

The scan bias corrections can only be calculated if scan angle information (the NESDIS mini-box number) is available. If not, $s_j(\theta)$ is set to zero for all θ. When the mini-box number is available, $d_j(\theta=0)$ is set to the mean value for the two central mini-boxes (numbers 9 and 10). The values of $s_j(\theta)$ are calculated from eq. 4.2 and stored.

5.4 Bias correction varying with air-mass

If the scan bias corrections have been calculated, they are applied to give corrected measurements and departures using eqs. 4.4 and 4.3 respectively. In this case, although the quality control procedure is again as described in section 5.2, it may have slightly different effects, as it is now applied to corrected data.

After the quality control, the bias correction coefficients are calculated using eqs. 4.6 and 4.7. For most of the work performed so far, the predictors have been MSU channels 2, 3 and 4. They were selected because they are always present (whereas most HIRS channels are unavailable for cloudy soundings). They appear to give satisfactory results for use in the 1DVAR scheme (see section 6). However recent experiments have suggested that the inclusion of HIRS channel 1 would lead to significant improvement in stratospheric channels.

6. RESULTS AND DISCUSSION

Table 1 gives results from the calculation of bias coefficients for May 1992 for NOAA-11. The radiosonde mask has been used, giving about 14 000 soundings for use in the coefficient generation. MSU channels 2, 3 and 4 have been used as predictors, and no scan bias correction has been applied. Note that the global standard deviations of the departures are significantly reduced by the bias correction procedure in several channels. The procedure ensures that the residual global bias will be zero for the dependent data set, but

this may disguise significant regional biases. For this reason, the residual biases (and standard deviations) have been calculated separately for the 5 latitude bands listed in section 5.1 by applying the coefficients back to all the data (i.e. without the radiosonde mask). The results are shown in Table 2; "band index 6" represents the total data set. Note that the effect of the radiosonde mask is negligible in most channels. Table 3 shows the results for the same data but using the coefficients calculated from data of April 1992. This simulates an operational scenario in which the coefficients are changed once per month. The results appear satisfactory: the biases in the departure after correction for each band are generally much smaller than the standard deviations, and there is little change when using coefficients from the preceding month. This has been confirmed by examining other pairs of months over the period May 1991 to May 1992 for NOAA-10, -11 and -12.

The effect of the bias correction is illustrated in Fig. 2 which shows the field of the local monthly mean bias before and after correction in MSU channel 3. This channel has one of the largest problems of air-mass-dependent bias. It is removed almost completely by the bias correction procedure. [The major cause of the air-mass-dependence in this channel (and to a lesser extent other MSU channels) has been identified with a problem in the coefficients which describe the temperature-dependence of transmittance. Clearly this type of error can be corrected very effectively using the MSU channels themselves as predictors, since they are sensitive to the temperature profile.]

Figure 3 gives maps of the local mean and standard deviation of the departure (after correction) for selected tropospheric temperature-sounding channels, again for May 1992. Figures 4 and 5 illustrate the results of monitoring such plots monthly for one year for NOAA-11. Figure 4 is a sequence of plots of residual standard deviation in MSU channel 2 and Fig. 5 shows the monthly mean residual biases in HIRS channel 11.

From studies of these and similar figures, the following points of interest emerge:

(a) For the critical tropospheric temperature sounding channels (HIRS 4-7 and 13-15 and MSU 2-3), the zonal biases are generally lower than the standard deviations — a good sign, suggesting that we have some chance of seeing the "signal" of forecast error above the additional local "noise" created by measurement or radiative transfer model bias.

(b) Nevertheless, the standard deviations in all these channels are surprisingly low. On the one hand this is a good sign, as it can only occur if all the contributions to the departures — from measurement, forward model and first-guess error — are low. On the other hand, it demonstrates how carefully these data must be handled if they are to lead to improvement on the forecast first-

guess. These data have been used to re-tune the error statistics of the forecast first-guess and the measurements in the 1DVAR system (see *Eyre et al.*, 1992).

(c) First-guess biases which are correlated with the regression predictors will be compensated by the correction procedure. Such biases cannot therefore be corrected subsequently in the data assimilation by the radiance information, and this is a weakness which can only be addressed by using another data source such as sondes (see section 2).

(d) However, local/regional forecast biases which are not correlated with the MSU predictors will appear as biases in the mean departure fields and can potentially be corrected in the data assimilation. In the figures, there are areas of bias which are probably caused by biases in the analysis/forecast system (or the data it uses, eg NESDIS retrievals). They could possibly be caused by regional biases in the measurements or radiative transfer model, but it is difficult to think of plausible mechanisms here. Also, when channels with similar weighting functions, but from different bands (e.g. HIRS channel 15 and MSU channel 2) show similar bias patterns, it suggests that the problem lies with the forecast field.

(e) The spatial variations of the residual standard deviation are broadly consistent with expectations, taking into account the season, conventional data density, distance from data dense areas, etc. It is also encouraging that they are found not to change greatly from one month to the next. Although the highest values are in the southern hemisphere mid-latitudes, it should be noted that the values here are less than a factor of 2 greater than over the northern hemisphere oceans. These data should be useful for studying the spatial variation of forecast error.

(f) The mid/upper tropospheric humidity channels — HIRS channels 11 and 12 — show interesting bias patterns (Fig. 5). They suggest that the NWP model is systematically too moist in the latitudes of the sub-tropical anticyclones and too dry along the inter-tropical convergence zone. This is consistent with results from comparisons between NWP model analysis and total precipitable water vapour derived from SSM/I data (*Phalippou*, 1992). The interpretation of these plots is not straightforward, as the relationship between brightness temperature difference and humidity profile difference depends on the lapse rates of both temperature and humidity. However a bias of 1 K in HIRS channel 11 represents a bias of about 10-20% in mid-tropospheric specific humidity (with positive biases on the figures corresponding to measurements dry with respect to NWP model). Note that there are monthly mean biases of magnitude 3 K in some areas, which correspond to very large biases in specific humidity. The measurements used are only cloud-free data, whereas the model values attempt to represent the local mean of clear and cloudy conditions. There is therefore

a concern that the measured values will tend to show a dry bias. However, in the moist areas of the deep tropics, where we might expect this effect to be a problem, we find that the model is currently drier than the measurements indicate. The model shows a moist bias in the subsidence regions of the sub-tropics, where problems of clouds at mid and upper levels are not expected to be significant.

(g) The residual biases in HIRS channel 1 show a marked latitudinal banding. This is reflected to a lesser extent in channels 2 and 3. The problem here lies mainly in the systematic errors in extrapolating the temperature profile above the top of the model. Clearly this error is not strongly correlated with the measurements in MSU channels 2, 3 and 4. When HIRS channel 1 is added to the predictors, the global residual standard deviation and the regional biases are strongly reduced in HIRS channel 1 itself and to a lesser extent in HIRS channels 2 and 3 (see Fig. 6). Other channels are not significantly affected. HIRS channel 1 has not been included in the predictors in the first operational implementation 1DVAR, but these results indicate that it should be added in future. When (as planned) SSU channels are added to the 1DVAR system, their use as bias correction predictions will also need to be considered.

7. CONCLUSIONS

A scheme has been developed for correcting the spatial-varying biases between measured TOVS brightness temperatures and those calculated from a forecast model. The scheme is relatively simple — an advantage for an operational system — using linear regression with measured brightness temperatures in a small number of TOVS channels as predictors. Despite this, it appears to be successful in its main task of controlling the bias in the critical channels which sound tropospheric temperature.

Other useful diagnostics have emerged as by-products of the bias correction work. The fields of residual standard deviation have already proved useful in re-tuning the error statistics of the 1DVAR, and they also show potential for studying the spatial variation of error in the assimilation system. The residual biases in the water vapour channels appear to be a valuable diagnostic of problems with the NWP model's hydrological cycle.

ACKNOWLEDGEMENTS

I am grateful to Graeme Kelly, Tony McNally and Erik Andersson at ECMWF for providing the data and parts of the software used in this work and for their comments on the interpretation of results. The analysis of the bias correction problem, as presented here, has benefitted from discussions with Phil Watts (UK Meteorological Office).

REFERENCES

Chedin, A and N A Scott, 1984. Improved Initialization Inversion Procedure ("3I"). Tech Proc 1st Int TOVS Study Conf; Igls, Austria; 29 August - 2 September 1983; Report of CIMSS, Univ of Wisconsin-Madison, Ed W P Menzel, pp 14-79.

Eyre, J R, 1989. Inversion of cloudy satellite sounding radiances by nonlinear optimal estimation. Q J R Meteorol Soc, 115, 1001-1037.

Eyre J R, 1991. A fast radiative transfer model for satellite sounding systems. ECMWF Tech Memo 176.

Eyre J R, G Kelly, A P McNally and E Andersson, 1992. Assimilation of TOVS radiance information through one-dimensional variational analysis. ECMWF Tech Memo 187.

Fleming, H E, D S Crosby and A C Neuendorffer, 1986. Correction of satellite temperature retrieval errors due to errors in atmospheric transmittances. J Clim Appl Meteorol, 25, 869-882.

Kelly, G A and J-F Flobert, 1988. Radiance tuning. Tech Proc 4th Int TOVS Study Conf; Igls, Austria; 16-22 March 1988; Report of CIMSS, Univ of Wisconsin-Madison, Ed W P Menzel, pp 99-117.

McMillin L M and C Dean, 1982. Evaluation of a new operational technique for producing clear radiances. J Appl Meteorol, 21, 1005-1014.

McMillin L M, L J Crone and D S Crosby, 1989. Adjusting satellite radiances by regression with an orthogonal transformation to a prior estimate. J Appl Meteorol, 28, 969-975.

Pailleux J, 1990. A global variational assimilation scheme and its application for using TOVS radiances. Preprints WMO Int Symp on "Assimilation of observations in meteorology and oceanography; Clermont-Ferrand; 9-13 July 1990; WMO Report, pp 325-328.

Pailleux J, W Heckley, D Vasiljevic, J-N Thépaut, F Rabier, C Cardinali and E Andersson, 1990. Development of a variational assimilation system. ECMWF Tech Memo 179.

Phalippou L, 1992. Comparisons between SSM/I and ECMWF total precipitable water. To appear in Proc Conf on "Microwave radiometry and remote sensing"; Boulder, Colorado; 14-16 January 1992; Ed: R Westwater; pp 22-26.

Reale, A L, D G Gray, M W Chalfant, A Swaroop and A Nappi, 1986. Higher resolution operational satellite retrievals. Preprints 2nd Conf. on Satellite Meteorology/Remote Sensing and Applications; 13-16 May 1986; Williamsburg, Virginia; Amer Meteorol Soc, pp 16-19.

Smith W L, H M Woolf, C M Hayden, D Q Wark and L M McMillin, 1979. The TIROS-N Operational Vertical Sounder. Bull Am Meteorol Soc, 60, 1177-1187.

Smith W L, H M Woolf, C M Hayden, A J Schreiner and J F Le Marshall, 1984. The physical retrieval TOVS export package. Tech Proc 1st Int TOVS Study Conf; Igls, Austria; 29 August - 2 September 1983; Report of CIMSS, Univ of Wisconsin-Madison, Ed W P Menzel, pp 227-278.

Susskind, J, J Rosenfield and D Reuter, 1983. An accurate radiative transfer model for use in the direct physical inversion of HIRS-2 and MSU temperature sounding data. J Geophys Res, 88, 8550-8568.

Uddstrom, M J, 1988. The effect of collocation radiosonde errors on the assessment of the performance of a physical retrieval estimator. Tech Proc 4th Int TOVS Study Conf; Igls, Austria; 16-22 March 1988; Report of CIMSS, Univ of Wisconsin-Madison, Ed W P Menzel, pp 371-389.

Uddstrom, M J, 1991. Forward model errors. Tech Proc 6th Int TOVS Study Conf; Airlie, Virginia; 1-6 May 1991; Report of Univ of Wisconsin-Madison, Ed W P Menzel, pp 501-516.

Watts P D, 1989. Tuning the UK Meteorological Office's TOVS processing scheme. Proc ECMWF/EUMETSAT Workshop on "The use of satellite data in operational numerical weather prediction: 1989-1993"; Reading, UK; 9-12 May 1989; ECMWF Report, Vol II, pp 137-152.

Table 1. Bias correction coefficients.
Data from May 92, NOAA-11, using radiosonde mask.

channel	data uncorrected mean	data uncorrected SD	data corrected SD	coefficients a_{22}	a_{23}	a_{24}	a_0
1	1.48	1.78	1.66	-0.01285	0.08991	0.04820	-25.974
2	-0.97	0.77	0.70	-0.03950	0.05051	0.00579	-3.761
3	-1.69	0.85	0.55	-0.07093	0.04957	0.01782	1.005
4	-0.12	0.48	0.37	-0.04378	0.10917	-0.07075	1.343
5	-0.22	0.58	0.47	-0.00815	0.04727	-0.04841	1.528
6	-0.48	0.72	0.63	0.00285	-0.01230	-0.03558	9.231
7	-0.52	1.12	1.03	0.04102	-0.06235	-0.01772	7.128
8	0.91	2.88	1.94	0.04581	0.32041	-0.22166	-35.329
10	-0.75	1.56	1.53	0.09209	-0.21749	0.06903	10.559
11	-1.48	2.38	2.20	0.03096	0.02412	-0.08445	3.465
12	-1.33	3.62	3.15	0.03816	0.22500	-0.18867	-21.182
13	-1.21	0.93	0.90	-0.01916	-0.03644	-0.01318	14.637
14	-0.88	0.63	0.59	-0.00117	-0.05930	0.01487	9.621
15	-0.32	0.58	0.47	-0.04484	0.03192	0.00220	3.197
22	-0.08	0.42	0.42	-0.00760	-0.00594	-0.00641	4.534
23	-0.25	0.85	0.28	0.01718	0.07770	-0.08529	-3.782
24	-1.16	0.46	0.44	-0.01240	0.05000	-0.02654	-3.657

channel 1-15 = HIRS channels 1-15
channel 22-24 = MSU channels 2-4

Table 2. Mean and standard deviation of corrected data in each latitude band. data from May 1992, NOAA-11, corrected using coefficients in Table 1. "Band 6" includes data in all latitude bands.

band	1		2		3		4		5		6	
no. of data	4259		3843		15983		6734		5161		35980	
channel	mean	SD	mean	SD	mean	SD	mean	SD	mean	SD	mean	SD
1	-1.46	2.98	-3.35	1.43	0.11	1.31	0.23	1.09	0.58	0.94	-0.36	1.94
2	-0.44	0.99	-0.87	0.62	0.07	0.68	-0.07	0.59	0.27	0.52	-0.09	0.76
3	-0.21	0.70	-0.60	0.50	0.05	0.60	0.02	0.48	0.17	0.45	-0.04	0.60
4	0.00	0.35	-0.06	0.36	0.06	0.42	-0.07	0.35	0.10	0.28	0.02	0.38
5	-0.02	0.48	0.04	0.46	0.11	0.55	-0.13	0.42	0.09	0.37	0.04	0.50
6	0.03	0.66	0.07	0.55	0.16	0.72	-0.18	0.53	0.11	0.58	0.06	0.65
7	-0.04	1.18	-0.13	0.78	0.16	1.06	-0.20	0.83	0.19	1.14	0.04	1.04
8	-0.74	2.30	-1.09	1.33	-0.17	1.70	-0.23	1.59	0.43	2.29	-0.26	1.87
10	-0.08	1.88	-0.40	1.07	0.07	1.34	-0.14	1.21	0.20	1.92	-0.02	1.48
11	0.30	1.95	1.21	2.41	0.58	2.72	-0.34	2.18	0.26	1.58	0.40	2.41
12	0.44	3.08	1.41	3.56	0.71	3.71	-0.32	3.15	0.34	2.24	0.51	3.38
13	-0.08	1.23	-0.36	0.64	0.00	0.56	-0.20	0.76	0.20	1.19	-0.06	0.84
14	0.00	0.81	-0.29	0.52	0.00	0.45	-0.07	0.53	0.08	0.74	-0.04	0.58
15	-0.04	0.65	-0.28	0.50	0.06	0.39	-0.07	0.46	0.08	0.46	-0.01	0.48
22	0.03	0.61	-0.24	0.46	0.06	0.39	-0.04	0.38	0.11	0.44	0.01	0.45
23	0.07	0.47	0.06	0.34	-0.03	0.23	0.06	0.25	0.00	0.35	0.02	0.30
24	0.04	0.50	-0.26	0.43	0.08	0.45	-0.15	0.41	0.20	0.40	0.01	0.46

Table 3. Mean and standard deviation of corrected data in each latitude band.
Data from May 1992, NOAA-11, corrected using coefficients from April 1992 data.
"Band 6" includes data in all latitude bands.

band	1		2		3		4		5		6	
no. of data	4259		3843		15983		6734		5161		35980	
channel	mean	SD	mean	SD	mean	SD	mean	SD	mean	SD	mean	SD
1	-2.44	2.20	-3.60	1.32	-0.20	1.35	0.25	1.05	2.55	1.19	-0.35	2.22
2	-0.70	0.86	-1.03	0.60	0.11	0.73	-0.18	0.54	0.63	0.57	-0.09	0.83
3	-0.14	0.68	-0.64	0.51	0.03	0.62	-0.02	0.45	0.45	0.47	-0.01	0.63
4	0.12	0.36	-0.10	0.35	-0.05	0.42	-0.15	0.35	0.19	0.29	-0.02	0.39
5	-0.07	0.47	0.00	0.45	-0.01	0.55	-0.17	0.41	0.20	0.38	-0.02	0.50
6	-0.06	0.67	0.03	0.55	0.05	0.72	-0.21	0.53	0.05	0.58	-0.02	0.65
7	-0.16	1.19	-0.19	0.81	0.11	1.07	-0.26	0.85	-0.13	1.15	-0.06	1.05
8	-2.30	2.22	-1.51	1.43	0.56	1.77	-0.43	1.65	-0.46	2.26	-0.33	2.10
10	0.22	1.94	-0.41	1.10	-0.03	1.35	-0.25	1.26	-0.53	1.95	-0.15	1.51
11	-0.47	1.94	0.72	2.40	0.34	2.71	-0.77	2.18	-0.08	1.58	0.02	2.41
12	-1.08	3.06	0.77	3.55	0.61	3.71	-0.76	3.16	0.25	2.26	0.12	3.41
13	-0.33	1.24	-0.33	0.69	0.09	0.56	-0.13	0.80	-0.01	1.21	-0.06	0.85
14	-0.05	0.82	-0.26	0.55	0.00	0.45	-0.04	0.55	-0.05	0.74	-0.05	0.59
15	0.00	0.64	-0.32	0.46	-0.05	0.39	-0.12	0.45	0.28	0.48	-0.04	0.48
22	-0.03	0.60	-0.20	0.48	0.04	0.40	0.02	0.39	0.11	0.44	0.01	0.45
23	0.22	0.43	0.09	0.32	-0.03	0.22	0.06	0.25	-0.12	0.35	0.02	0.30
24	-0.17	0.52	-0.36	0.43	0.28	0.47	-0.22	0.40	0.13	0.38	0.04	0.51

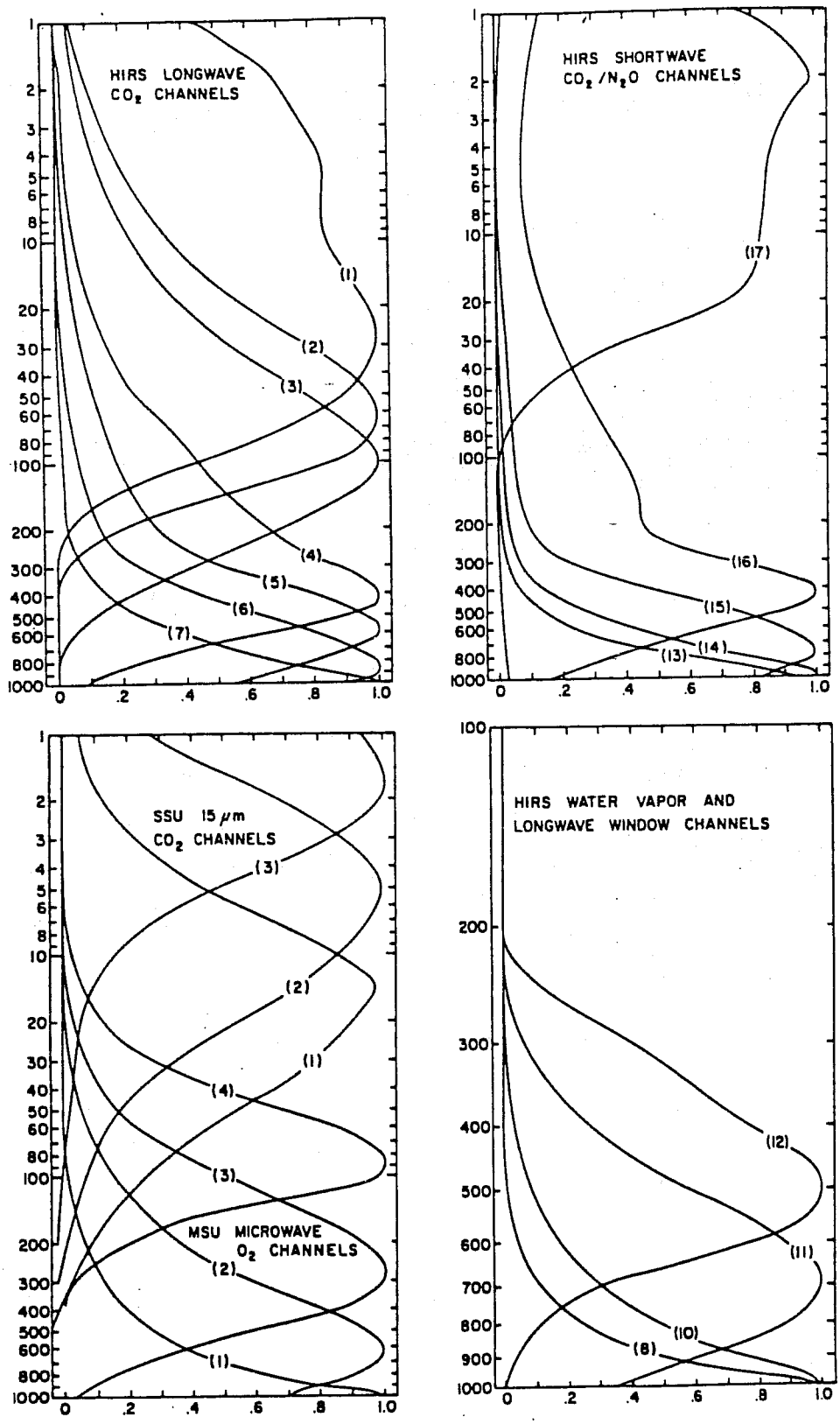

Fig. 1 TOVS weighting functions (taken from *Smith et al.*, 1979).

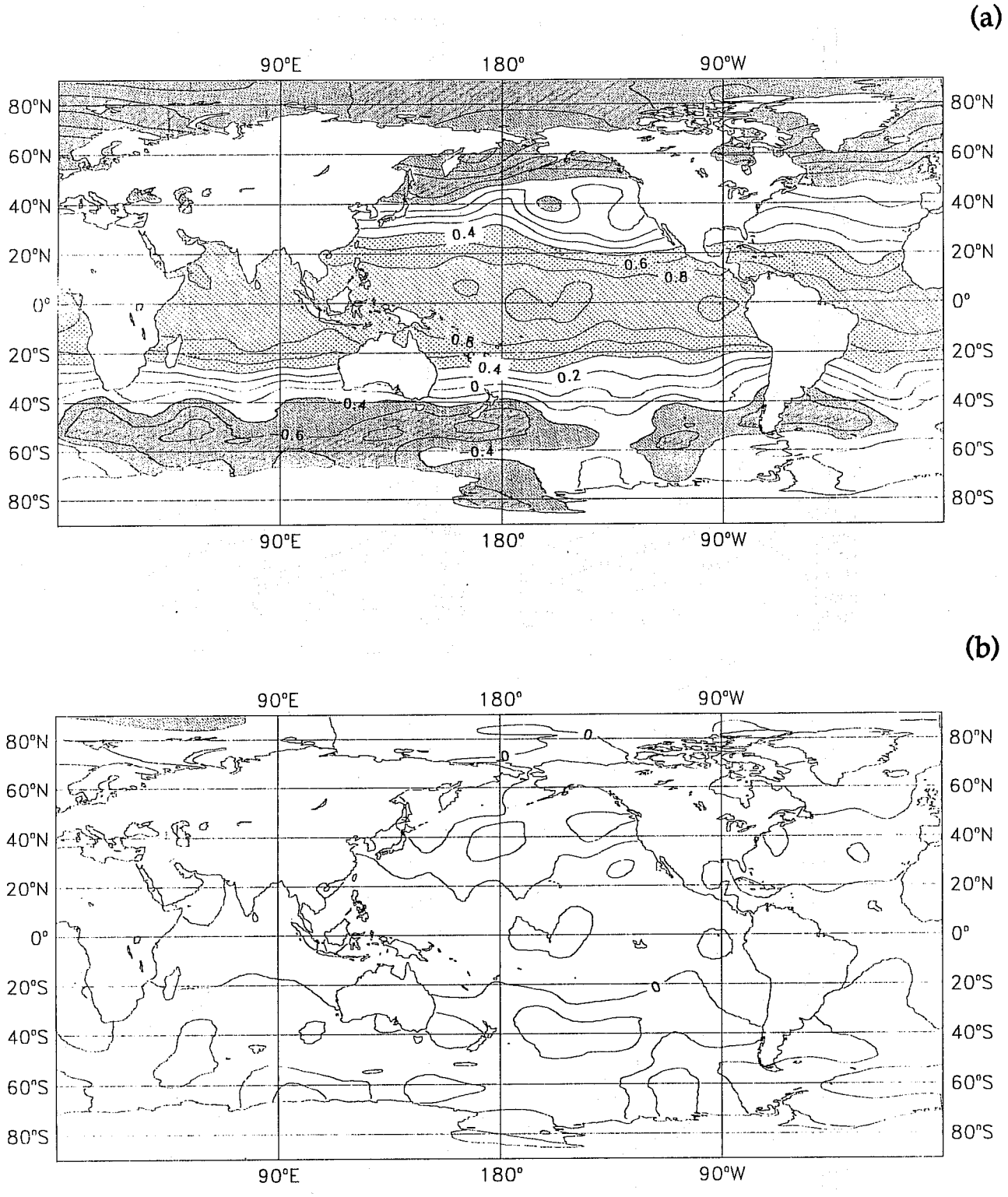

Fig.2 Local mean difference between measured and forecast brightness temperatures in MSU channel 3, NOAA-11, in May 1992 (a) before bias correction and (b) after bias correction. Contour interval = 0.2K; light shading > 0.4K; dark shading < -0.4K.

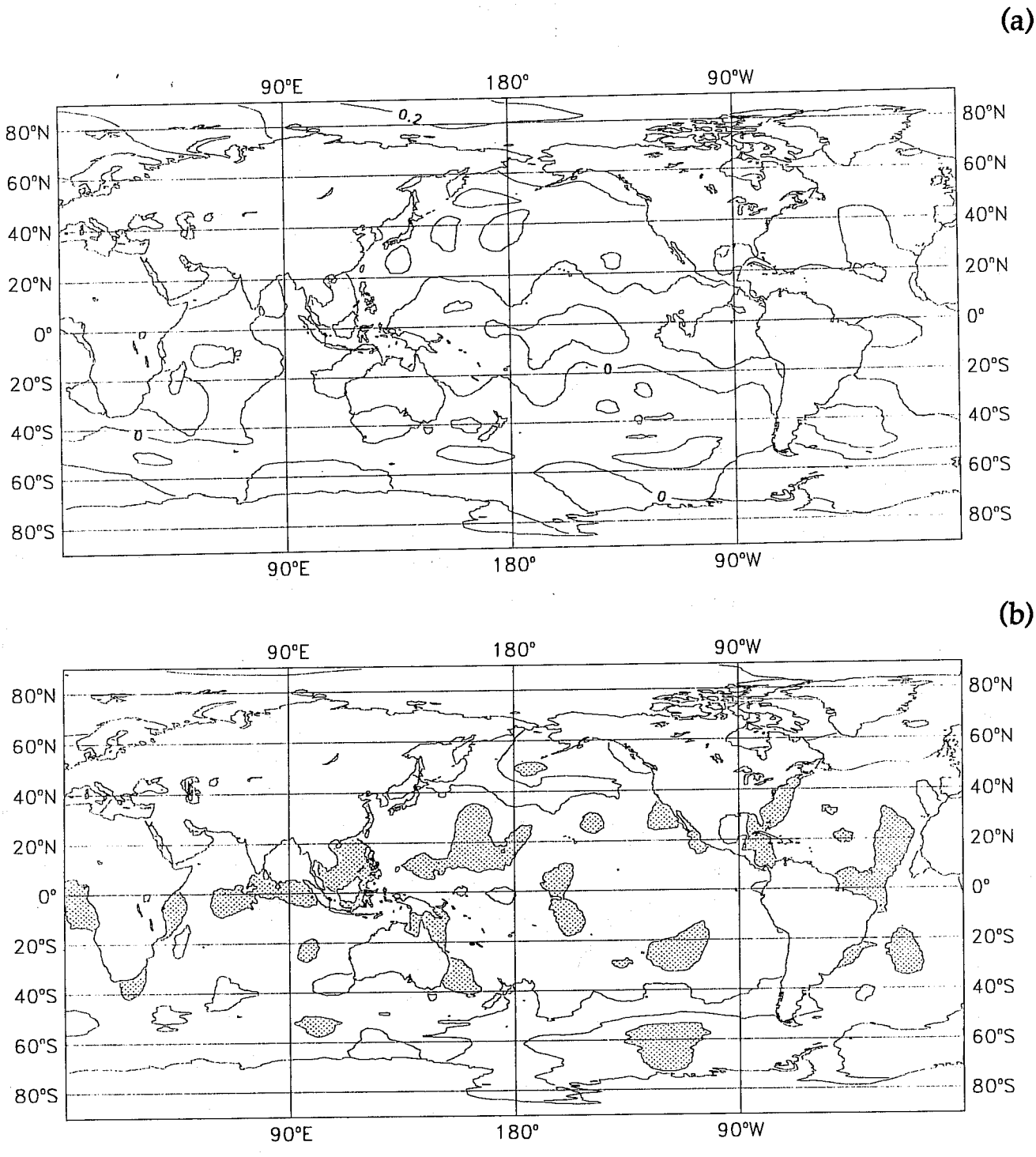

Fig.3 Local mean and standard deviation (SD) of the difference between measured and forecast brightness temperatures (after bias correction) in TOVS channels for NOAA-11, in May 1992:
HIRS channel 4 (a) mean and (b) SD, HIRS channel 5 (c) mean and (d) SD, HIRS channel 15 (e) mean and (f) SD, and MSU channel 2 (g) mean and (h) SD.
For mean plots: contour interval = 0.2K; light shading > 0.4K; dark shading < -0.4K.
For SD plots: contour interval = 0.1K; shading > 0.4K.

HIRS channel 5

(c)

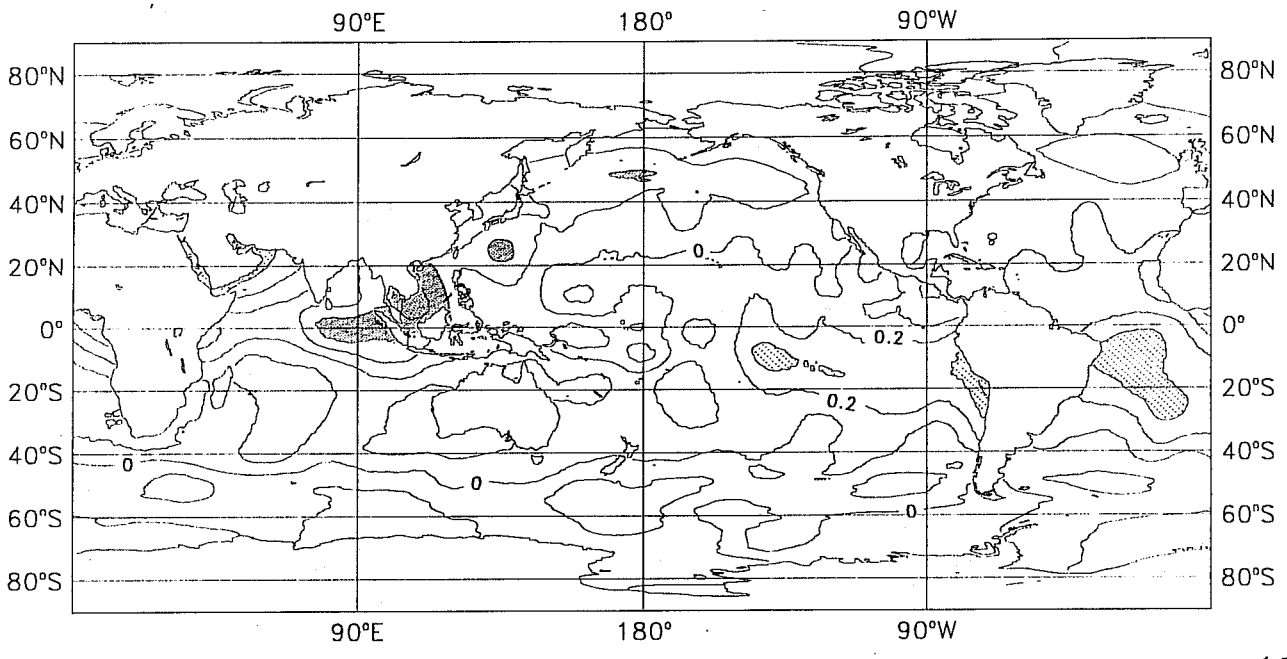

(d)

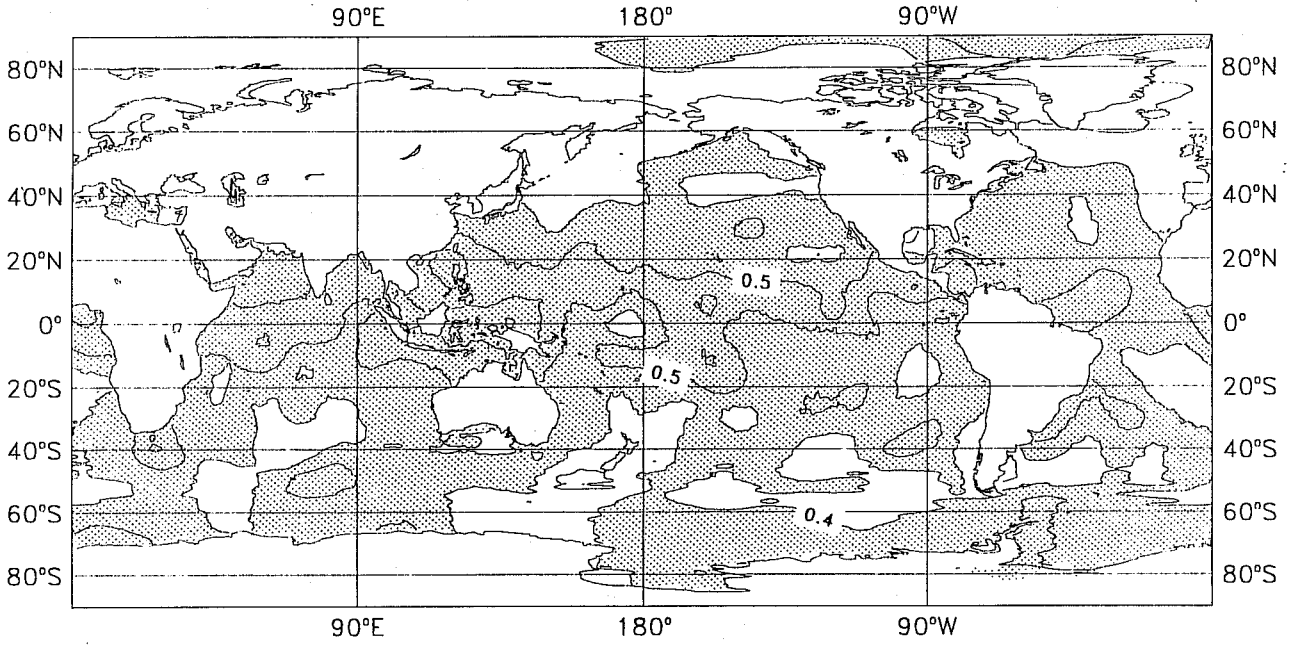

Fig. 3 (continued)

HIRS channel 15

(e)

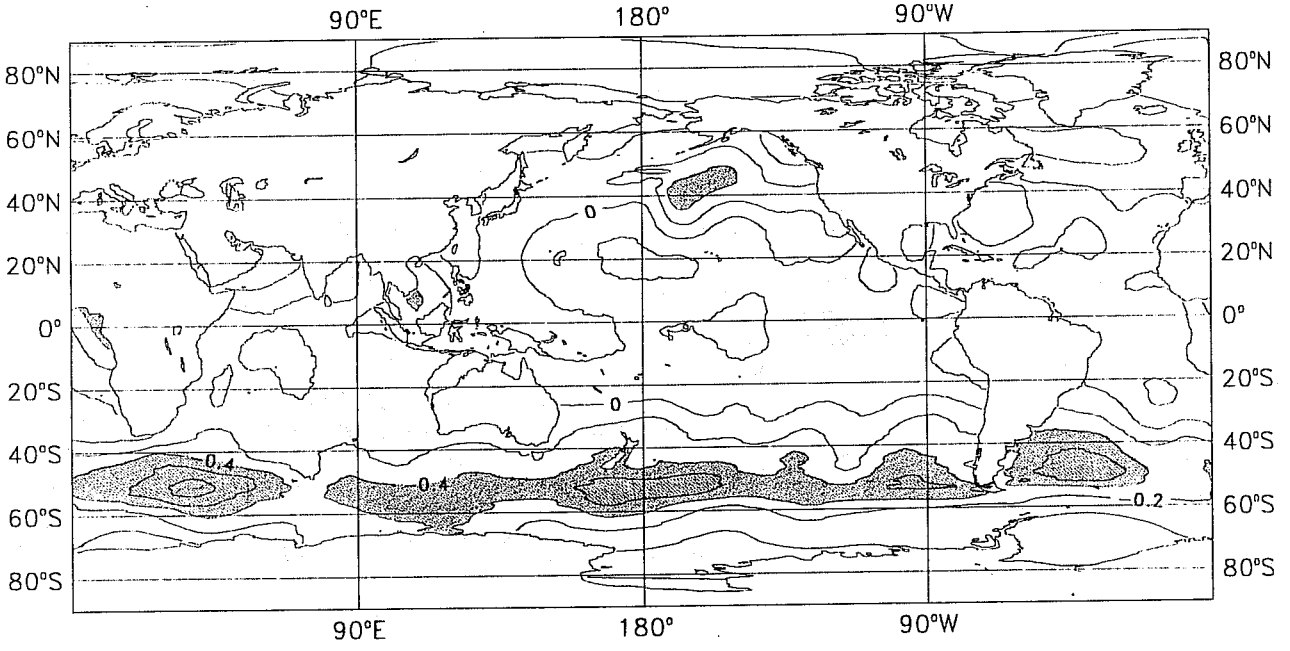

(f)

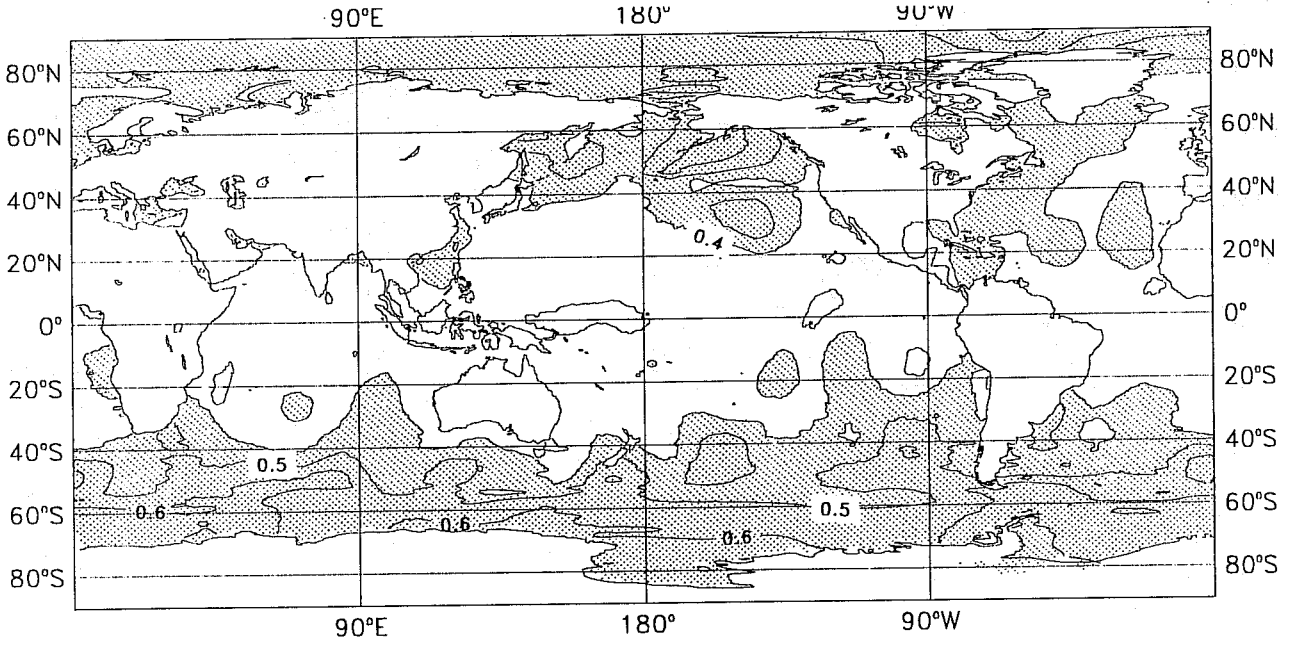

Fig. 3 (continued)

MSU channel 2

(g)

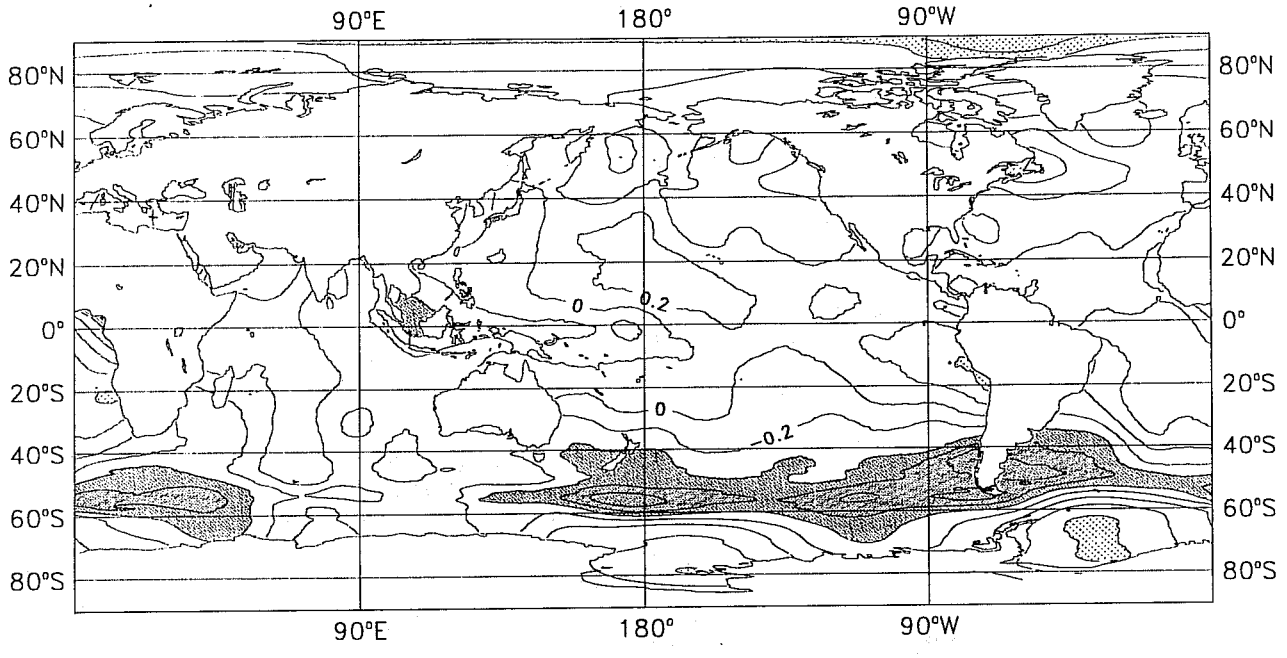

(h)

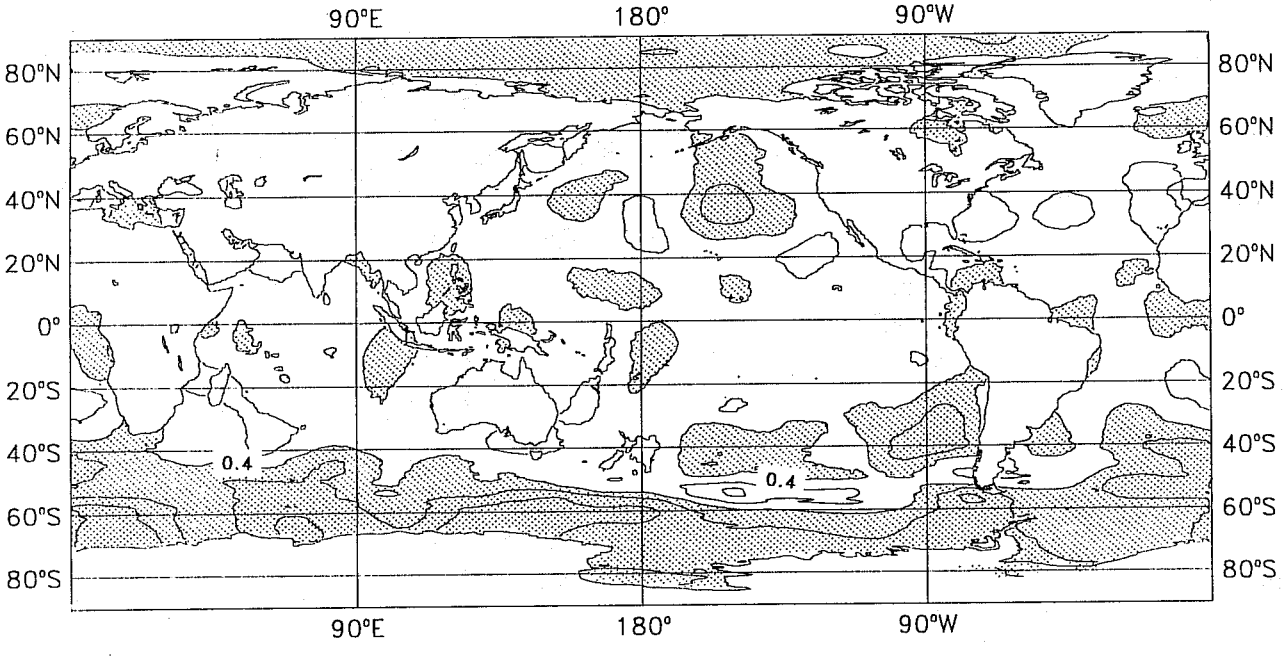

Fig. 3 (continued)

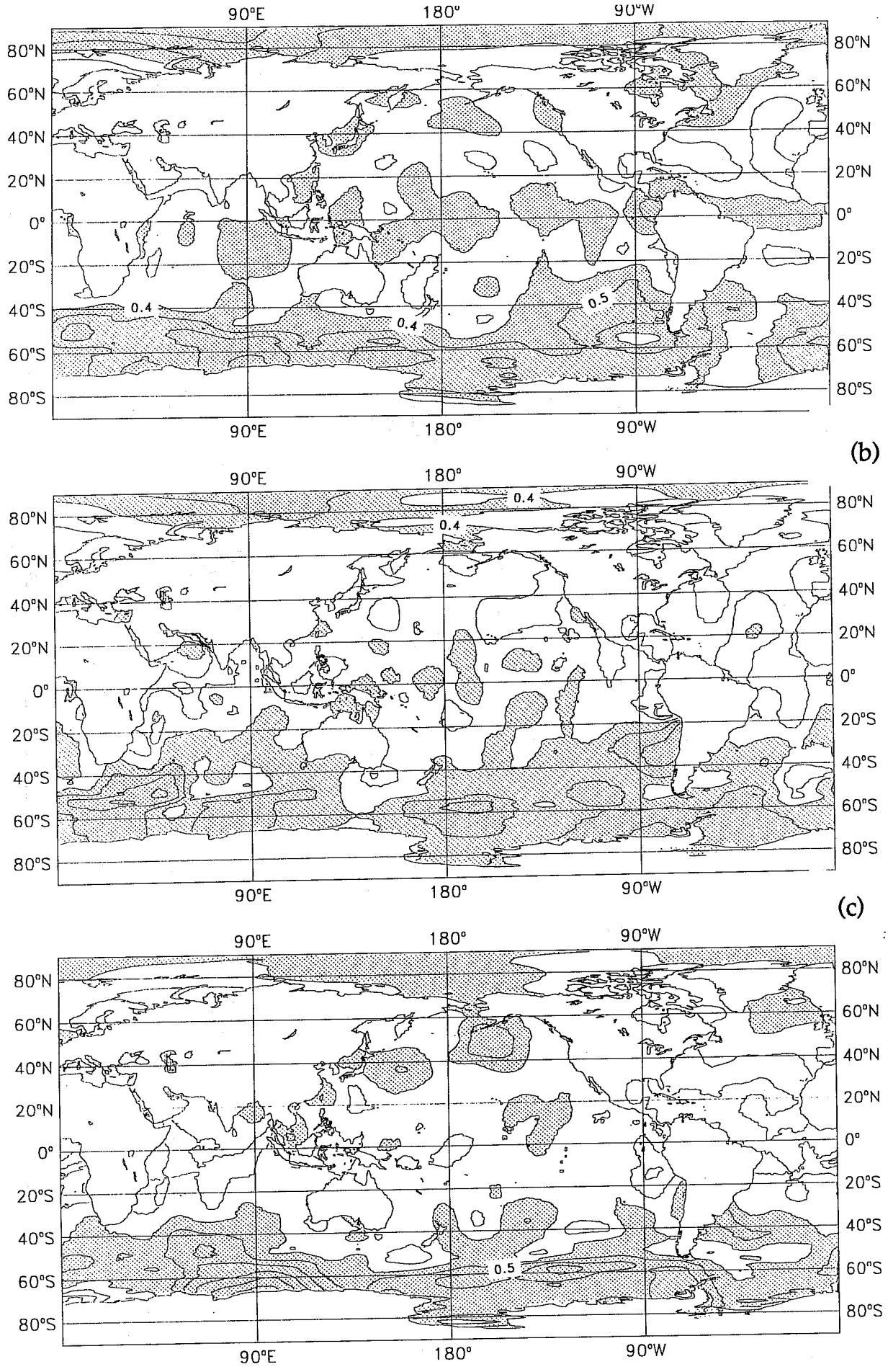

Fig.4 Local standard deviation of the difference between measured and forecast brightness temperatures (after bias correction) in MSU channel 2, NOAA-11: (a) May 1991, (b) July 1991, (c) September 1991, (d) November 1991, (e) January 1992 and (f) March 1992.
Contour interval = 0.1K; shading > 0.4K.

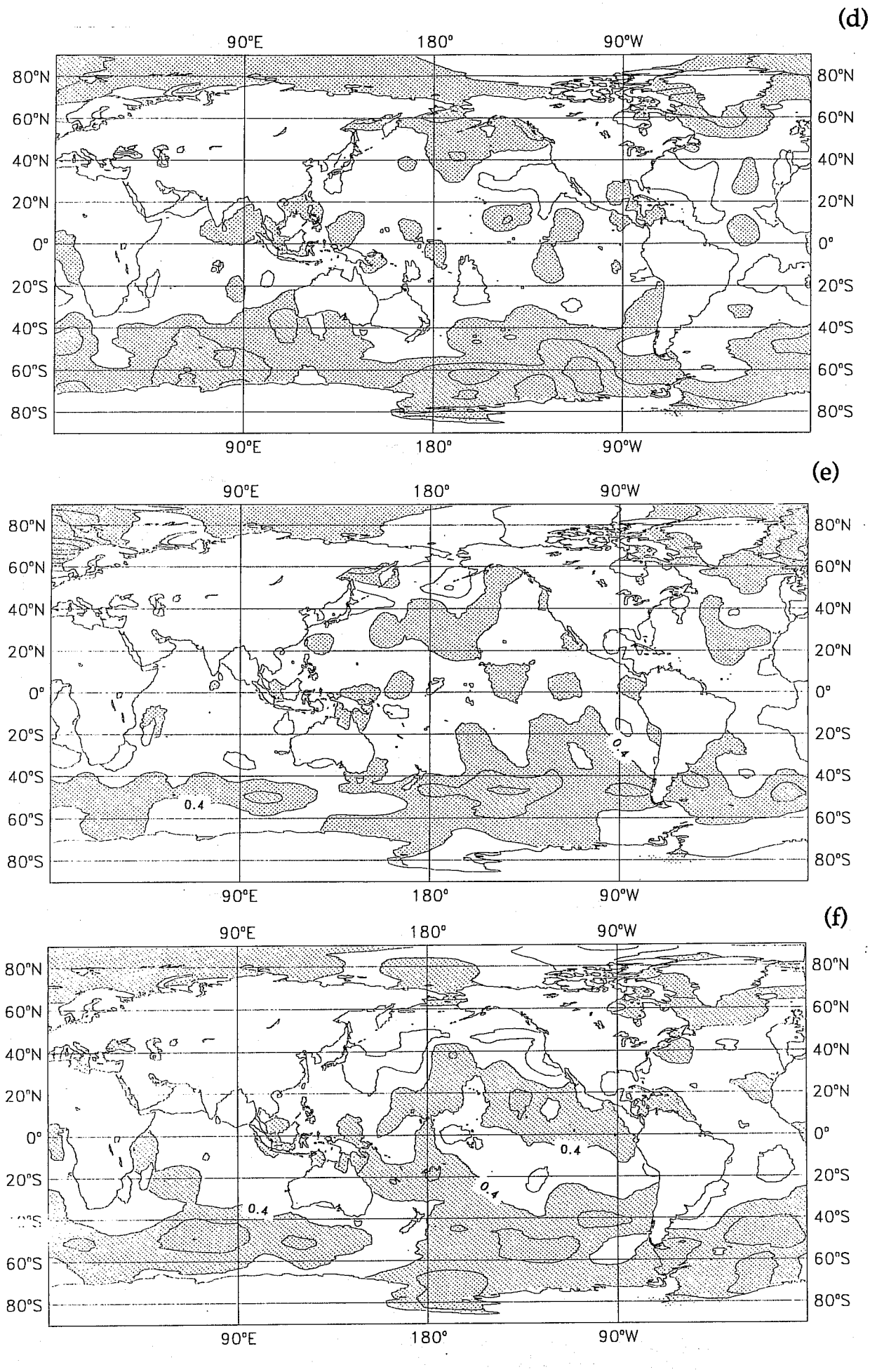

Fig. 4 (continued)

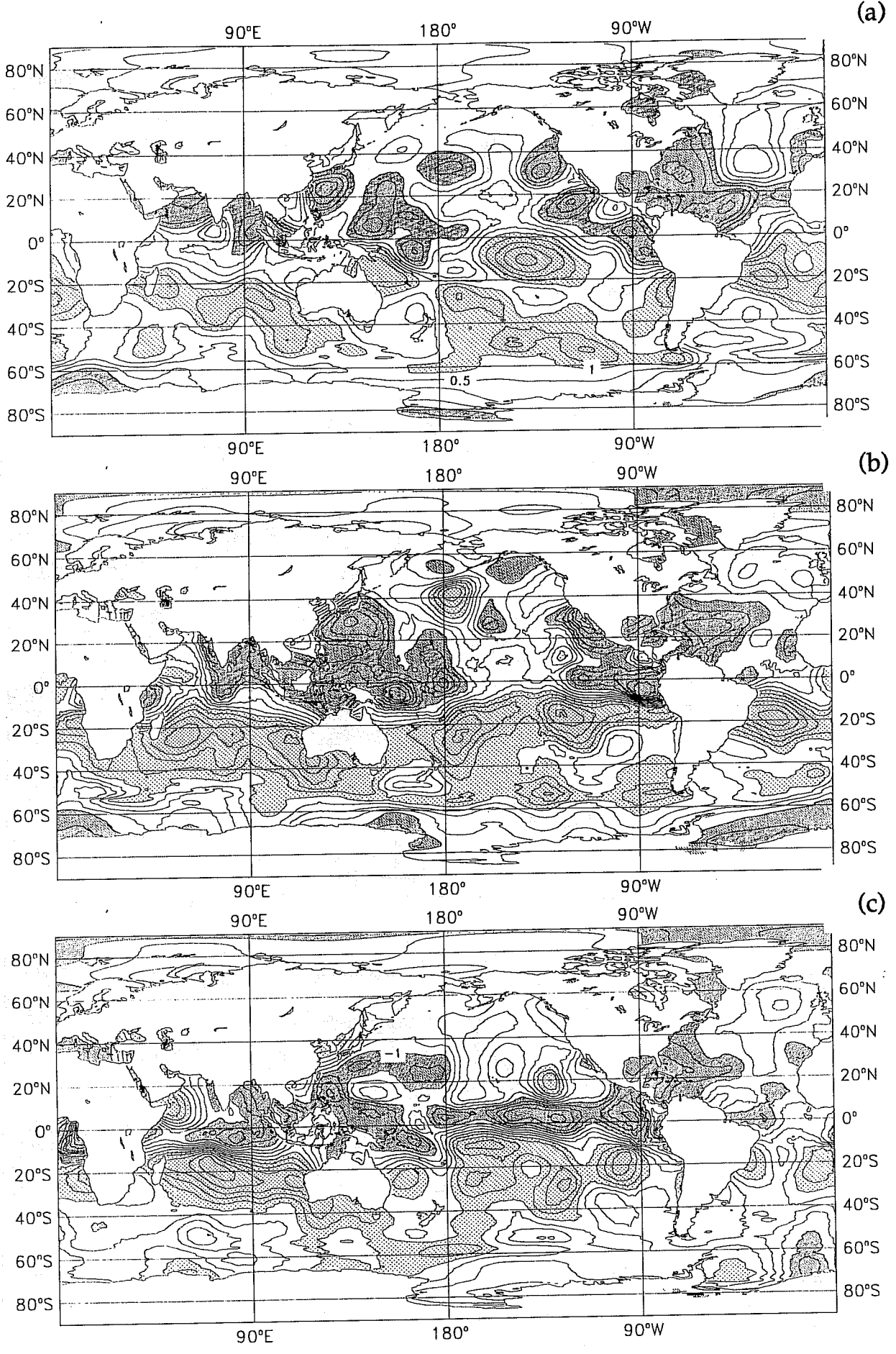

Fig.5 Local mean difference between measured and forecast brightness temperatures (after bias correction) in HIRS channel 11, NOAA-11: (a) May 1991, (b) July 1991, (c) September 1991, (d) November 1991, (e) January 1992 and (f) March 1992.
Contour interval = 0.5K; light shading > 1.0K; dark shading < -1.0K.

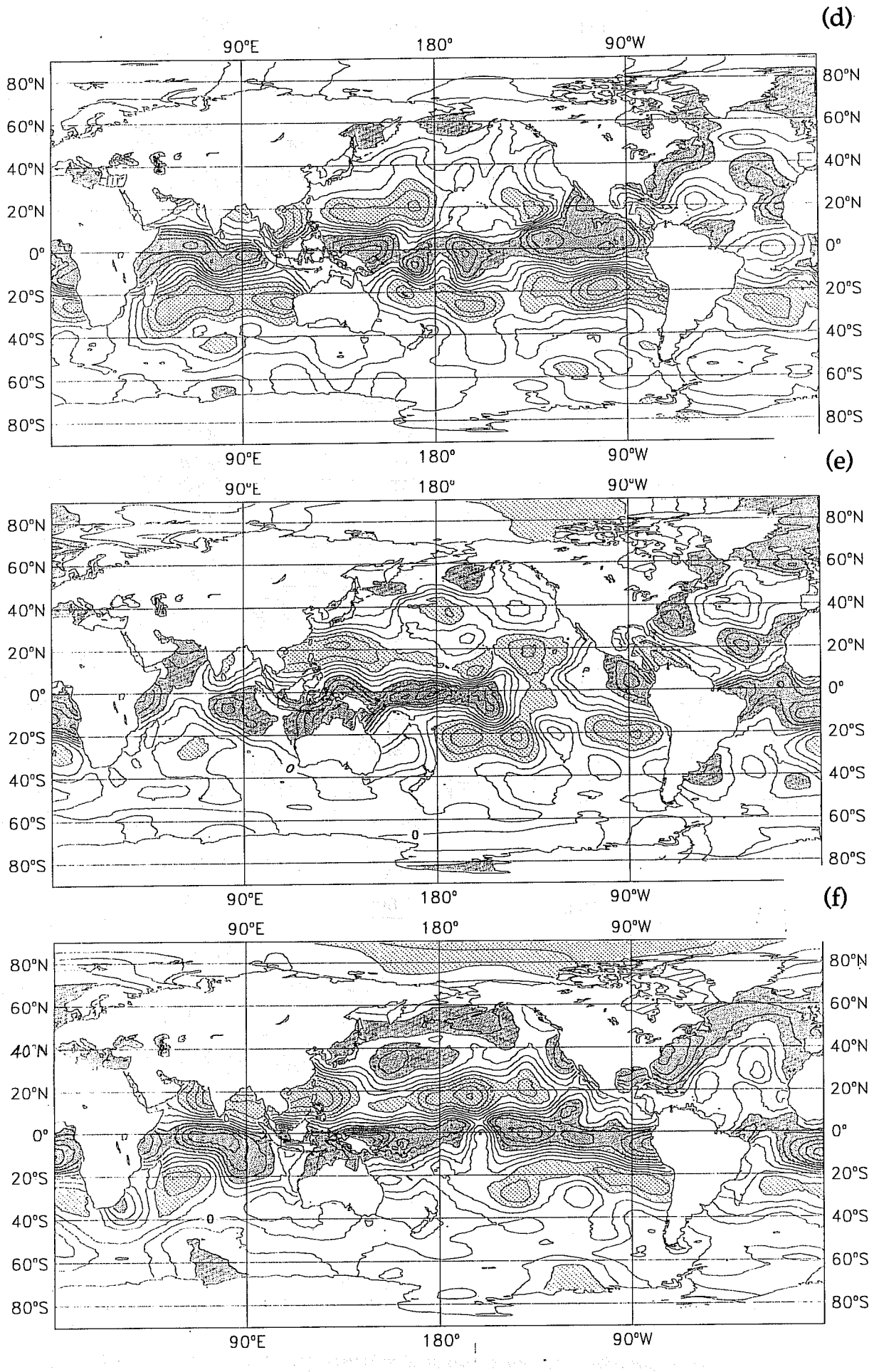

Fig. 5 (continued)

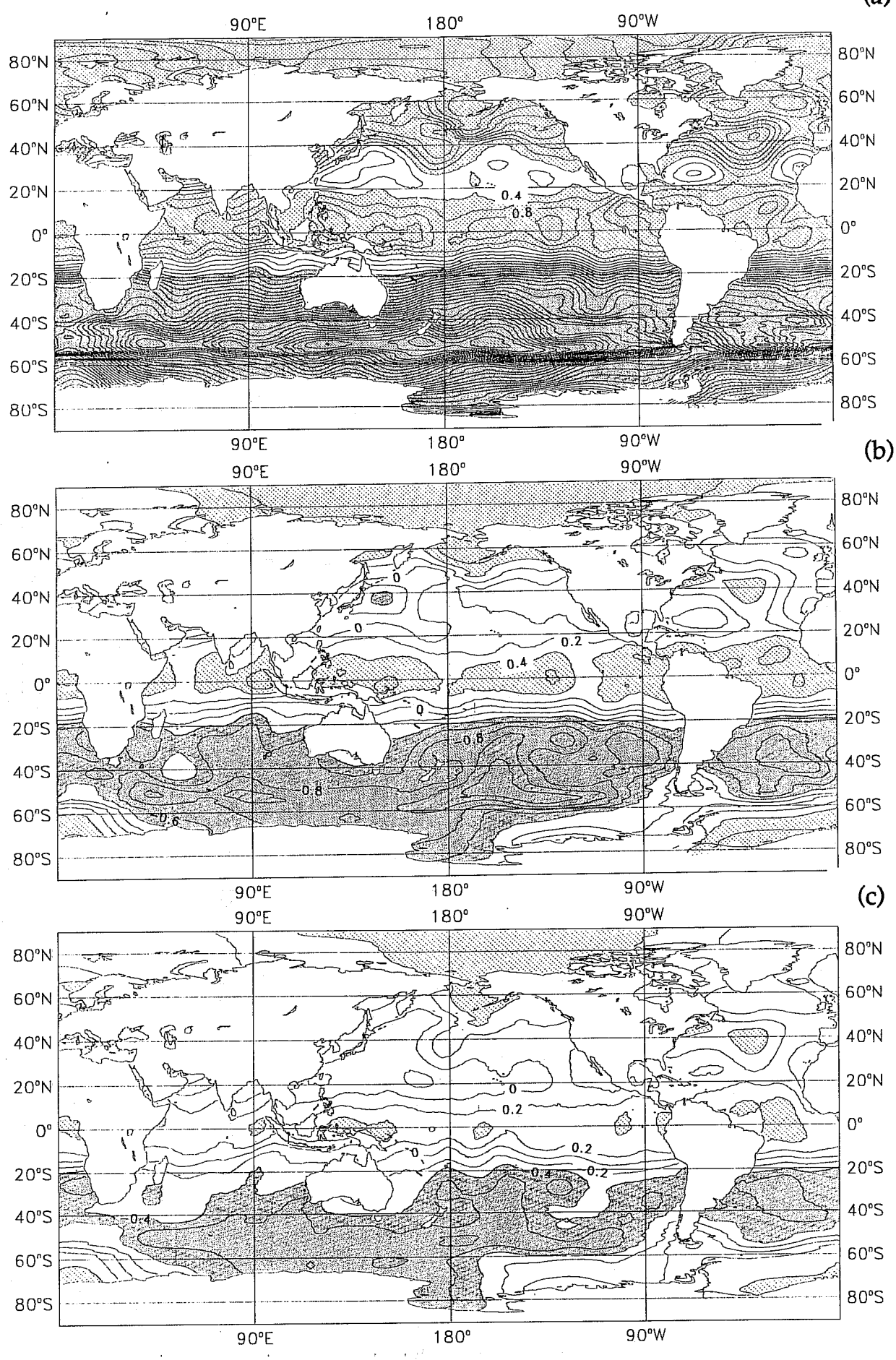

Fig.6 Local mean difference between measured and forecast brightness temperatures (after bias correction) in HIRS channels 1, 2 and 3, NOAA-11, for May 1992: (a)-(c) with and (d)-(f) without HIRS channel 1 as a bias predictor.
Contour interval = 0.2K; light shading > 0.4K; dark shading < -0.4K.

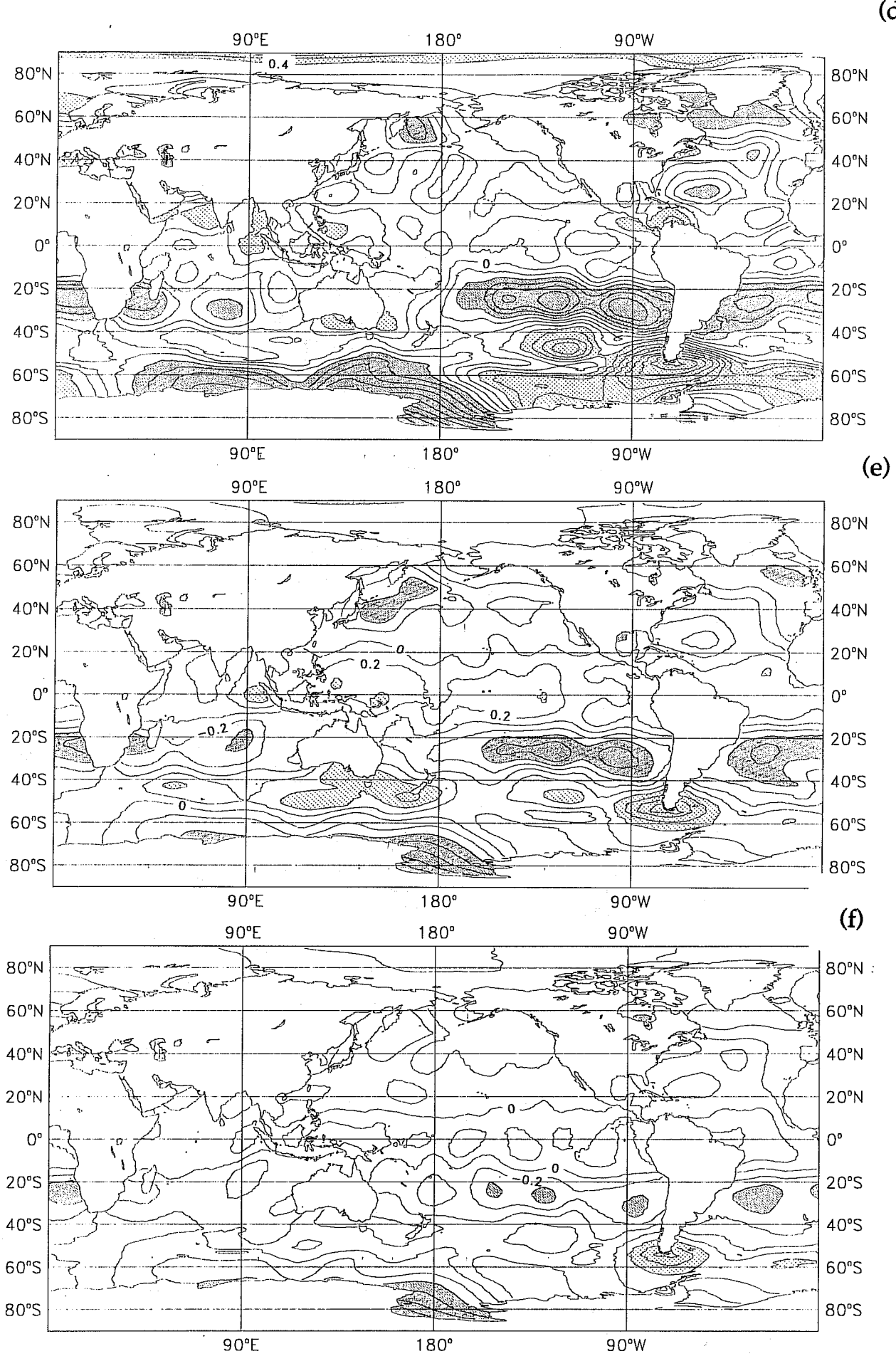

Fig. 6 (continued)

ANNEX A.

USER GUIDE TO BIAS CORRECTION PROGRAMS.

1. PROGRAMS

1.1 Data selection

This is described in section 5.1.

Jobs are in: .STE.CRAY_JOBS.BIASPREP92_##,
where ## = 11 for NOAA-11, = 12 for NOAA-12.

Each job contains 2 FORTRAN programs: the first (BIASPREP) selects data for the required satellite and cloud-clearing route (currently set to "clear" soundings only) and concatenates data for required days. The second (BIASSELE) selects data for sea or land (set to sea at present) and equalises data quantities for different latitude bands.

Input from ECFILE: /ANALF/O/PRESAT1D/STAT/yymmddhh.
Output to ECFILE: /STE/UNICOS/PRESAT92/BIASPREP_mm_##.

To modify for new month, make changes shown in Figure A.1.

1.2 Scan bias correction

This is described in sections 5.2 and 5.3. The job is not currently active.

Source code is in .STE.BIAS.SOURCE_LIBRARY, with main program BIASSCAN. (Currently requires some modification to make consistent with other programs.)

Input:
- TOVS data from ECFILE: /STE/UNICOS/PRESAT92/BIASPREP_mm_##,
- radiosonde mask: /ec/ste/rsmask.

Output:
- scan bias corrections.

1.3 Spatially-varying bias correction

This is described in sections 5.2 and 5.4.

Jobs are in: .STE.CRAY_JOBS.BIAS92_##rs,
where ## = 11 for NOAA-11, = 12 for NOAA-12.

Source code is in .STE.BIAS.SOURCE_LIBRARY, with main program BIASCOR.

Input:
- TOVS data from ECFILE: /STE/UNICOS/PRESAT92/BIASPREP_mm_##,
- radiosonde mask: /ec/ste/rsmask,
- scan bias corrections (not currently active).

Output:
- bias correction coefficients: /STE/UNICOS/PRESAT92/COEF_mm_##R,
- corrected TOVS data: /STE/UNICOS/PRESAT92/BIASCOR_mm_##R,
- uncorrected TOVS data: /STE/UNICOS/PRESAT92/BIASUNC_mm_##R.

To modify for new month, make changes shown in Figure A.2.

BIASCOR can also be run in a mode in which it reads in "external coefficients" calculated beforehand (e.g. from the previous month) and uses these to generate corrected data.

1.4 Creation of radiosonde mask

Job is in: .STE.CRAY_JOBS.RSMASK. Source code is in:
.STE.PPEMISC.SOURCE_LIBRARY, with main program RSMASK_CRAY.

Input:
- list of active radiosonde stations (obtained from Met.Ops): /ec/ste/templist.

Output:
- mask, with resolution of 1 deg x 1 deg, denoting points within a radius of X degrees (latitude equivalent) of an active radiosonde station (currently X = 5 deg): /ec/ste/rsmask.

1.5 Plotting fields of local bias and standard deviation

Job is in: .STE.CRAY_JOBS.PLOTBIAS.

Input:
- output of BIASCOR, either corrected or uncorrected data:
/STE/UNICOS/PRESAT92/BIASCOR_mm_##R,
/STE/UNICOS/PRESAT92/BIASUNC_mm_##R.

Output:
- contoured plots of local mean and standard deviation of data.

To modify for new month or channels, make changes shown in Figure A.3. Appropriate contour intervals are 0.5K for HIRS channels 10, 11 and 12, and 0.2K for other channels.

2. PROCEDURE TO GENERATE AND CHECK NEW BIAS CORRECTIONS

The current practice is to generate bias corrections once per month as soon as the PRESAT output is available for all days in the preceding month, and to use data from all cycles on alternate days.

2.1 Edit BIASPREP92_## and BIAS92_##rs to new month for both satellites.

2.2 Run BIASPREP92_##, then BIAS92_##rs, for each satellite. Check that the coefficient files have been successfully stored.

2.3 Check the application of bias correction using PLOTBIAS: edit it to the appropriate month. Run one job for each batch of channels (e.g. 1-4, 5-8, 10-12, 13-15, 22-24).

Fig. A.1 Job for data selection.

.ste.cray_jobs.biasprep92_11 (selected parts)

```
|
#QSUB -r biasprep              # Job name
|
cat > test.f <</EOF
      PROGRAM BIASPREP
C
C          ACCUMULATE PRESAT OUTPUT STATS FOR BIAS CORRECTION PROGS
|
      CHARACTER*80      YPARMS, YPFTABB
      CHARACTER*6       YTABB
      CHARACTER*2       YTIM(4)
      DATA YTIM/'00','06','12','18'/
|
      ILFN=JYEAR*10000+JMON*100+JDAY
      WRITE (YTABB,'(16)') ILFN
      YPFTABB='/tmp/ste/prss'//YTABB//YTIM(ITIM)
      YPARMS='-p /analf/o/presat1d/stat'//YTABB//YTIM(ITIM)//'get'
     1//YPFTABB
      CALL ECFILE(NFAIL,IRSN,YPARMS)
|
      END
EOF
|
assign -a biasprep_07[1]_11.d fort.20
./a.out <<\EOF
201 32
92 07 01 92 07 31 02[2]
EOF
#
cat >biassele.f <<\EOF         # put code from stdin into file bias.f
      PROGRAM BIASSELE
C
C**** *BIASCOR* - TO SELECT DATA FOR BIAS CORRECTION PROGRAMS.
C
|
      END
EOF
|
assign -a biasprep_07[1]_11.d fort.10
assign -a /tmp/ste/biasprep_07[1]_11 fort.11
./biassele.out
#
ecfile -h O -v U/PUB/R/-/S -p /STE/UNICOS/PRESAT92/BIASPREP_07[1]_11 save \
/tmp/ste/biasprep_07[1]_11
#
fi
```

[1] month

[2] start year, month, day; end year, month, day; day-increment

Fig. A.2 Job for spatially-varying bias correction.

.ste.cray_jobs.bias92_11rs (selected parts)

```
PROC RUN_BIAS( )
|
#QSUB -r stebias                # Job name
|
#       SCAN BIASES
#ecfile -p /STE/UNICOS/SCANBIAS_89R11 get /tmp/ste/scanbias_89r11
#assign -a /tmp/ste/scanbias_89r11 fort.15
#       INPUT DATA FROM SELECT
ecfile -p /STE/UNICOS/PRESAT92/BIASPREP_07[1]_11 get /tmp/ste/biasprep_07[1]_11
assign -a /tmp/ste/biasprep_07[1]_11 fort .10
#       INTERNAL COEFFICIENTS
assign -a /tmp/ste/coef_07[1]_11r fort.11
#       EXTERNAL COEFFICIENTS
#ecfile -p /STE/UNICOS/PRESAT92/COEF_01_11 get /tmp/ste/coef_01_11
#assign -a /tmp/ste/coef_01_11 fort.21
#       CORRECTED OUTPUT
assign -a /tmp/ste/biascor_07[1]_11r fort.12
#       UNCORRECTED OUTPUT
assign -a /tmp/ste/biasunc_07[1]_11r fort.13
#       mask
assign -a /ec/ste/rsmask fort.39
#
cat > biasdata << EOFB
201 0 0 1
sat id, int/ext coeffs (0/1), scan corr: no/yes (0/1), raob mask: no/yes (0/1)
EOFB
bias.out < biasdata
#
fi
#
ecfile -h O -v U/PUB/R/-/S -p /STE/UNICOS/PRESAT92/COEF_07[1]_11R save \
/tmp/ste/coef_07[1]_11r
ecfile -h O -v U/PUB/R/-/S -p /STE/UNICOS/PRESAT92/BIASCOR_07[1]_11R save \
/tmp/ste/biascor_07[1]_11r
ecfile -h O -v U/PUB/R/-/S -p /STE/UNICOS/PRESAT92/BIASUNC_07[1]_11R save \
/tmp/ste/biasunc_07[1]_11r
```

[1] month

Fig. A.3 Job for plotting local bias and standard deviation.

.ste.cray_jobs.plotbias (selected parts)

```
PROC UNL_RADS_ANAL_MAIN( )
|
#QSUB -r steplot                    # Job name
|
cat > pltrad.f <<\EOF
        PROGRAM ANALRAD
C
|
        END
EOF
|
ecfile -p /ste/unicos/presat92/biascor_06[1]_12[2]r get fort.50          # input
#ecfile -p /ste/unicos/presat92/biasunc_03_11r    get fort.50          # input
a.out << \eof
 $namin
        anwlon= 0., aselon=360., anwlat=90., aselat=-90., xlen=10.,
        NLNDSEA=1, NRET=0, NDEV=0, cint=.2[3],
        NCHS=|$VALUE(NCHS)|,
        NCHE=|$VALUE(NCHE)|,
        NSAT=|$VALUE(NSAT)|,
 $end
 $namtx
        CTEXT='presat92 06/cor rsmask'[4]
 $end
eof
if [ $? -ne 0 ]; then
        debug; exit 1
fi
# rename plotfile
#
#mv qms pltrad.qms
# gksplot -f qms pltrad.qms
mv ps pltrad.ps
gksplot -d ps -f ps -n pltrad.ps
exit
??end
disv' Submitting rads_anal job to CRAY ...'
subcj $fname(cray_job_file)
procend UNL_RADS_ANAL
??
$local.rads_anal          'ste' '920601'[5] '12'[2] '22'[6] '24'[6]
disv ' End of MAIN VE-procedure, OK!
"delf $user.rads_anal
procend UNL_RADS_ANAL_MAIN
```

1 month
2 satellite
3 contour interval
4 plot title
5 start date
6 channel limits

Abstract

Radiative transfer models for simulating measurements from satellite sounding radiometers are subject to systematic errors which are found to vary as a function of the atmospheric profile. The radiance measurements themselves, particularly if they have been pre-processed, may also contain systematic errors. The magnitudes of these errors are often comparable with the radiance changes corresponding to typical errors in the temperature field from a short-range forecast, and yet we hope to use these radiance measurements to help us improve the accuracy of the temperature field during the data assimilation process. It is therefore necessary to have a scheme which compensates adequately for the biases in the measurements and the radiative transfer model.

This paper describes the bias correction procedure developed at ECMWF for application to the difference between measured and simulated brightness temperatures of the TIROS Operational Vertical Sounder (TOVS). The scheme is being used in the context of the one-dimensional variational analysis scheme used at ECMWF for operational assimilation of TOVS radiance data. A data base of the differences between measured and forecast brightness temperatures has been generated and used to develop a correction for bias in two stages. Firstly, a constant correction is applied at each scan position to remove the relative bias between measurements at different scan positions. Secondly, a regression correction, using measured brightness temperatures in a sub-set of channels as predictors, is applied to remove the bias between measured and forecast brightness temperatures. The paper describes the details of the bias correction method and discusses the results of some brightness temperature statistics obtained through its application.

8 Appendix 2: relationship between analysis error covariance matrix and Hessian matrix.

Let us write the cost-function as

$$J(X_0) = \frac{1}{2}\sum_{i=0}^{n}(\mathcal{M}(t_i,t_0)X_0 - Y_i)^t Q^{-1}(\mathcal{M}(t_i,t_0)X_0 - Y_i) \tag{18}$$

where $\mathcal{M}(t_i,t_0)$ represents the integration of the model from the initial conditions X_0 at time t_0 up to time t_i, Y_i stands for the observations at the same time and Q is the matrix defining the scalar product $< .,. >$ used in 11 interpreted here as the covariance matrix of observation error:
the observations Y_i at each time step are of the form

$$Y_i = X_{it} + \epsilon_i \tag{19}$$

where the subscript t stands for true, and the observational errors (ϵ_i; i=1,n) satisfy the relations

$$\left.\begin{array}{l} E(\epsilon_i) = 0 \\ E(\epsilon_i\epsilon_i^t) = Q \\ E(\epsilon_i\epsilon_j^t) = 0 \end{array}\right\} \tag{20}$$

The gradient (first derivative of J) with respect to the Euclidean inner product can be written

$$\nabla_{X_0} J = \sum_{i=0}^{n}\mathcal{R}(t_i,t_0)^t Q^{-1}(\mathcal{M}(t_i,t_0)X_0 - Y_i) \tag{21}$$

and the Hessian matrix

$$J'' = \sum_{i=0}^{n}\mathcal{R}(t_i,t_0)^t Q^{-1}\mathcal{R}(t_i,t_0) + \sum_{i=0}^{n}\mathcal{H}(t_i,t_0)^t Q^{-1}(\mathcal{M}(t_i,t_0)X_0 - Y_i) \tag{22}$$

where $\mathcal{R}(t_i,t_0)$ represents the first derivative of $\mathcal{M}$ (tangent linear model) and $\mathcal{H}(t_i,t_0)$ the second derivative of $\mathcal{M}$.
Since the tangent linear model $\mathcal{R}$ is a good approximation to $\mathcal{M}$, the Hessian matrix reduces to

$$J'' = \sum_{i=0}^{n}\mathcal{R}(t_i,t_0)^t Q^{-1}\mathcal{R}(t_i,t_0) \tag{23}$$

and the gradient of J is zero. Using the expression of Y_i and the tangent linear approximation, one gets

$$\sum_{i=0}^{n}\mathcal{R}(t_i,t_0)^t Q^{-1}(\mathcal{R}(t_i,t_0)(X_0 - X_{0t}) - \epsilon_i) = 0 \tag{24}$$

which can be inverted in order to get the difference between the analysed state and the truth

$$X_0 - X_{0t} = (\sum_{i=0}^{n} \mathcal{R}(t_i, t_0)^t Q^{-1} \mathcal{R}(t_i, t_0))^{-1} . (\sum_{i=0}^{n} \mathcal{R}(t_i, t_0)^t Q^{-1} \epsilon_i) \tag{25}$$

Thus, the error covariance matrix at the minimum is

$$E((X_0 - X_{0t})(X_0 - X_{0t})^t) = (\sum_{i=0}^{n} \mathcal{R}(t_i, t_0)^t Q^{-1} \mathcal{R}(t_i, t_0))^{-1} \tag{26}$$

and the following relationship applies:

$$E((X_0 - X_{0t})(X_0 - X_{0t})^t) = (J'')^{-1} \tag{27}$$

In order to evaluate the Hessian matrix, we can, as in Gauthier(1990) consider the gradient as a random variable due to the observational errors. Replacing Y_i by its expression (Eq. 19) and defining the "true" gradient by

$$\nabla_{X_0} J_t = \sum_{i=0}^{n} \mathcal{R}(t_i, t_0)^t Q^{-1} (\mathcal{M}(t_i, t_0) X_0 - X_{it}) \tag{28}$$

one obtains

$$\nabla_{X_0} J = \nabla_{X_0} J_t - \sum_{i=0}^{n} \mathcal{R}(t_i, t_0)^t Q^{-1} \epsilon_i \tag{29}$$

The gradient error covariance may then be written as

$$E((\nabla_{X_0} J - \nabla_{X_0} J_t)(\nabla_{X_0} J - \nabla_{X_0} J_t)^t) = \sum_{i=0}^{n} \mathcal{R}(t_i, t_0)^t Q^{-1} \mathcal{R}(t_i, t_0) = J'' \tag{30}$$

In practice, we create 50 sets of observations with errors having the appropriate error covariance of Q, and we compute the empirical gradient error covariance to evaluate the Hessian.

9 References.

Buckley, A. and A. Lenir, 1983: QN-like Variable Storage Conjugate Gradients. *Mathematical Programming*, **27**, 155-175.

Courtier, P., C. Freydier, J-F Geleyn, F. Rabier and M. Rochas 1991: The ARPEGE Project at Meteo-France. *ECMWF Seminar proceedings, September 1991.*

Gauthier,P. 1991: Chaos and quadri-dimensional data assimilation : a study based on the Lorenz model. To appear in *Tellus.*

Gill A.E., 1982: Atmosphere-Ocean Dynamics. *Academic Press*, 662pp.

Jarraud, M., J.Goas and C.Deyts, 1989: Prediction of an exceptional storm over France and Southern England (15-16 October 1987). *Wea. For.*, **4**, 517-536.

Lacarra, J.F. and O. Talagrand, 1988: Short range evolution of small perturbations in a barotropic model. *Tellus*, **40A**, 81-95.

Lorenc, A.C., R.S.Bell, T.Davies and G.J.Shutts, 1988. Numerical forecast studies of the October 1987 storm over southern England. *Meteorol. Magazine*, **117**, 118-130.

Navon, I.M., X. Zou, K. Johnson, J. Derber and J. Sela, 1991: Variational data assimilation with an adiabatic version of the NMC spectral model. *Tech. Rep. FSU-SCRI-91-13, Tallahassee, FL 32306-4052*, 43 pp.

Pedlosky, J., 1970: Finite-Amplitude Baroclinic waves. *J.Atmos.Sci.* **27**, 15-30.

Simmons, A. and D.Burridge, 1981: An energy and angular momentum conserving vertical finite difference scheme and hybrid vertical coordinates. *Mon.Wea.Rev.*, **109**, 758-766

Simmons, A.J. and B.J.Hoskins, 1978: The Life Cycles of Some Nonlinear Baroclinic Waves. *J. Atmos. Sci.*, **35**, 414-431.

Thépaut, J.N. and P.Courtier, 1991: Four dimensional variational data assimilation using the adjoint of a multilevel primitive equation model . To appear in *Q. J. R. Meteorol. Soc.*. Also available from ECMWF as Technical Memorandum 178

Thépaut, J.N. and P.Moll, 1991: Variational inversion of simulated TOVS radiances using the adjoint technique. *Q. J. R. Meteorol. Soc.*, **116**,1425-1448.

Thorncroft, C.D. and B.J.Hoskins, 1990: Frontal Cyclogenesis. *J.Atmos.Sci.*, **47**, 2317-2336.

Vukicevic, T. 1991. Nonlinear and Linear Evolution of Initial Forecast Errors. *Mon. Wea. Rev.*, **119**, 1602-1611.

185

Abstract

The paper analyses the performance of different schemes aimed at computing the clear sky brightness temperature from measurements affected to some degree by clouds. Both the ability to detect clouds and to estimate the equivalent clear sky brightness temperature were examined. The simulated brightness temperatures computed from the ECMWF operational analysis using the fast radiative transfer model have been used as control variable, together with AVHRR-derived sea surface temperature and cloud content within HIRS field of views. Cloud-masks obtained from the cloud-detection schemes were compared with cloud-masks obtained from AVHRR data; clear-column brightness temperatures for HIRS/2 channels 4, 7 and 13 were compared with the simulated ones; simulated clear-column brightness temperatures in the HIRS/2 window channel 8 were validated with equivalent products from AVHRR data.

1. INTRODUCTION

Radiometric accuracy for infrared sounders is largely independent of scene brightness temperature (BT) and high quality radiometry of cloudy, as well as of clear, scenes is therefore a reality. However most of the scientific attention and research has been devoted to the processing of clear radiances, for at least two reasons. Firstly, most of the scientific attention was concentrated on the problem of retrieving the temperature and humidity profiles. Over the years more physics has been introduced in the inversion algorithms and a steady reduction of the differences among various retrieval methods, when applied to the same clear radiance set, has been attained, differences still arising depending on the choice of the first guess, whether based on forecast fields or on climatological databases. Secondly, operational practice in handling TIROS Operational Vertical Sounder (TOVS) data in Numerical Weather Prediction (NWP) has been until now to analyse some sounding products obtained by inverting cloud cleared radiances and very little, if any, use is presently made of cloudy measurements, which could provide information on aspects of the water cycle in the atmosphere; to use them still a large effort is required, to model the satellite data for what they really are and interpret all the information that today's measurements contain.

Lesser attention has been paid to the cloud detection and clearing step, aimed at producing clear column radiances from measurements contaminated to some degree by clouds, the matter being considered as a necessary preprocessing step with little scientific content. However the quality of retrieved products and their usefulness in NWP is fundamentally limited by the quality of the cloud cleared BTs and the ability to specify this quality in any optimal inversion process (*McNally*, 1990).

Currently TOVS data are received at ECMWF in two formats. The first is the so-called full resolution output at about 120 km global resolution and contains cloud cleared radiances together with the temperature and humidity profiles produced by the National Environmental Satellite and Data Information Service (NESDIS). This data is then passed to a pre-processing program to quality control and reduce the data to a resolution of about 250 km for input to the ECMWF analysis. A second, which is a backup data set, contains only temperature and humidity data and is an operational GTS NESDIS product. The horizontal resolution of this data is only 500 km.

Impact studies began at ECMWF soon after FGGE. *Uppala et al.* (1984) carried out some observing system experiments on NESDIS statistical retrievals in the FGGE period, using the 1982/83 ECMWF operational system. In the Southern Hemisphere the impact always was large and positive. In the Northern Hemisphere the impact was positive in some cases to neutral in others. A second study by *Kelly and Pailleux* (1988) using the 1987 ECMWF system confirmed these previous results. Later *Andersson et al.* (1991), using the 1988 version of the ECMWF system, showed the impact of 250 km statistical SATEM retrievals produced by NESDIS in the Northern Hemisphere had become very variable and often negative and *Kelly et al.*

(1991) showed that the SATEMS produced by the NESDIS physical retrieval had just as serious errors and biases as the statistical retrievals. The outcome of these studies lead to removing NESDIS TOVS retrievals from the Northern Hemisphere below 100 hPa and completely from the Tropics. The clear signal coming out from the impact studies at ECMWF is that TOVS data is not used in an optimum way.

Schemes have been developed to handle cloudy radiances, either by iterating between the cloud clearing and the inversion steps (*Susskind et al.*, 1984) or by eliminating the need for a separate clearing stage. *Huang and Smith* (1985) perform a simultaneous retrieval that includes atmospheric profiles, surface parameters together with cloud top pressure and amount. *Eyre* (1989) applies the principles of nonlinear optimal estimation to extract the same parameters for use in NWP. Although these techniques could in principle provide the needed profiles and the cloud parameters, no impact study has been done so far.

Despite the growing awareness of the relevance of cloud clearing to the retrieval problem, comparison among different techniques and validation studies are still lacking, despite the International TOVS Working Group has been recommending them since its first Study Conference. The present study was intended to begin to correct the situation by comparing three different cloud-clearing schemes. One is the NESDIS scheme, operational at February 1989 (*Reale et al.*, 1986), which relies on an adjacent spot technique described in *McMillin and Dean* (1982), a variation on the N^* clearing method (*Smith*, 1968). The second one is the scheme routinely running at the UK Meteorological Office (UKMO), which is based on the technique developed by *Eyre and Watts* (1987). Finally, the third technique is the one described in *Andretta et al.* (1989) and *Amato et al.* (1991) and will be referred to as MR59.

While the NESDIS-method and UKMO-method are operational, MR59 is not and relies on some operational parameters and information which were provided by UKMO. In particular it uses UKMO operational coefficients involved in the prediction of HIRS from MSU via a regression relation, and the UKMO cloud-mask, which is produced by their preliminary cloud-detection algorithm. As a consequence, the differences found between the two schemes are due only to the different techniques used to reduce local bias and to filter the first guess clear radiance field.

Three type of comparisons were performed and analysed:

1. Cloud-masks obtained from the cloud-detection schemes of NESDIS and UKMO were compared with cloud-masks obtained from the Advanced Very High Resolution Radiometer (AVHRR) data;

2. clear-column BTs for HIRS/2 channels 4, 7 and 13 produced from NESDIS, UKMO and MR59 were compared with BTs calculated from the ECMWF operational analyses;

3. clear-column BTs in the HIRS/2 window channel 8 produced from NESDIS, UKMO and MR59 were compared to equivalent products from AVHRR data.

This report is organized as follows. Section 2 is devoted to a brief description of the data we used to compare and validate products; section 3 describes the results according to the three items above. Conclusion are drawn in section 4.

2. THE DATA SET

The initial dataset consists of five NOAA 11 nighttime orbits of February 11 (2 consecutive orbits) and 12 (3 consecutive orbits), 1989. The orbits cover the European and North Atlantic areas. A subsequent screening was performed, based on similarity between the orbits and on the availability of AVHRR data and the set which will be presented consists of three orbits, two of which are mostly over the ocean (passes A and D) and one (pass C) covering the European area. Since passes A and D were characterized by quite similar cloud coverage, the attention was focused in the low latitude portion of orbit D in order to have a dataset with significantly different cloud coverage from pass A.

The level 1-B navigated and located data were processed using the International TOVS Processing Package to generate the so-called sounder data files. The latter were sent to the UKMO which sent back the cloud cleared BTs and the output of their cloud detection algorithm ("cloud mask"). The sounder data files and the UKMO cloud masks were then sent to the Dipartimento di Scienze Fisiche (DSF) of Napoli, which sent back the cleared BTs and the final error estimate at each field of view (FOV).

The data produced by NESDIS were already available at ECMWF, written in DSD3 file format. The navigation information contained in the DSD3 sets were checked against the sounder files FOV location and the quality of the NESDIS products were checked using quality flags contained in the DSD3 files themselves.

Simulated radiances were computed using the ECMWF TOVS forward model (*Eyre*, 1991) using the analyses produced operationally, interpolated to the time of the passes. Both limb corrected and non limb corrected simulated datasets were generated but, since all three processing schemes operate on limb corrected radiances no use, until now, has been made of the latter simulated dataset. No bias correction has been applied to the simulated BTs which therefore constitute only a reference field for the products obtained with the various techniques. Note that a bias correction is built into the UKMO and MR59 techniques while NESDIS data handling does not require a bias correction. Since the ITPP and NESDIS processing software produce a HIRS/2 channel 8 BT "corrected" for water vapour attenuation, all references to BT in channel 8 will identify a corrected value. Since UKMO processing does not include this correction, it is possible that some degradation of the quality of the cloud mask resulted. Also, since the UKMO HIRS-MSU regression coefficients assume an uncorrected channel 8, local biases have possibly been generated by the regression prior to the debiasing procedure in UKMO and MR59 processing.

The simulated BT in channel 8 is the analysed value of sea surface temperature with climatology as first guess, from the averaged monthly values of the blended SST analysis produced by NMC (*Reynolds*, 1988), which uses in situ and satellite observations (*McClain et al.*, 1985).

Figs. 1a, 1b, and 1c are grey scale (12 levels) images of BT in HIRS/2 channel 8 for passes A, C and D. Pass D and was cut in order to have a measured average minimum distance (MAMD) between clear FOVs (for the definition of MAMD and of the Random Average Minimum Distance, see *Amato et al.*, 1991) significantly different from pass A. Table 1 summarizes some relevant information about the three orbit portions mentioned above.

Pass	scan lines	MAMD	RAMD	Clear fovs %
A	102	7.0	1.42	15
C	72	4.7	1.34	18
D	62	4.4	1.20	25

Table 1: Summary of some relevant information for the three passes which were used in the analyses. Percentage of clear FOVs were computed according to the cloud mask provided by UKMO.

Along with the data above, AVHRR HRPT data and products were also available for passes A and D, provided by CMS (Centre de Meteorologie Spatiale) in Lannion, France. The products used were cloud masks (*Derrien et al.*, 1990) and skin temperatures (*Castagne et al.*, 1986), collocated at HIRS/2 FOVs. These played a significant role in the exercise, allowing us to obtain highly accurate estimates of SST at HIRS/2 spots contaminated by clouds, thus permitting to validate the different cloud-clearing schemes in the most transparent channels. Furthermore, cloud-masks derived from AVHRR allowed us to intercompare and validate the different cloud-detection schemes based solely on TOVS data.

Cloud-detection from AVHRR permits to establish with high accuracy the amount of cloud coverage at every HIRS/2 spot, expressed as a number, C_c, which takes values from 0 to 100, the latter indicating that the HIRS/2 FOV is completely clear. Intermediate values give the fraction of area of the HIRS/2 FOV which is cloud-free (e.g. $C_c = 90$ means that 90% of the HIRS/2 spot area is clear). Based on the HIRS/2 spots completely clear over the sea, 67 FOVs in pass A and 129 in pass B in all, a linear regression relation was derived between the BT in HIRS/2 corrected channel 8 and AVHRR SST (a similar relation was established and used in *Lloyd et al.* 1985). The linear relation, shown in Fig. 2, is:

$$\hat{T}_c(8) = a + b \cdot \hat{T}_s$$

with b =1.045 and a =-13.94 K; the standard error is 0.03 K; $\hat{T}_s$ denotes the skin temperature derived from AVHRR data and $\hat{T}_c(8)$ is the clear-column BT estimate in HIRS/2 channel 8 (corrected).

The regression relation was used in order to estimate the BT in channel 8 at partially cloudy HIRS/2 FOVs, in which AVHRR data still permitted us to obtain skin temperatures ($C_c \geq 5$). These data were then used to validate the cloud-cleared products obtained with the different techniques. Of course, the use of this regression relation is limited to the orbit A and D from which it was derived. The map in Fig. 3 show the locations (black spots) where it was possible to obtain clear-column BTs in HIRS/2 channel 8 from AVHRR data.

Finally, we note that although a more accurate regression relation might be obtained by correlating radiances directly, we had to use limb corrected BTs for compatibility with the available data.

3. RESULTS

3.1 Comparative performance of the cloud detection schemes

The first step in any cloud-clearing scheme is cloud detection. This is a very important task because the quality of the clear-column BT estimates at cloudy FOVs depends critically on the accuracy of cloud detection.

Figs. 4a and 4b show the cloud masks produced by NESDIS for passes A and D, whereas Figs. 5a and 5b show the one produced by UKMO. They can be compared to the C_c =100 maps obtained from AVHRR, shown in Figs. 6a and 6b, and to the C_c = 90 maps, Figs. 7a and 7b, which include all FOVs for which at least 90\% of the area is free of clouds. The comparison clearly shows that the overall number of NESDIS clear FOVs is very small, some of the clear FOVs are quite severely cloud contaminated and that the processing does not identify most of the clear spots. A first quantitative assessment, in terms of cloud percentage, is shown in Tables 2, 3 and 4. Table 2 displays the number, and percentage, of FOVs in the various C_c channels. Table 3 shows the number of NESDIS clear FOVs, flagged 32 in the DSD3 file, in each C_c channel. In Table 4 the same subdivision is done for UKMO cloud mask data.

The effect of assuming clear FOVs can also be evaluated quantitatively by computing, in all FOVs over sea, the differences:

$$\Delta T = \hat{T}(8) - \hat{T}_c(8)$$

between the BT in HIRS/2 channel 8 and the value of the SST, estimated from AVHRR data as explained in the previous section. Fig. 8 shows histograms of such differences in the case of NESDIS. It is possible to see that on average the cloud masks introduce a cold bias of about 2 K. The effect is less serious in the case of UKMO in Fig. 9, where a cold bias of less than 0.5 K is introduced. Comparison of results in Tables 3 and 4 with Figs. 8 and 9 shows that the C_c test is quite selective in pointing out the FOVs in which clouds are present but that the amount of contamination can best be judged in terms of BT difference.

3.2 Comparing clear-column products in channel 4, 7, 13

The channels 4, 7 and 13 were selected as test channels to compare the different clear-column products. HIRS/2 channel 4 peaks at 400 hPa and of the three channels selected is the one less affected by clouds, although it is still sensitive to high clouds. Both channels 7 and 13 look near the surface (900 and 1000 hPa respectively) but have central wavelengths in different spectral ranges (nominally 748 and 2190 cm^{-1}) and are characterised by different principal absorbing constituents (CO_2/H_2O and N_2O respectively).

C_c class	nr. of FOVs	%
0 - 4	3071	64.5
5 - 24	554	11.6
25 - 49	338	7.1
50 - 74	284	6.0
75 - 89	181	3.8
90 - 99	257	5.4
100	75	1.6
	4760	

Table 2a: Number of FOVs belonging to the given C_c class for pass A obtained using AVHRR data.

C_c class	nr. of FOVs	%
0 - 24	2184	65.0
25 - 49	267	7.9
50 - 74	225	6.7
75 - 89	159	4.7
90 - 99	335	10.0
100	190	5.7
	3360	

Table 2b: Number of FOVs belonging to the given C_c class for pass D obtained using AVHRR data.

C_c class	nr. of FOVs	%
0 - 24	14	26.4
25 - 49	12	22.6
50 - 74	7	13.2
75 - 89	9	17.0
90 - 99	11	20.8
100	0	0
	53	

Table 3a: Number of NESDIS clear (code 32) FOVs belonging to each AVHRR C_c class for pass A.

C_c class	nr. of FOVs	%
0 - 24	11	18.0
25 - 49	7	11.5
50 - 74	14	23.0
75 - 89	7	11.5
90 - 89	17	27.8
100	5	8.2
	61	

Table 3b: Number of NESDIS clear FOVs (code 32) belonging to each AVHRR C_c class for pass D.

C_c class	nr. of FOVs	%
0 - 24	105	15.1
25 - 49	106	15.2
50 - 74	129	18.5
75 - 89	116	16.6
90 - 99	186	26.6
100	56	8.0
	698	

Table 4a: Number of UKMO clear FOVs belonging to each AVHRR-C_c class for pass A.

C_c class	nr. of FOVs	%
0 - 24	63	9.7
25 - 49	84	12.9
50 - 74	99	15.3
75 - 89	91	14.0
90 - 99	207	31.9
100	105	16.2
	649	

Table 4b: Number of UKMO clear FOVs belonging to each AVHRR-C_c class for pass D.

Products from MR59, UKMO and NESDIS were compared with the simulated data and the mean difference (bias) standard deviation (std) and root mean square error (rms) are given in Tables 5 to 7 for the three passes under examination. Although the simulated data should be regarded as a simple reference, and NESDIS processing does not involve an internal bias correction, while the two other schemes do, it is again evident that NESDIS products compare least favourably whereas MR59 is almost always characterised by the lowest rms with respect to the simulated data. We recall that the comparison is extended to FOVs for which the following conditions hold:

a. they are located only over sea for passes A and D;

b. cloud cleared BTs from NESDIS are available whose quality is good, according to the filter flag in the DSD3 file; hence both clear (code 32) FOVs and partially cloudy ones (code 16), for which the N^* technique has been applied to derive the clear values, enter the comparison.

channel 4	bias	std	rms
NESDIS	- 0.67	0.41	0.78
MR59	- 0.41	0.34	0.53
UKMO	- 0.70	0.34	0.78
channel 7	bias	std	rms
NESDIS	- 1.76	2.15	2.77
MR59	- 0.35	0.77	0.84
UKMO	- 0.85	0.92	1.25
channel 13	bias	std	rms
NESDIS	- 2.89	2.99	4.16
MR59	- 0.85	0.75	1.14
UKMO	- 1.74	1.56	2.34

Table 5a: Pass A. Comparison of cloud-clearing schemes against simulated data. The table shows mean value (bias), standard deviation (std) and root mean square error (rms) between the clear-column products and simulated data computed for each scheme. The statistics is done on NESDIS clear and N* FOVs (62 data points).

	bias	std	rms
NESDIS ch 4	- 0.60	0.37	0.71
NESDIS ch 7	- 0.95	1.24	1.56
NESDIS ch 13	- 1.75	1.48	2.29

Table 5b: Same as Tab. 5a but the statistics is based only on NESDIS clear FOVs (49 data points).

channel 4	bias	std	rms
NESDIS	- 1.27	0.32	1.31
MR59	- 1.29	0.24	1.31
UKMO	- 1.31	0.22	1.33
channel 7	bias	std	rms
NESDIS	- 0.08	1.63	1.64
MR59	0.24	1.20	1.22
UKMO	0.26	1.39	1.41
channel 13	bias	std	rms
NESDIS	- 0.69	1.88	2.01
MR59	- 0.22	1.49	1.51
UKMO	- 0.35	1.74	1.78

Table 6 : Pass C. Comparison of cloud-clearing schemes against simulated data. The table shows mean value (bias), standard deviation (std) and root mean square error (rms) between the clear-column products and simulated data computed for each scheme. The statistics is done on NESDIS clear and N* FOVs (132 data points).

channel 4	bias	std	rms
NESDIS	- 0.44	0.32	0.55
MR59	- 0.56	0.19	0.59
UKMO	- 0.51	0.20	0.55
channel 7	bias	std	rms
NESDIS	- 0.62	1.48	1.61
MR59	- 0.32	0.64	0.71
UKMO	- 0.31	0.62	0.69
channel 13	bias	std	rms
NESDIS	- 1.70	1.58	2.31
MR59	- 1.19	0.41	1.26
UKMO	- 1.23	0.66	1.40

Table 7: Pass D. Comparison of cloud-clearing schemes against simulated data. The table shows mean value (bias), standard deviation (std) and root mean square error (rms) between the clear-column products and simulated data computed for each scheme. The statistics is done on NESDIS clear and N^* FOVs (59 data points).

	bias	std	rms
NESDIS ch 4	- 0.44	0.32	0.54
NESDIS ch 7	- 0.56	1.30	1.42
NESDIS ch 13	- 1.61	1.35	2.10

Table 7b: Same as Tab. 7a but the statistics is based only on NESDIS clear FOVs (57 data points)

It is possible to eliminate the effects introduced by the N^* technique and the results are shown in Tables 5b and 7b, for passes A and D only. In this case condition b. above is modified to select only the clear NESDIS FOVs. Although both bias and standard deviation are reduced, they still are the highest.

Since MR59 and UKMO are able to produce cleared BTs at every FOVs, the comparison can be performed on a much larger statistical base. Tables 8 to 10 summarize the results. In most of the cases MR59 exhibits the lowest bias and the lowest rms.

channel 4	bias	std	rms
MR59	- 0.56	0.67	0.87
UKMO	- 0.83	0.47	0.96
channel 7	bias	std	rms
MR59	- 0.33	1.32	1.34
UKMO	- 1.02	1.24	1.60
channel 13	bias	std	rms
MR59	- 1.14	1.44	1.84
UKMO	- 2.27	1.48	2.71

Table 8: Pass A. Comparison of cloud-clearing schemes against simulated data. The table shows mean value (bias), standard deviation (std) and root mean square error (rms) between the clear-column products and simulated data computed for each scheme. The statistics are based on 4561 data points.

channel 4	bias	std	rms
MR59	- 1.23	0.28	1.27
UKMO	- 1.29	0.28	1.32
channel 7	bias	std	rms
MR59	0.44	1.86	1.91
UKMO	0.16	2.20	2.21
channel 13	bias	std	rms
MR59	0.066	2.18	2.19
UKMO	0.40	2.70	2.73

Table 9: Pass C. Comparison of cloud-clearing schemes against simulated data. The table shows mean value (bias), standard deviation (std) and root mean square error (rms) between the clear-column products and simulated data computed for each scheme. The statistics are based on 3472 data points.

channel 4	bias	std	rms
MR59	- 0.64	0.26	0.69
UKMO	- 0.54	0.23	0.59
channel 7	bias	std	rms
MR59	- 0.18	0.78	0.80
UKMO	- 0.33	0.74	0.78
channel 13	bias	std	rms
MR59	- 1.30	0.61	1.43
UKMO	- 1.49	1.21	1.92

Table 10: Pass D. Comparison of cloud-clearing schemes against simulated data. The table shows mean value (bias), standard deviation (std) and root mean square error (rms) between the clear-column products and simulated data computed for each scheme. The statistics are based on 2894 data points.

Further comparisons between the above two schemes were performed by computing the linear correlation coefficient between the clear products and the simulations to see how close (in a linear sense) are the two sets whatever the bias may be. Two parallel curves displaced by a fixed amount δ, for example, produce a correlation coefficient of 1 since the two curves have exactly the same shape. Computing the correlation along every scan line give therefore better insight on how closely the dynamics along the scan lines are. This is a very important test, since although the simulated data may be biased, their dynamics along every scan line is expected to be a "good" dynamics, quite representative of the true one, at least within the resolution of the analyses. The results of the comparison show that differences are small for channel 4 while the UKMO scheme starts worsening in channel 7 and finally it becomes practically inconsistent with ECMWF simulated radiances in channel 13, as shown in Fig. 10.

Mesh surfaces of channel 13 for pass A show that the UKMO product (Fig. 11a) has quite serious problems on the boundaries of the field, that could be caused by instability in the 2 dimensional filter triggered by large BT variations at large scan angles. There is also a big hole near the bottom of the mesh surface which is not present in the simulated data (Fig. 11b). Conversely, even though differences are evident, MR59 (Fig. 11c) has quite the same smoothness as the simulated data, since the filter is adaptive and its resolution can be tuned. The UKMO method has not the same flexibility since filtering is performed using only adjacent FOVs, irrespective of the actual spatial resolution of the field to be filtered. As a result, spurious high frequency components have migrated from the borders to the interior of the fields.

3.3 COMPARING CLEAR-COLUMN BTs IN THE WINDOW CHANNEL 8

Based on the regression relation, described in section 2, between AVHRR SST and the BT in HIRS/2 (corrected) channel 8, independent estimates of clear-column BT in channel 8 can be produced at HIRS/2 FOVs over the sea provided some AVHRR pixels are detected cloudfree. These values were compared to the clear-column BTs produced by the different schemes. Table 11 shows the mean value of these differences (bias), the standard deviation (std) and the root mean square error (rms) for passes A and D. The computation is performed on the FOV subset defined by the two conditions:

a. a NESDIS clear value is available (including N^*)

b. the FOV has a value of $C_o \geq 5$.

Orbit A (49)	bias	std	rms
NESDIS	- 2.13	1.56	2.64
MR59	0.20	0.58	0.91
UKMO	- 0.70	1.41	1.58
Orbit D (48)	**bias**	**std**	**rms**
NESDIS	- 1.91	0.64	2.01
MR59	- 0.33	0.60	0.69
UKMO	- 0.19	0.66	0.69

Table 11: Comparing clear-column brightness temperatures in HIRS corrected channel 8 (sst). The table shows mean value (bias), standard deviation (std) and root mean square error (rms) between the clear-column products and SST estimates obtained from AVHRR data. The statistics are based on 49 data points (pass A) and 48 data points (pass D).

Also in this case NESDIS gets by far the worst results, whereas MR59 produces the lowest rms. The low number of points included in the statistics is due to the relatively large number of FOVs defined by condition a. but failing b. above.

A comparison with a larger statistics is possible for MR59 and UKMO since both such schemes produce clear products at every FOV on every scan line. Fig. 12 shows the histogram of the differences of MR59 and UKMO with the regressed values for pass A and D computed at all FOVs for which data derived from AVHRR (with $C_o \geq 5$) were available. It is quite evident that MR59 introduces a smaller bias and has a lower variance. The superiority of MR59 over UKMO is more evident when the FOVs which were flagged clear according to the UKMO cloud-detection processing are eliminated from the statistics; in other words, including only the FOVs where clouds were detected. As it was expected, now the histograms become

broader (Fig. 13), MR59 still introducing a small bias, whereas UKMO produces values clearly cold biased for pass A. Finally, in the case of MR59 products the histograms are nearly symmetric, whereas UKMO products show either long left-tails or complex (bimodal) structures.

The simulated BT in channel 8 can also be compared to the AVHRR SST, in order to assess the bias and variance of the forward model. Fig. 14 shows that the bias in both passes is below 0.5 K, the variance being caused probably by the use of monthly averaged SST data. There is an indication that the simulations for the window channels and for channels having a significant contribution from the lower boundary, as well as any processing requiring an estimate of SST (like any cloud detection algorithm) would greatly benefit from SST data averaged over a shorter period.

3.4 FURTHER DISCUSSION ON NESDIS CLOUD CLEARING PRODUCTS

A better understanding of the underlying reasons for NESDIS' puzzling performance is needed and it can be done for pass A with the help of AVHRR channel 4 imagery. In Fig. 15 the location of some of the FOVs selected by NESDIS as being clear is superimposed to an image constituting the central portion of pass A. The symbols 100 and 50 denote respectively the clear FOVs (code 32) and the FOVs undergoing a cloud clearing based on the N^* technique. There are several points to be raised:

1. A large fraction of the FOVs in which the N^* technique is applied lies on top of a frontal region;
2. the value of C_0 for all the FOVs to the west of the front is below 25%;
3. the selected clear FOVs immediately to the east of the front are not the clearest to be found in the region and are in any case contaminated ($C_0<75$).

To illustrate point 3. Fig. 16 shows the location of the FOVs for which $C_0 \geq 75$. It is not at all evident why locations eastward to the one selected as clear by NESDIS have not been selected altogether, especially for the mid and lower orbit portion in which all 56 FOVs should be scanned by the processing software. North of 58^0 N, corresponding roughly to the upper limit in Figs. 17b and 18 to 20, a selection criterium causes the extreme "boxes" (as defined in NESDIS processing) to be rejected on the grounds that the same region has been scanned during the previous orbit with a smaller scan angle (*Reale*, 91). Figs. 17a and 17b are enhancements to show the radiance gradients eastward of the front; the region appeared dark (warm) in Fig. 16 and is now showing various degrees of cloudiness and clear areas as well.

Finally the difference in BT between NESDIS and simulated data for channel 8, 7 and 6 are shown respectively in Figs. 18 to 20 on top of the usual image. The application of the N^* technique within the frontal region, in areas where there seem to be no portion of the FOV seeing the surface of the sea and clouds appear as thick enough to be totally opaque, cannot produce any reliable estimate of clear column

BT in channel 8 (SST). It was pointed out that the simulated data agree quite well with AVHRR SST estimates (Fig. 14) and therefore there is no evidence supporting that the bulk of the still large differences found westward of the front are due to real features not present in the SST data used to compute the BT. Moreover the higher value of C_0 (percentage of clear AVHRR FOVs in any HIRS FOV) to be found westward of the front is 25.

Similar discussion and results apply to the large differences found over the frontal region in channel 7 and 6: these "clear" radiances could very well be interpreted as a temperature gradient across the front. However the effect of residual cloud contamination eastward and westward of the front are probably mixed with the effects induced by a temperature gradient across the front which could be stronger than the one contained in the ECMWF temperature analysis. In terms of an "extra gradient" to be added to the latter, both UKMO and MR59 processing indicate values ranging around zero (extra gradient) in the south central portion of the area shown in Fig. 20, and values going from -1 in the southwestern portion to -2 in the northwestern part; there is indeed an indication that the temperature analysis used for the BT simulations is underestimating the temperature gradient across the front in the north portion of the area shown in Fig. 20.

4. CONCLUSIONS

In this work a comparison among different cloud-clearing schemes has been performed. Clear-column BTs produced by NESDIS, UKMO and DSF have been compared against ECMWF analyses and against AVHRR products. Three types of comparisons were performed, as described in the introduction.

The comparison clearly shows that the overall number of NESDIS clear FOVs is very small, some of the clear FOVs are quite severely cloud contaminated and that the processing does not identify most of the clear spots. As a consequence the quality of clear-column products is poor.

The UKMO cloud-detection scheme is quite able to provide effective operational cloud-masks also in severe overcast conditions. However their cloud-clearing scheme tends to give cold biased values when applied to the lowest HIRS/2 sounding channels (7 and 13 in our case). It appears that the products of the filter should be extensively controlled. The filter itself may be refined since at the moment does not permit to tune the amount of smoothing and there is evidence of numerical instability.

MR59 products turn out to give the best results. They compare well with both ECMWF forecasts and AVHRR products. The ability of the method to tune the amount of smoothing has proved to be quite useful in producing data with the needed smoothness and consistency. Furthermore, the elimination of the N^*-method seems to limit the cold bias effect. Although the superiority of MR59 over UKMO is sometimes not significant (e.g., channel 4), the former appears to be the most flexible technique among the ones that were analysed in this study. A further point is that MR59 does not mix cloudy and clear radiance measurements when producing the filtered clear BT fields, hence in principle information on cloud amount is retrievable as a weighted difference between the measurements and the filtered data, although this implication has yet to be explored.

A limitation to the present study is the amount of data that has been analysed; two or three orbit portions do not permit to draw many firm conclusions. However there are no grounds to expect that problems arisen in the data examined would not show in different parts of the globe. Moreover the quality of meteorological information inserted in an analysis scheme, coming from satellite or any other data source, needs to be locally good, not only globally. Indeed global statistics may even lead to results that, although numerically correct, do hide local and significant problems.

Acknowledgements

Beside the authors, the present work would not have been possible without the active participation of a number of individuals and institutions. We wish to thank Phil Watts and Paul Dibben of the UK Met. Office for the full range of support given prior and during the comparison exercise as well as for the very valuable discussions on the final results. We also acknowledge the active support by Guy Rochard of C.M.S., Lannion, that allowed us to make use of AVHRR data which showed extremely valuable, and the interesting discussions with a number of researchers in NESDIS which were useful in getting a better understanding of the results.

Carmine Serio and Valerio Tramutoli were supported by C.N.R. Progetto Strategico Clima Ambiente e Territorio nel Mezzogiorno Grants n. 88.3582 and 89.2015.

References

Andersson, E., A. Hollingsworth, G. Kelly, P. Lönnberg, J. Pailleux and Z. Zhang, 1991: Global Observing System Experiments on Operational Statistical Retrievals of Satellite Sounding Data. Mon.Wea.Rev., 119, 8, 1851-1864.

Amato, U., V. Cuomo, G. Pavese, R. Rizzi, C. Serio and V. Tramutoli, 1991: Cloud-clearing with Radial Basis Functions. Proceedings of the 6th International TOVS Conference, Airlie, VA, USA (CIMSS, Madison).

Andretta, A., M.M. Bonzagni, V. Cuomo, R. Rizzi and C. Serio, 1990: A three-step Cloud Clearing Procedure for Infrared Sounder Measurements. International Journal of Remote Sensing, Vol. 11, 8 1349-1368.

Castagne N., P. Le Borgne, J. Le Vourch and J.P. Olry, 1986: Operational Measurements of Sea Surface Temperatures at CMS Lannion from NOAA-7 AVHRR Data. International Journal of Remote Sensing, Vol. 7, 8 953-984.

Derrien M., H. Legleau, L. Lavanant, L. Harang, A. Noyalet, D. Pochic, 1990: Detection Automatique des Nuages avec l'Imageur AVHRR du Satellite defilant NOAA-11. EERM n. 4.

Eyre, J.R., 1989: Inversion of Cloudy Satellite Soundings Radiances by Nonlinear Optimal Estimation: Application to TOVS Data. Quarterly Journal of the Royal Meteorological Society, 115, 1027-1037.

Eyre, J.R., 1991: A Fast Radiative Transfer Model for Satellite Sounding Systems. ECMWF Tech.Memo. No. 176.

Eyre, J.R. and P.D. Watts, 1987: A Sequential Estimation Approach to Cloud-Clearing for Satellite Temperature Sounding. Quarterly Journal of the Royal Meteorological Society, 113, 1349-1376.

Huang, H.-L A. and W.L. Smith, 1986: An Extension of the Simultaneous TOVS Retrieval Algorithm with the inclusion of cloud. Tech.Proc. 3rd. Int. TOVS Study Conference, Madison Wisconsin 13-19 August 1986. CIMSS Report, University of Wisconsin.

Kelly, G. and J. Pailleux, 1988: Use of Satellite Vertical Sounder Data in the ECMWF Analysis System. ECMWF Tech.Memo. 143.

Kelly, G., E. Andersson, A. Hollingsworth, P. Lönnberg, J. Pailleux and Z. Zhang, 1991: Quality Control of Operational Physical Retrievals of Satellite Sounding Data. Mon.Wea.Rev., 119, 8, 1866-1880.

Lloyd, P.E., J.J. Barnett and J.R. Eyre, 1985: Investigations of AVHRR data to improve TOVS Retrievals. Tech.Proc. 2nd Int. TOVS Study Conference, Igls 18-22 Feb. 1985, CIMSS, University of Wisconsin.

McClain, E.P., W.G. Pichel and C. Walton, 1985: Comparative Performance of AVHRR-based Multichannel Sea Surface Temperatures. J.Geophys.Res., 90, 11587-11601.

McMillin, L.M. and C. Dean, 1982: Evaluation of a New Operational Technique for Producing Clear Radiances. Journal of Applied Meteorology, 21, 1005-1014.

McNally, A.P., 1990: Satellite Sounding of Tropospheric Temperature and Humidity. D.Phil. Thesis, University of Oxford.

Reale, A.L., D.G. Gray, M.W. Chalfant, A. Swaroop, A. Nappi, 1986: Higher Resolution Operational Satellite Retrievals. Proc. Second Conference on Satellite Meteorology-Remote Sensing and Applications, Am.Met.Soc.

Reale, A.L., 1991, private communication.

Reynolds, R.W., 1988: A Real--Time Global Sea Surface Temperature Analysis. J.of Climate, 1, 75-86.

Smith, W.L., 1968: An Improved Method for Calculating Tropospheric Temperature and Moisture from Satellite Radiometer Measurements. Mon.Wea.Rev., 96, 387-396.

Susskind, J., J. Rosenfield, D. Reuter, and M.T. Chahine, 1984: Remote Sensing of Weather and Climate Parameters from HIRS-2/MSU on TIROS-N. J.Geophys.Res., 89, 4677-4697.

Uppala, S., A. Hollingsworth, S. Tibaldi and P. Källberg, 1984: Results from two Recent Observing System Experiments at ECMWF. Proc. of the ECMWF Seminar/Workshop Data Assimilation Systems and Observing System Experiments with Particular Emphasis on FGGE, vol. 1.

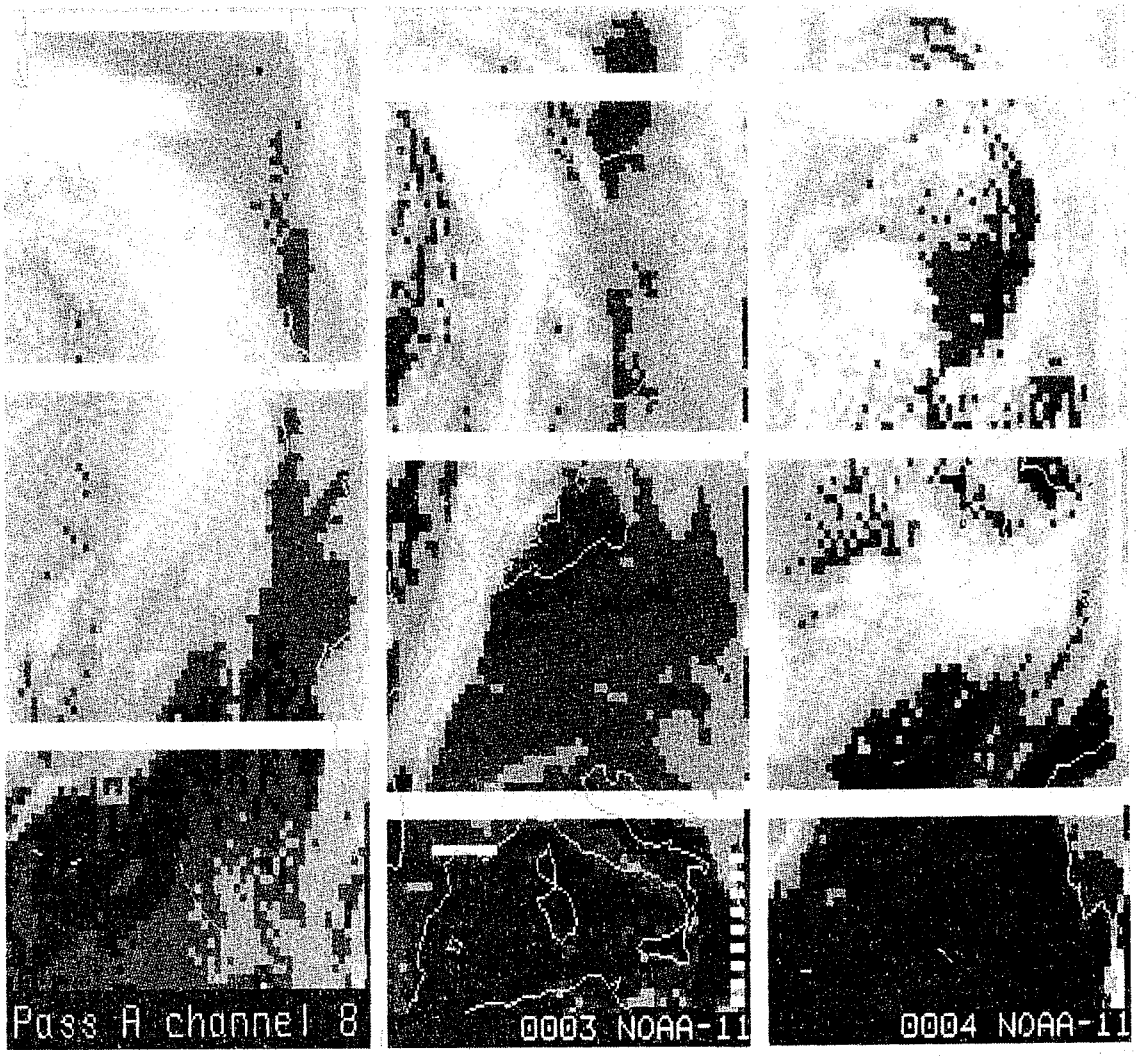

Fig. 1 HIRS/2 channel 8 BT: a)- for pass A; b)- pass C; c)- pass D.

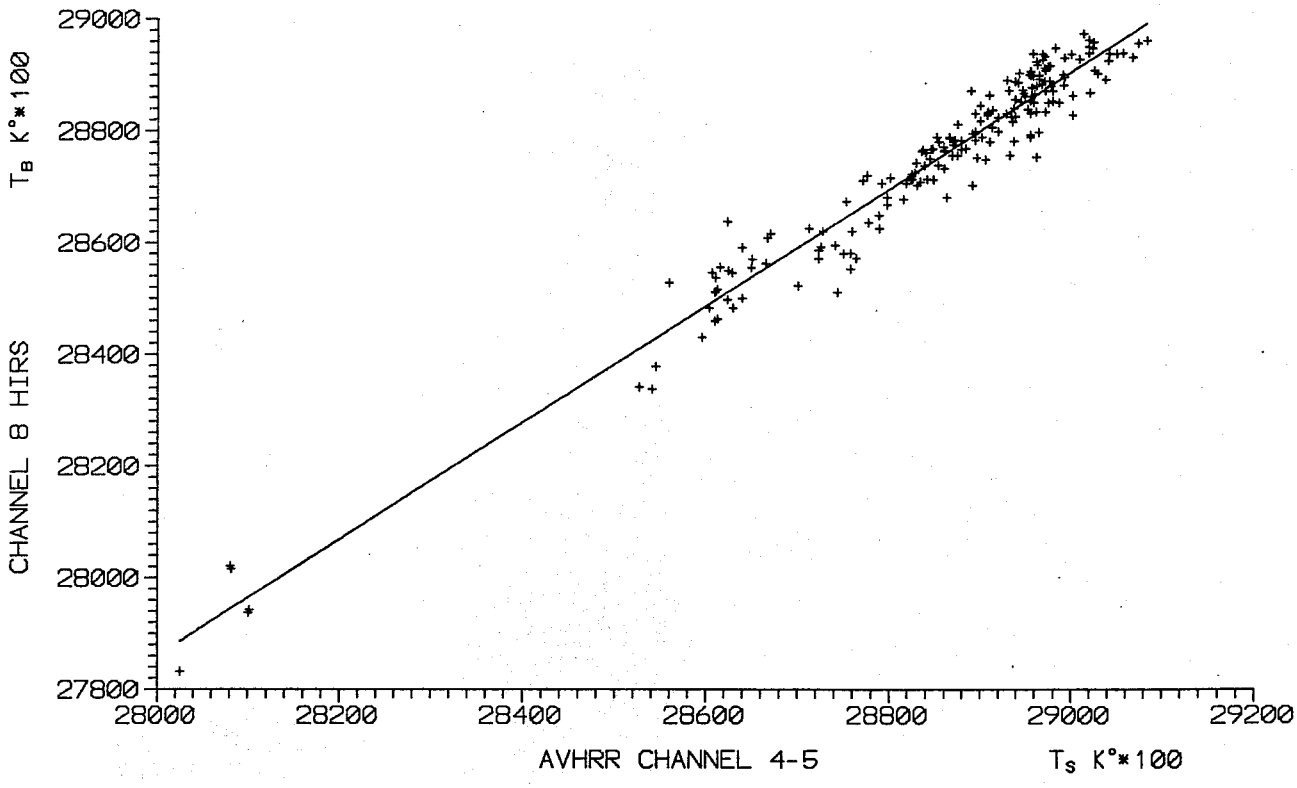

Fig. 2 **Plot of HIRS/2 channel 8 BT against skin temperature. The plot include only clear FOVs from both pass A and D. Clear FOVs were identified according to the cloud-mask derived from AVHRR data. Skin temperature estimates were derived from AVHRR data, too. The linear best-fit is also shown in figure.**

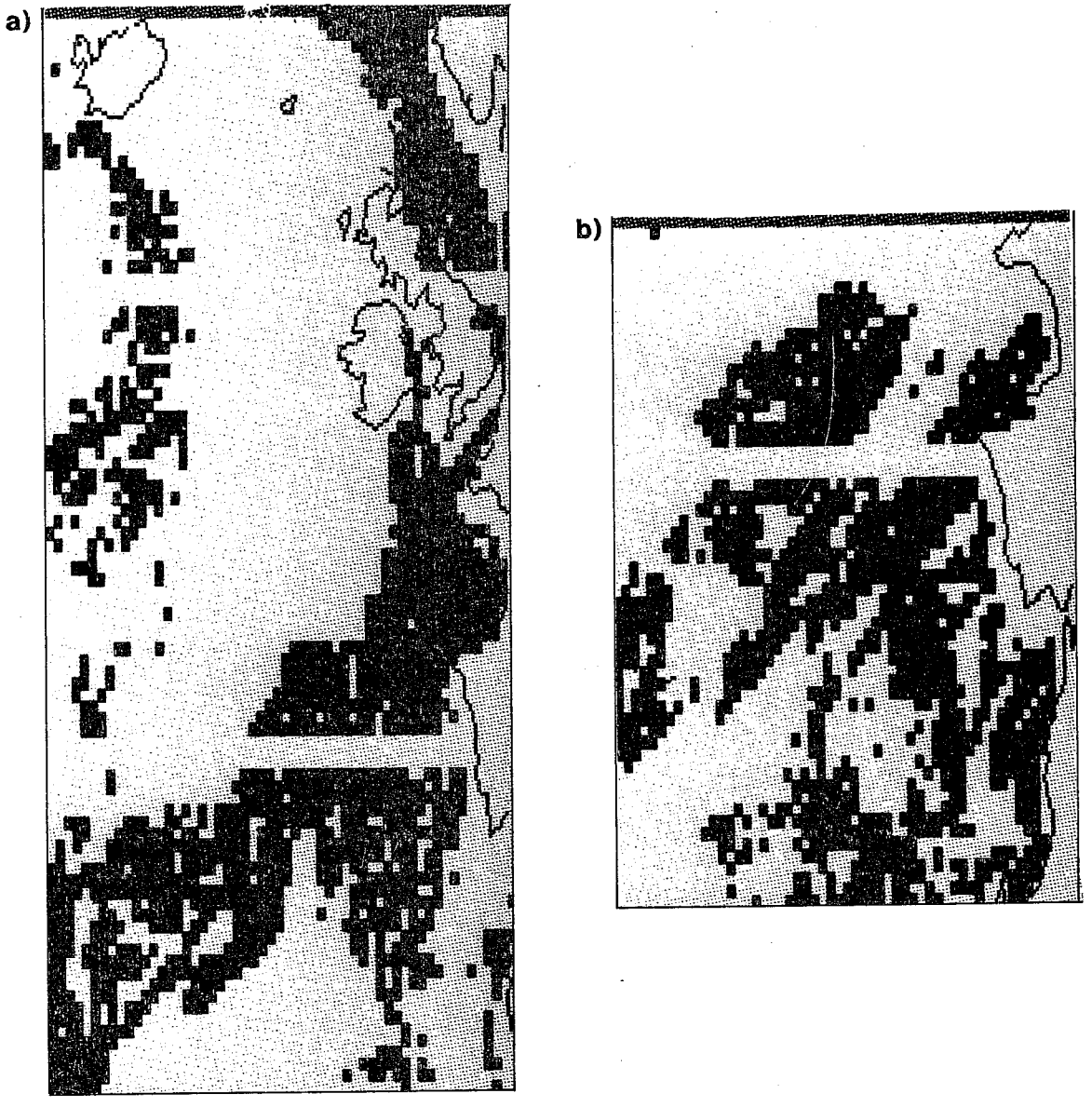

Fig. 3 The figure shows the FOVs (dark grey) for which it was possible to estimate clear-column BT in HIRS/2 channel 8 from AVHRR data. a)- pass A; b)- pass D.

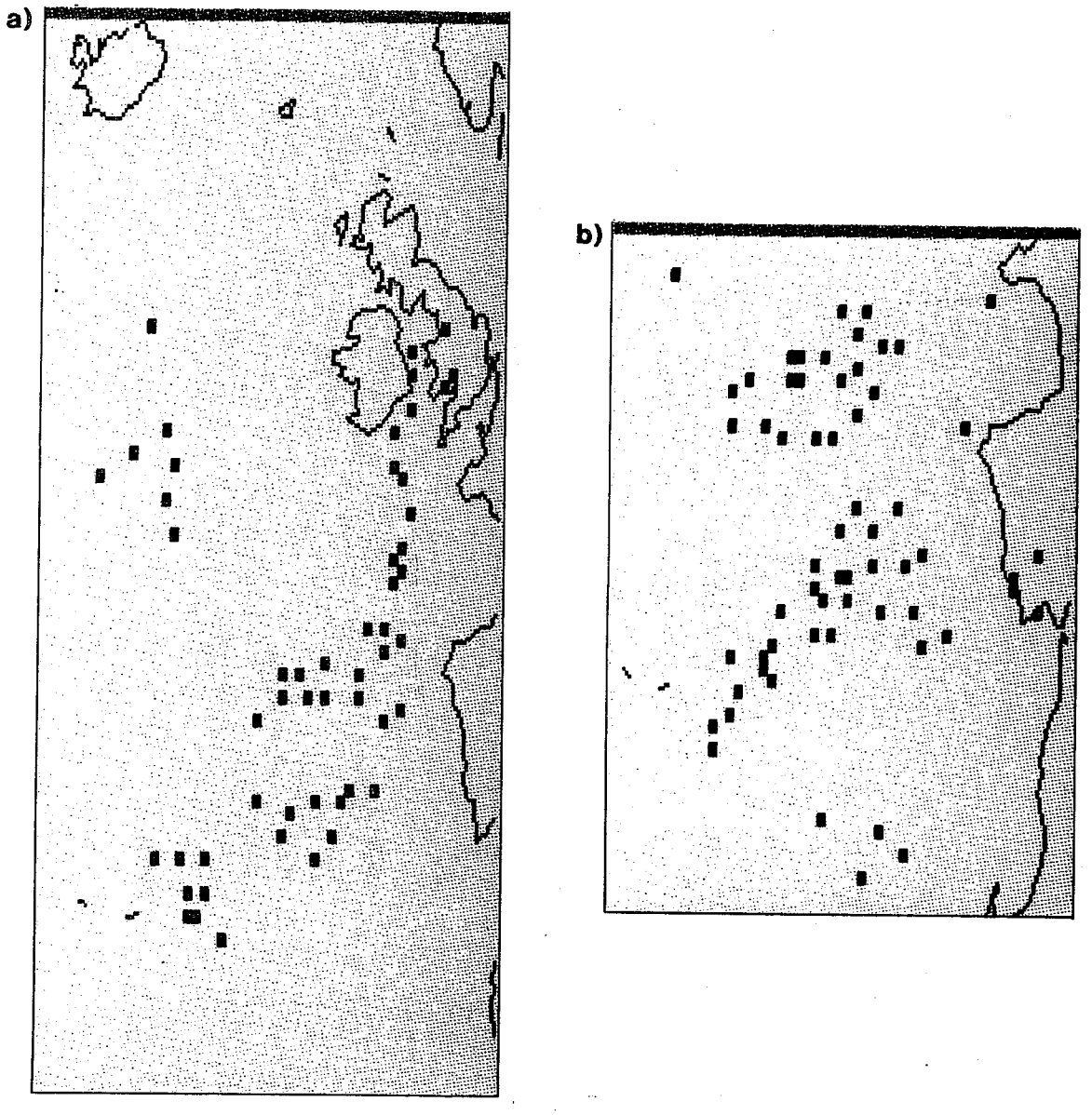

Fig. 4 Cloud-mask produced by NESDIS. Light grey indicates cloudy FOVs, whereas dark grey clear FOVs. a)- Pass A; b)- Pass D.

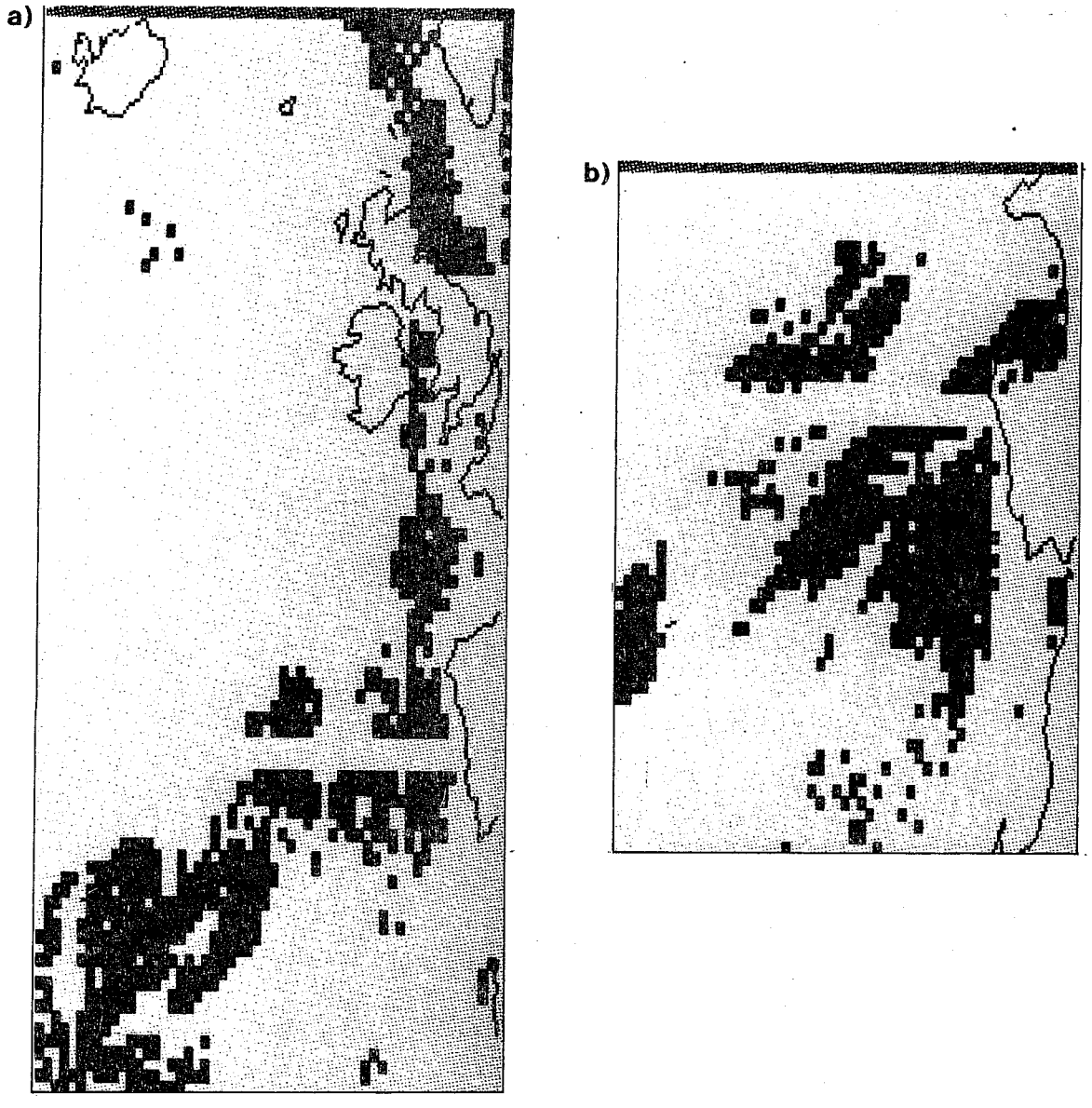

Fig. 5 Cloud-mask produced by UKMO. Light grey indicates cloudy FOVs, whereas dark grey clear FOVs. a)- Pass A; b)- Pass D.

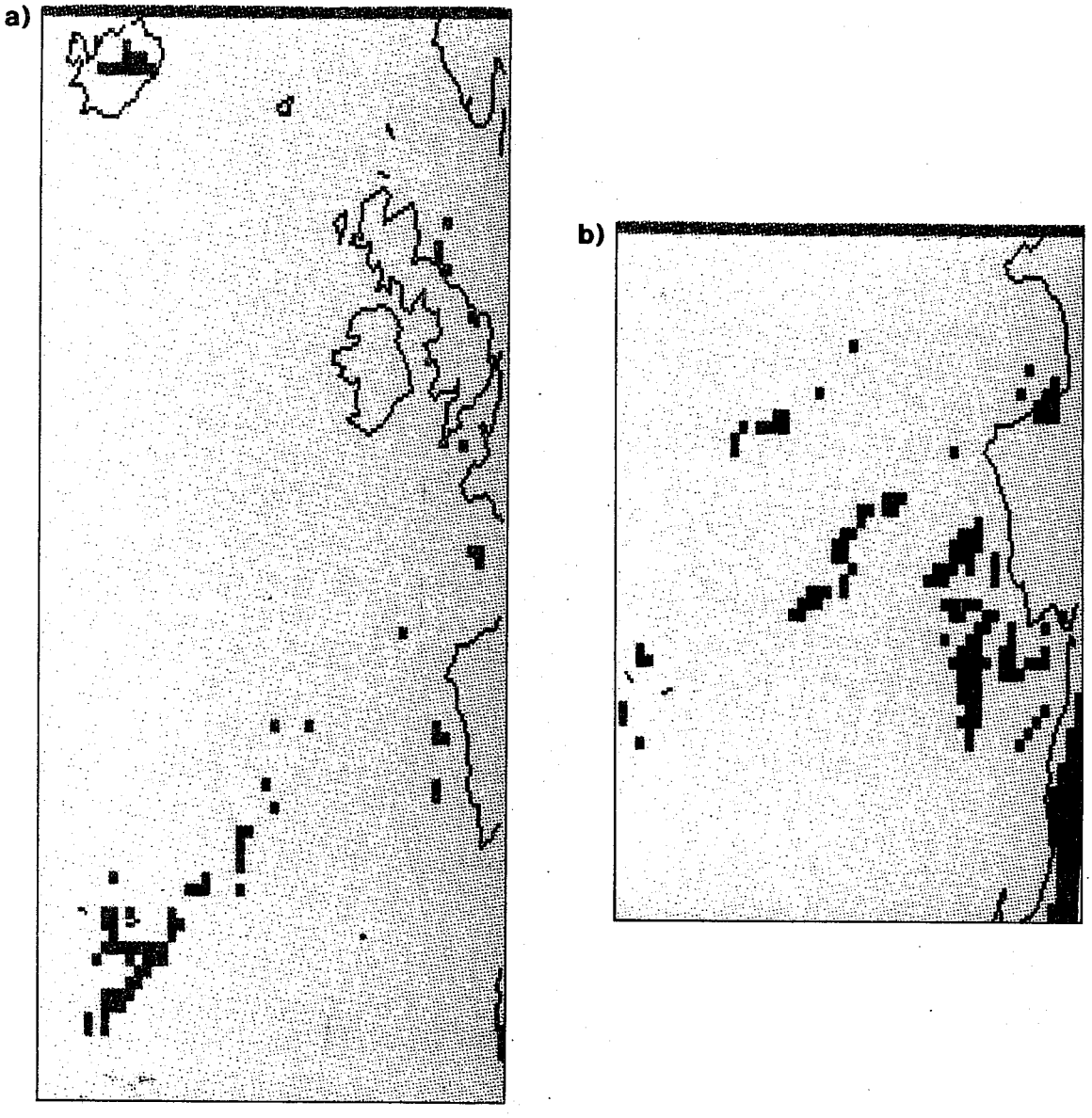

Fig. 6 Cloud-mask derived from AVHRR data. Light grey indicates cloudy FOVs, whereas dark grey clear FOVs. The cloud-masks include FOVs totally clear only. a)- Pass A; b)- Pass D.

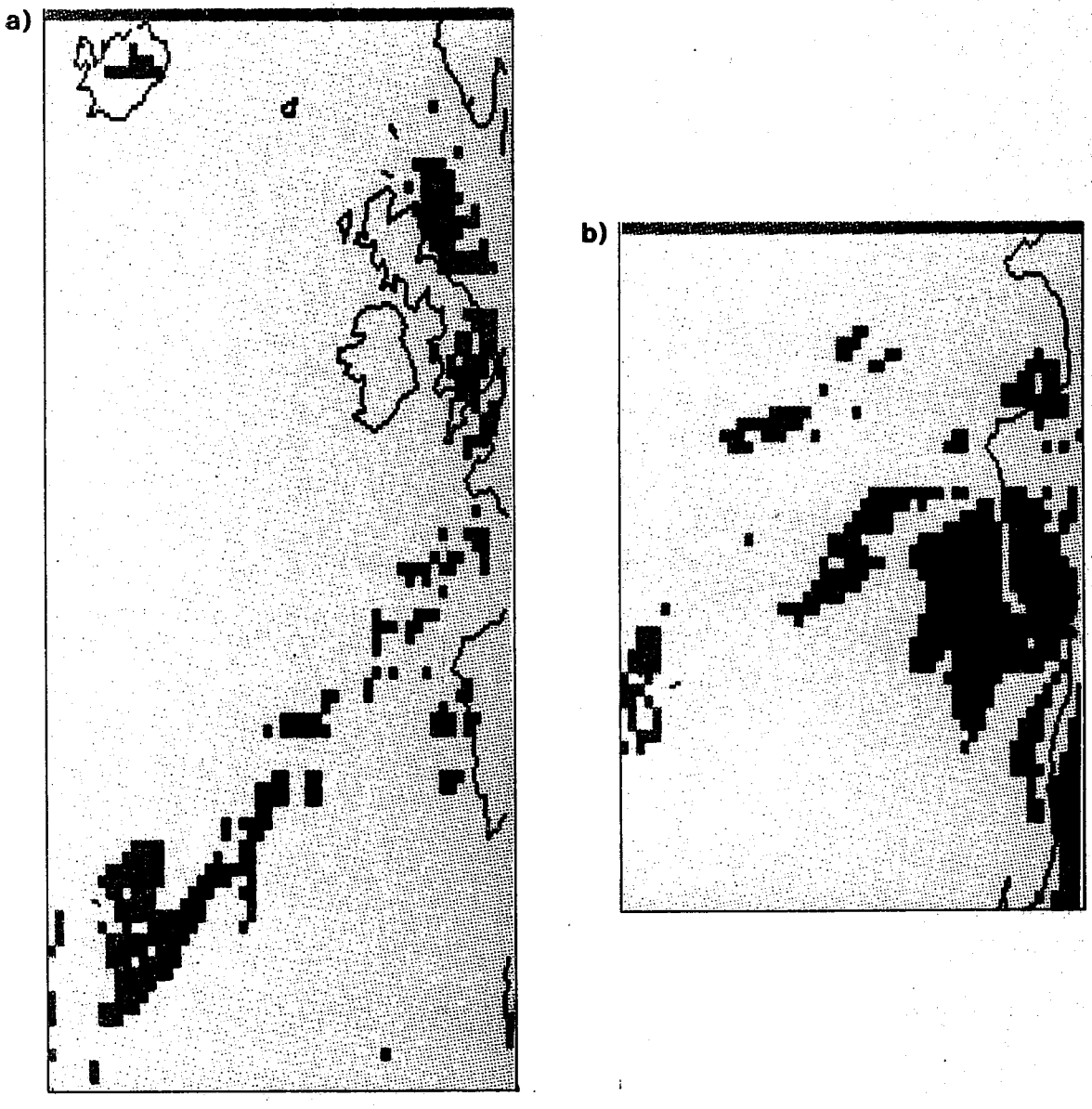

Fig. 7 **Cloud-mask derived from AVHRR data. Light grey indicates cloudy FOVs, whereas dark grey clear FOVs. The cloud-masks include all the FOVs with a clear area more than 90%. a)- Pass A; b)- Pass D.**

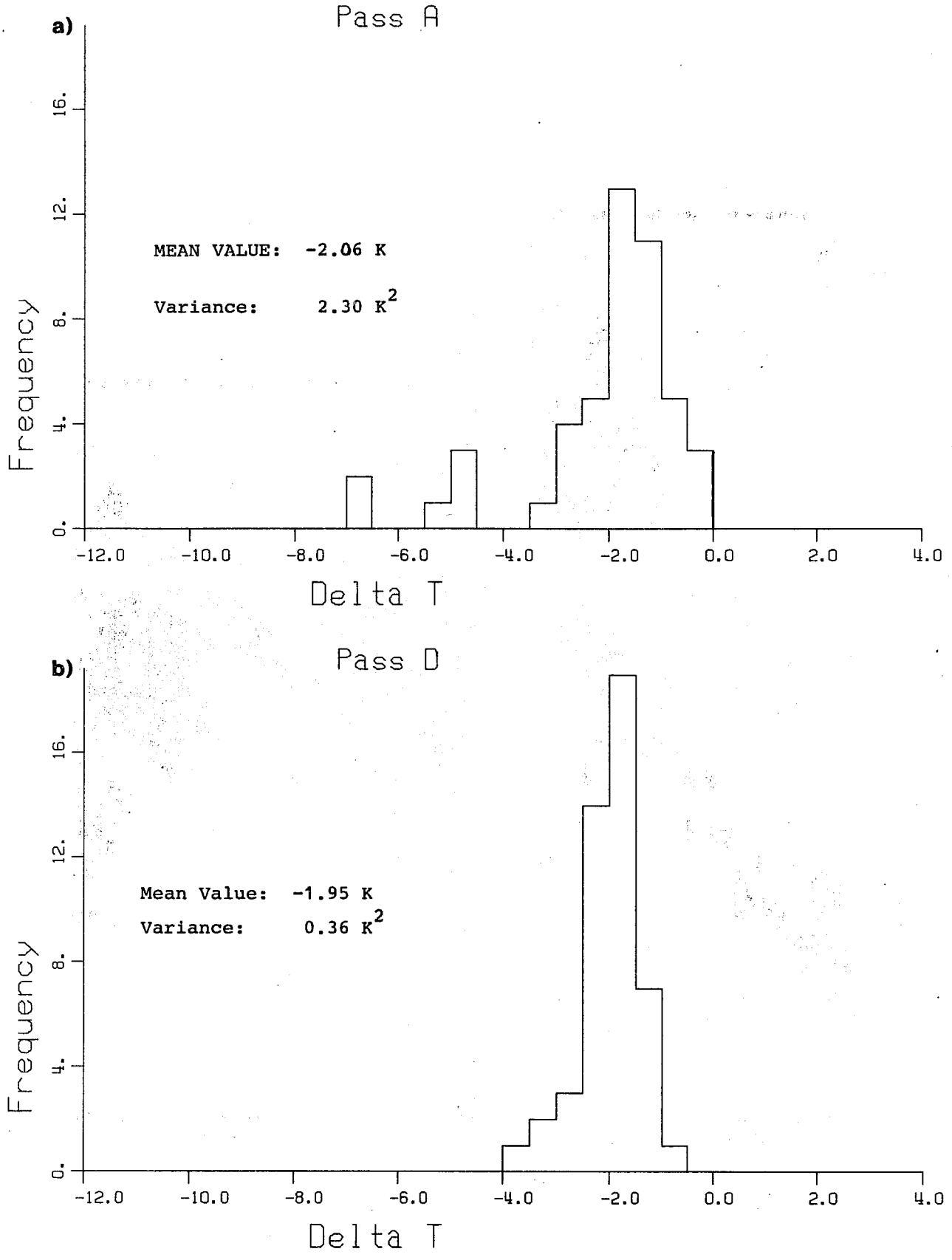

Fig. 8 Validating the cloud-masks produced by NESDIS. Histogram of the differences $\Delta T = \hat{T}(8) - \hat{T}_c(8)$ computed at clear FOVs according to the cloud-mask produced by NESDIS. $\hat{T}(8)$ is the BT from NESDIS at clear FOVs, $\hat{T}_c(8)$ gives an independent estimate at the same location obtained from AVHRR data. a)- Pass A; b)- Pass D.

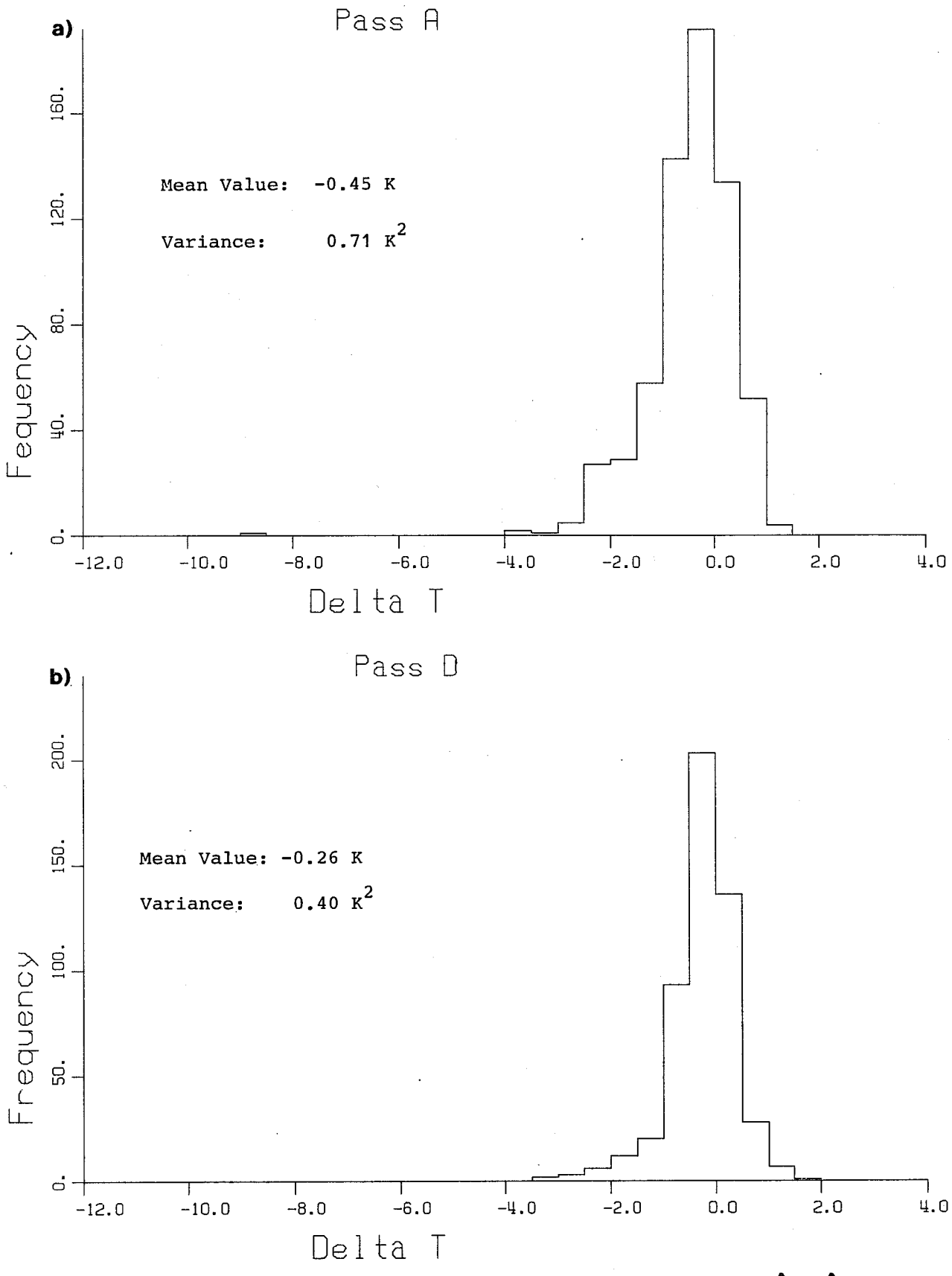

Fig. 9 Validating the cloud-masks produced by UKMO. Histogram of the differences $\Delta T = \hat{T}(8) - \hat{T}_c(8)$ computed at clear FOVs according to the cloud-mask produced by UKMO. $\hat{T}(8)$ is the BT from UKMO at clear FOVs, $\hat{T}_c(8)$ gives an independent estimate at the same location obtained from AVHRR data. a)- Pass A; b)- Pass D.

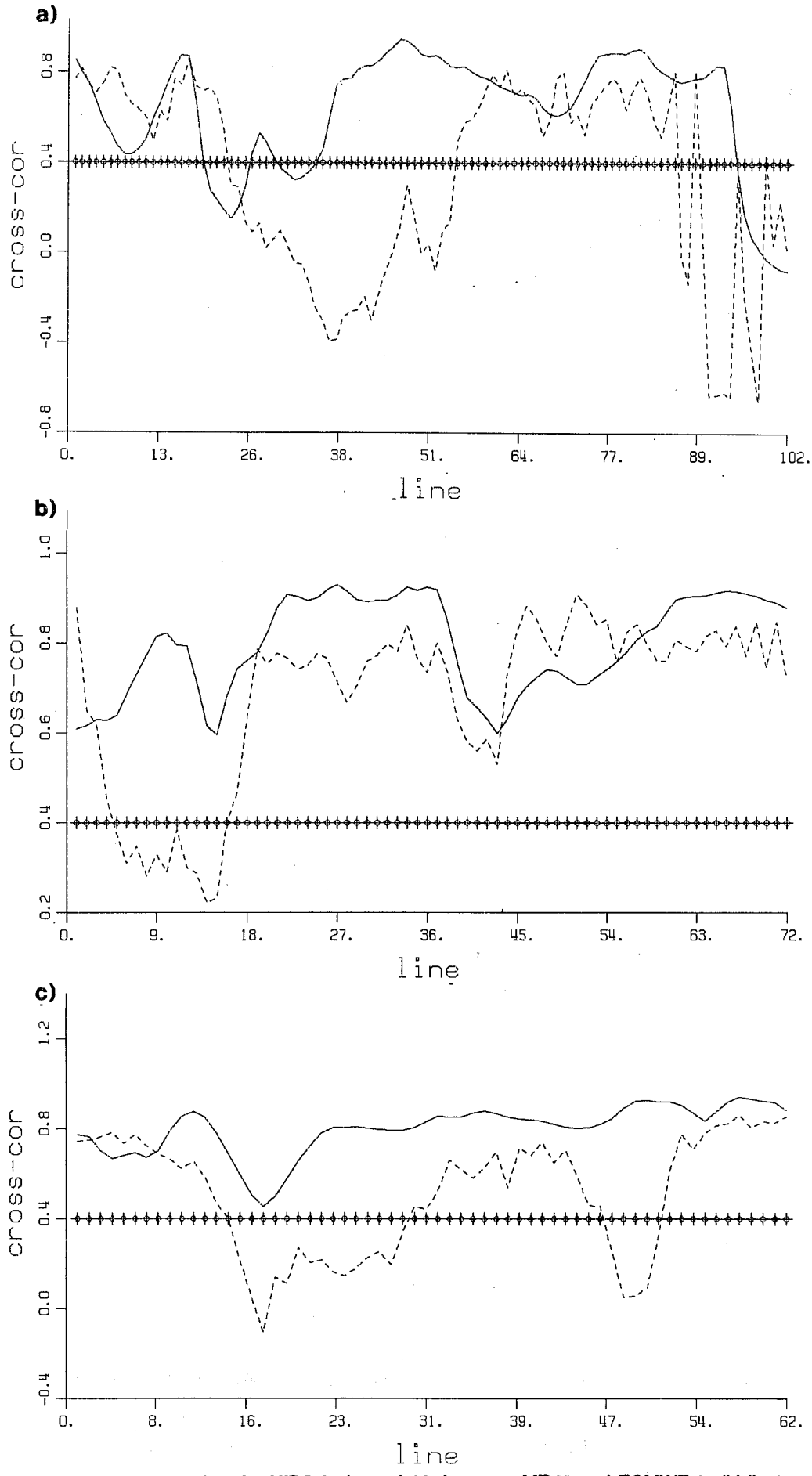

Fig. 10 Plots of correlation coefficient for HIRS/2 channel 13, between MR59 and ECMWF (solid line) and between UKMO and ECMWF (dashed lines). a)- Pass A; b)- pass C; c)- pass D. The horizontal line at $\rho = .4$ (circle with plus) roughly separate the zone of high correlation from the one of low correlation.

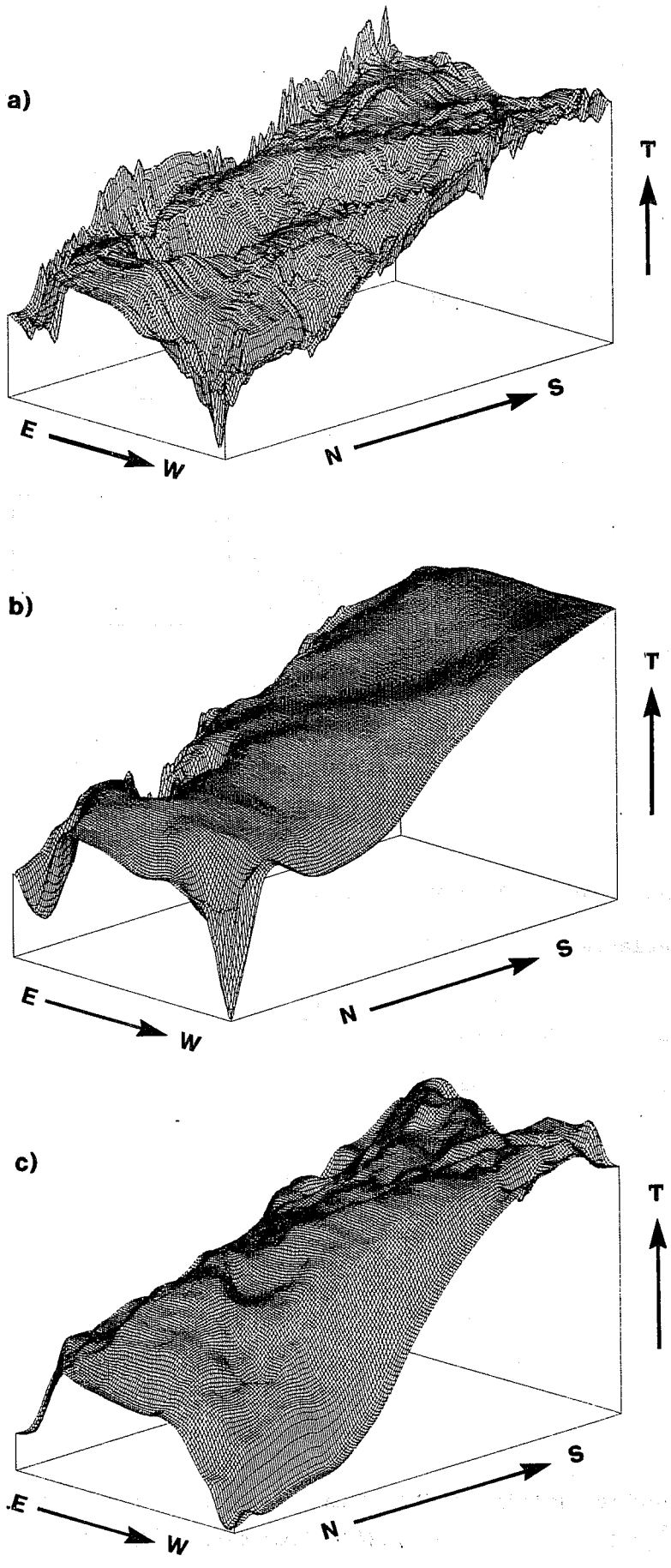

Fig. 11 Overpass A. Mesh surfaces of clear-column BT in HIRS/2 channel 13: a)- UKMO; b)- ECMWF; c)- MR59.

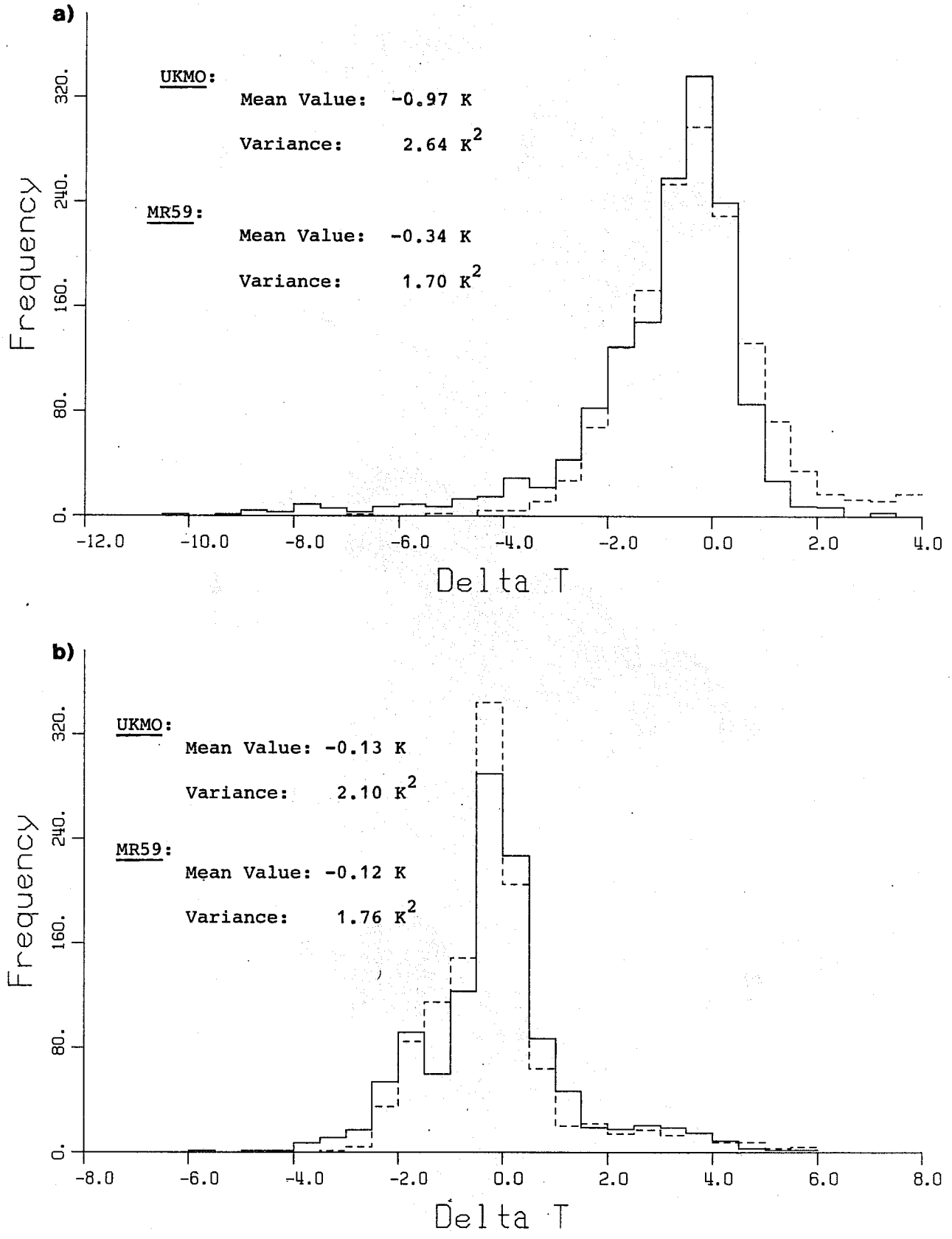

Fig. 12 Validating clear-column products in HIRS/2 channel 8. Figure shows the histogram of the differences $\Delta T = \hat{T}(8) - \hat{T}_c(8)$ for UKMO (solid line) and MR59 (dashed line). $\hat{T}(8)$ is the clear-column BT from either UKMO or MR59, $T_c(8)$ gives an independent estimate at the same location obtained from AVHRR data. The comparison covers all the FOVs for which $\hat{T}_c(8)$ was available; a)- pass A; b)- pass D.

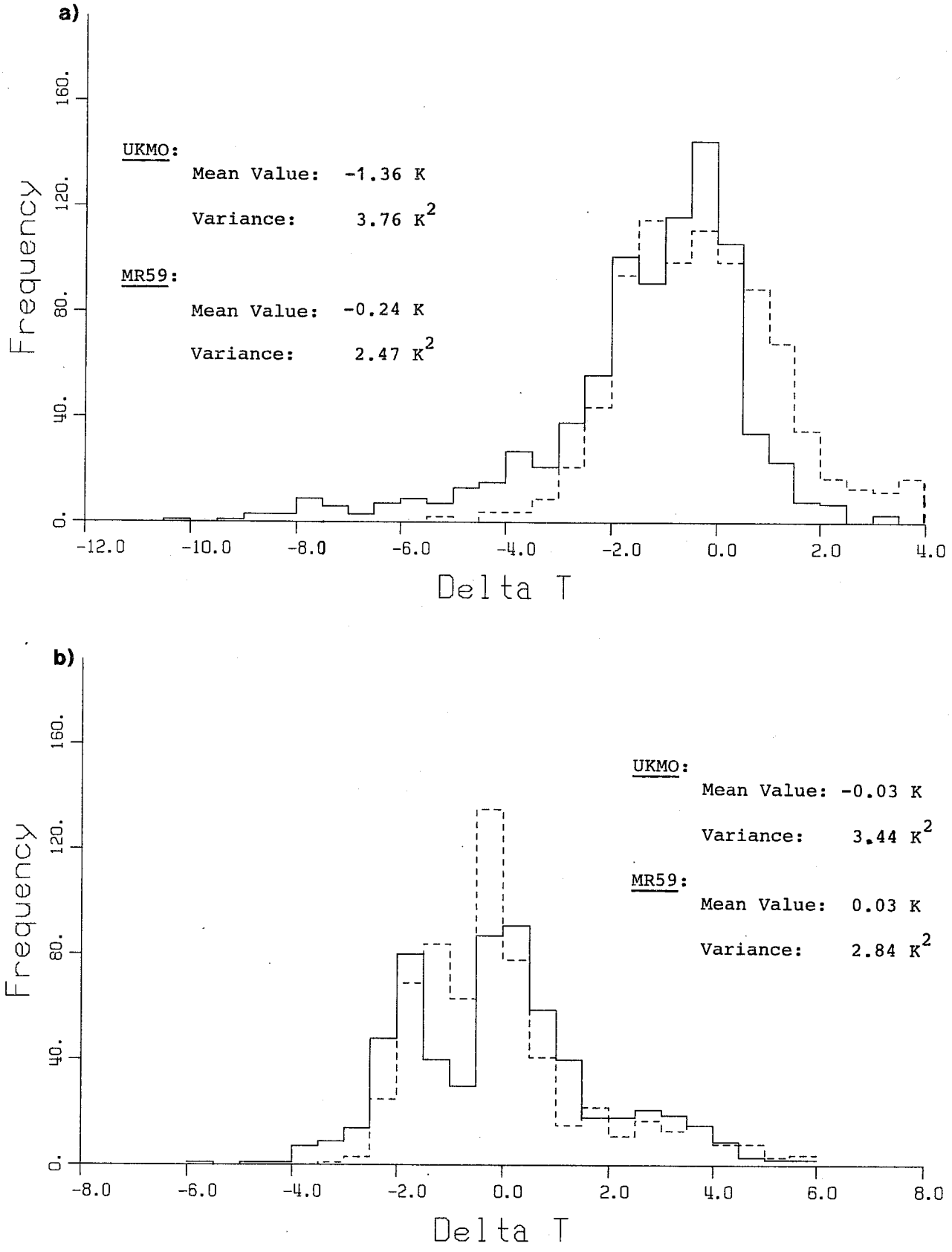

Fig. 13 As Fig. 12 but now the comparison covers only FOVs which were detected cloudy by the preliminary cloud-detection processing; a)- pass A; b)- pass D.

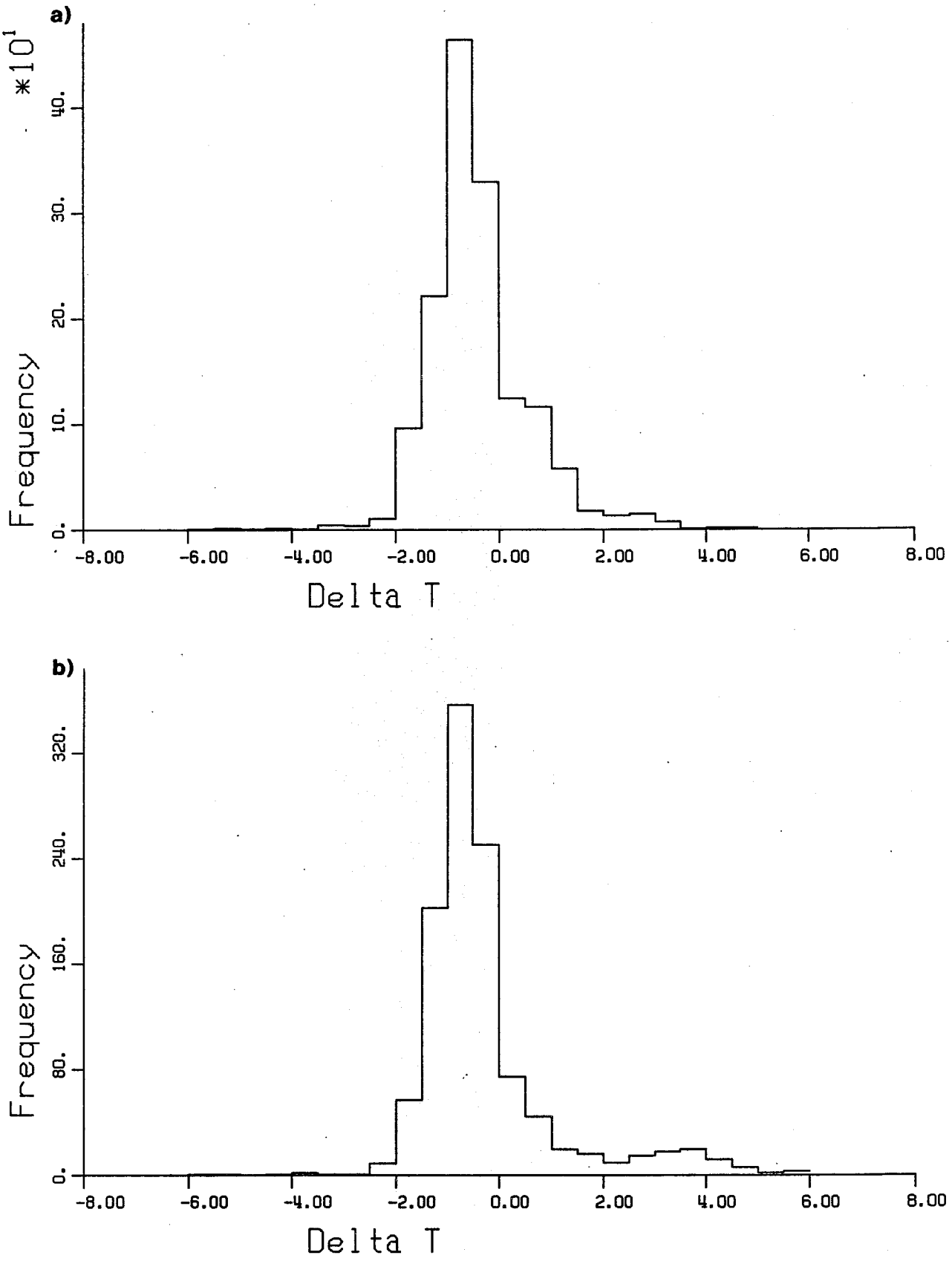

Fig. 14 Histograms of the difference between simulated BT in HIRS channel 8 and SST from AVHRR: a)- pass A; b) pass D.

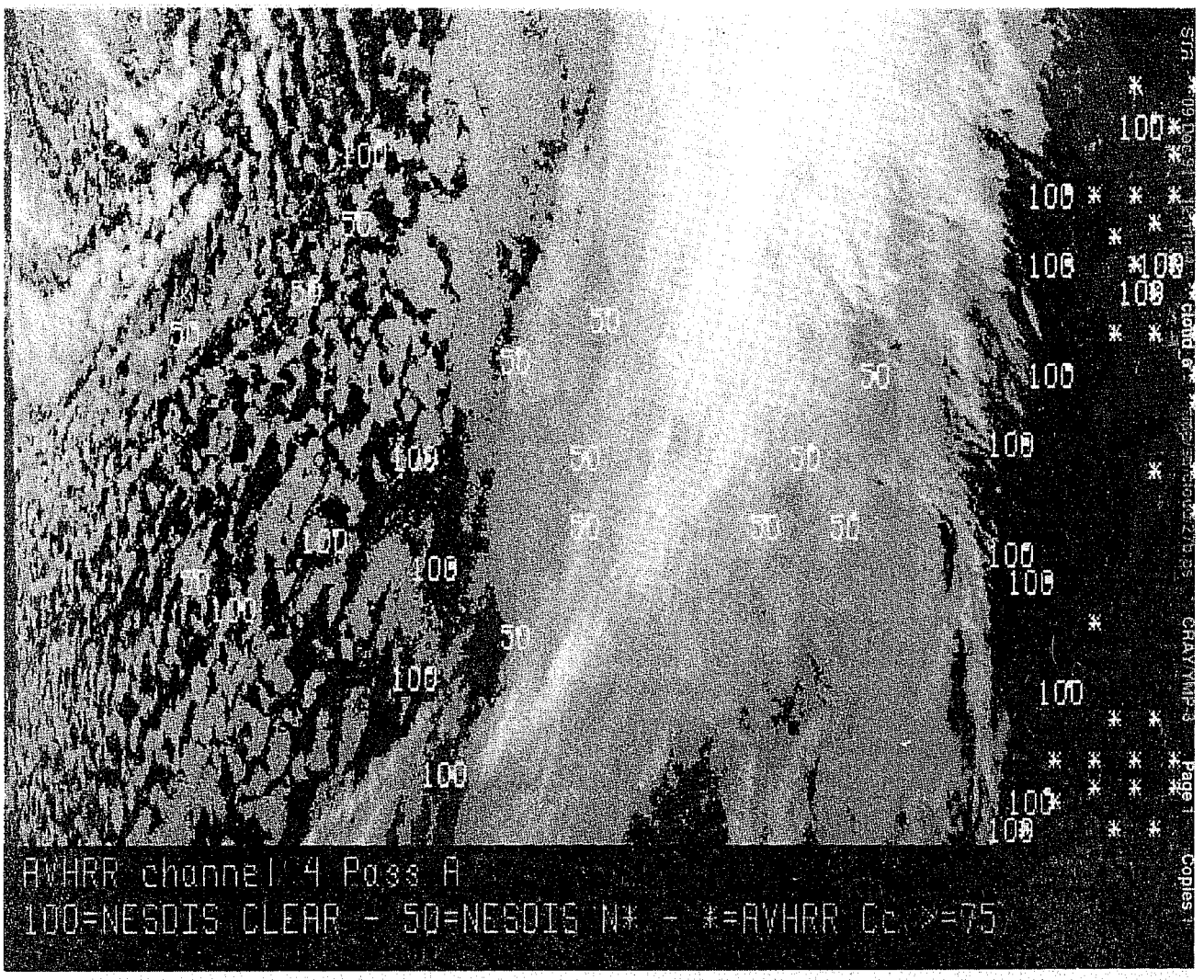

Fig. 15 Location of NESDIS clear (denoted by 100), NESDIS N^* FOVs (marked by 50) and FOVS with $C_c \geq 75$ (marked *) for the mid portion of pass A on top of AVHRR channel 4.

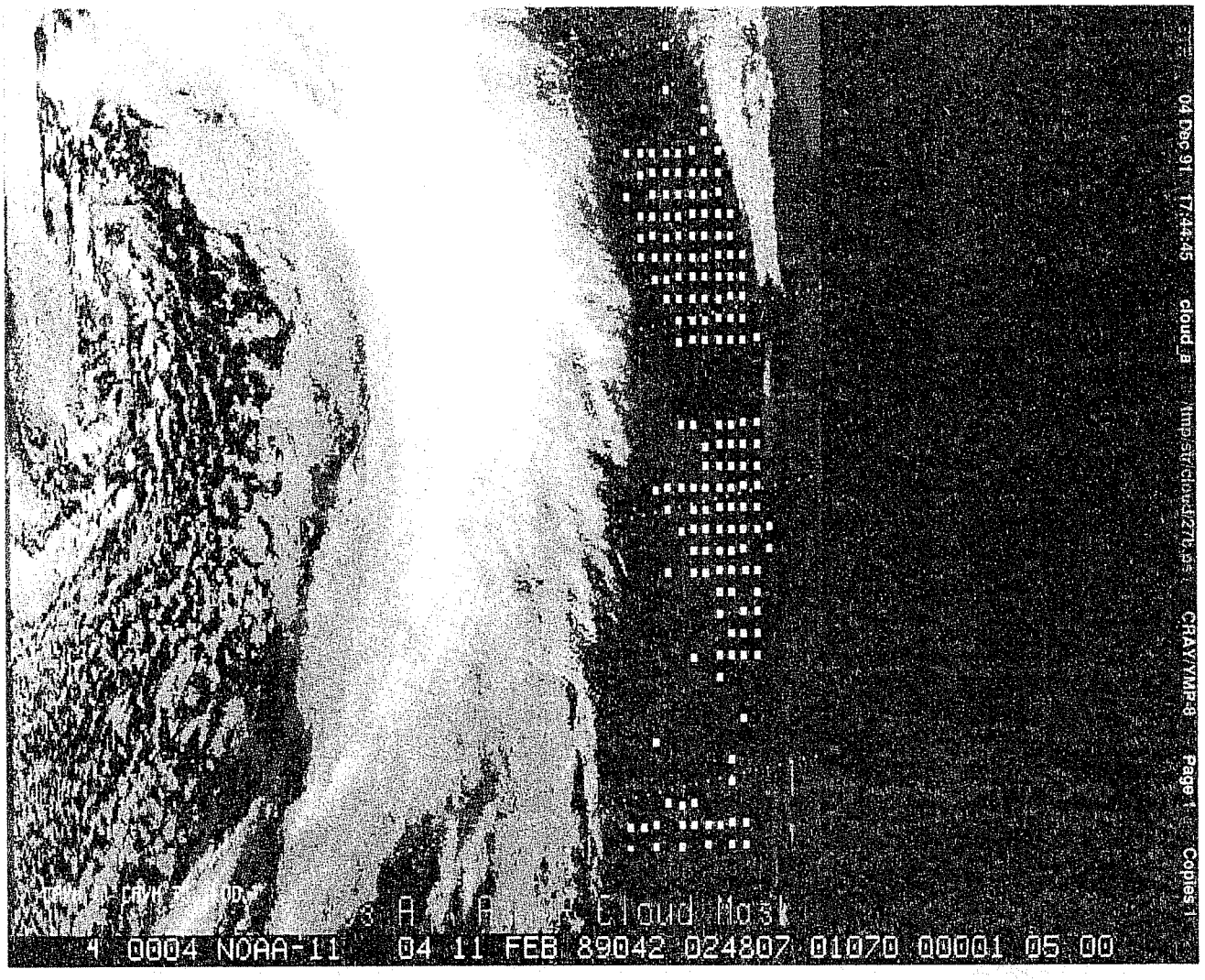

Fig. 16 Location of FOVs for which $C_c \geq 75$ on top of AVHRR channel 4.

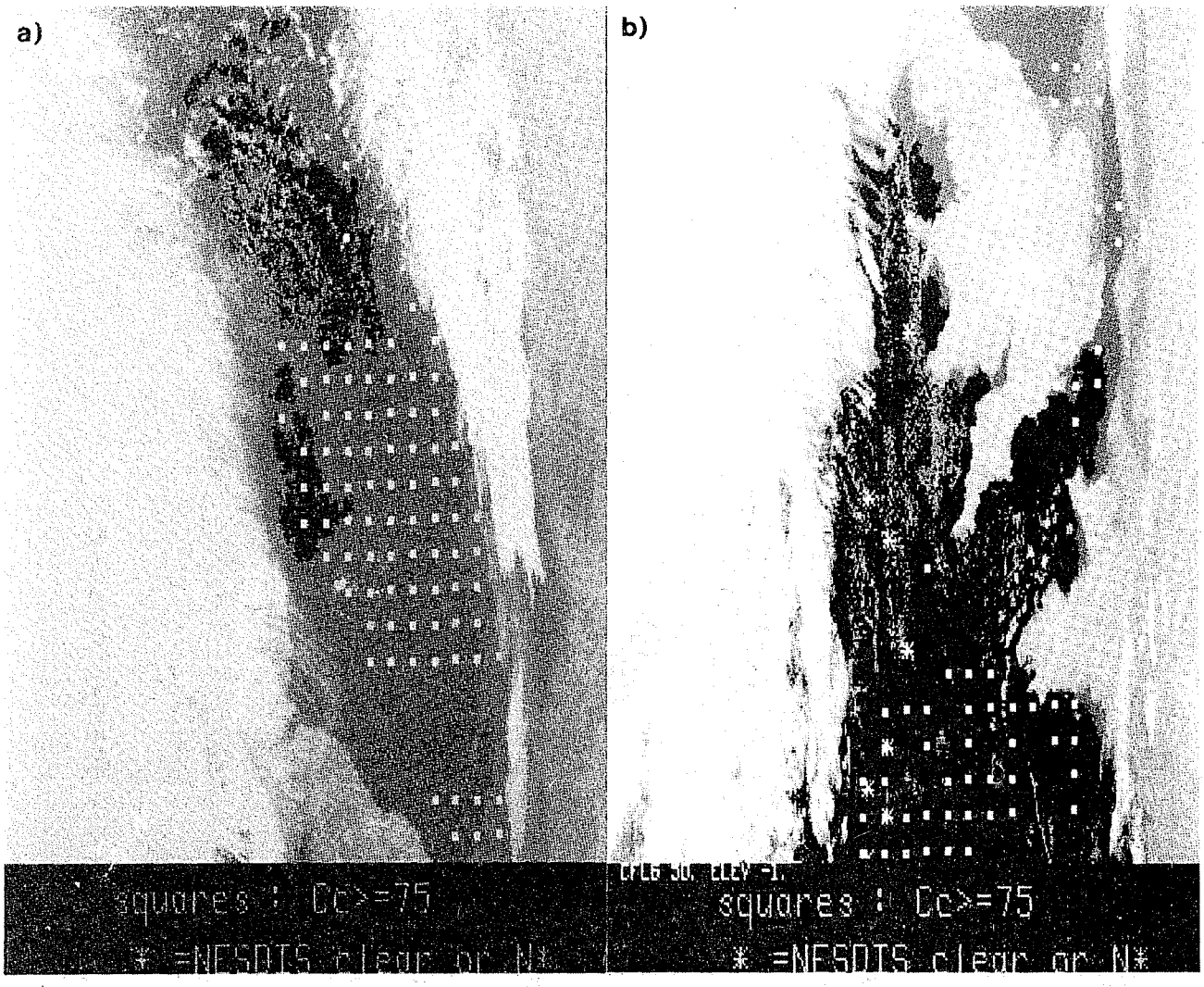

Fig. 17 Enhanced view of AVHRR channel 4 (pass A) to show location of FOVs for which $C_c \geq 75$ (bright squares) and NESDIS FOVs (*) over the sea; a)- northern portion of pass A; b)- southern portion of pass A.

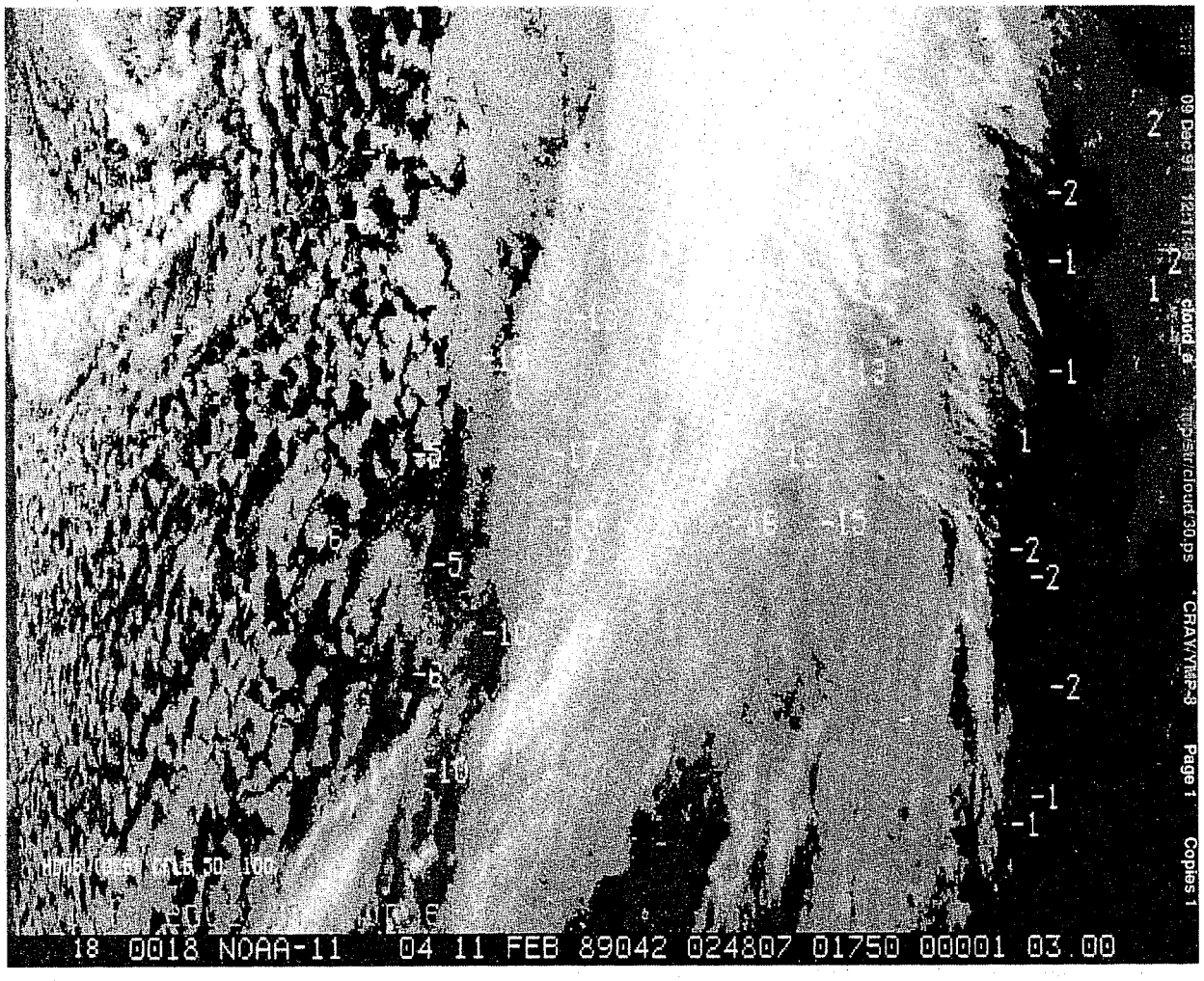

Fig. 18 Difference between NESDIS and simulated BT for HIRS/2 channel 8 (corrected) superimposed on AVHRR channel 4.

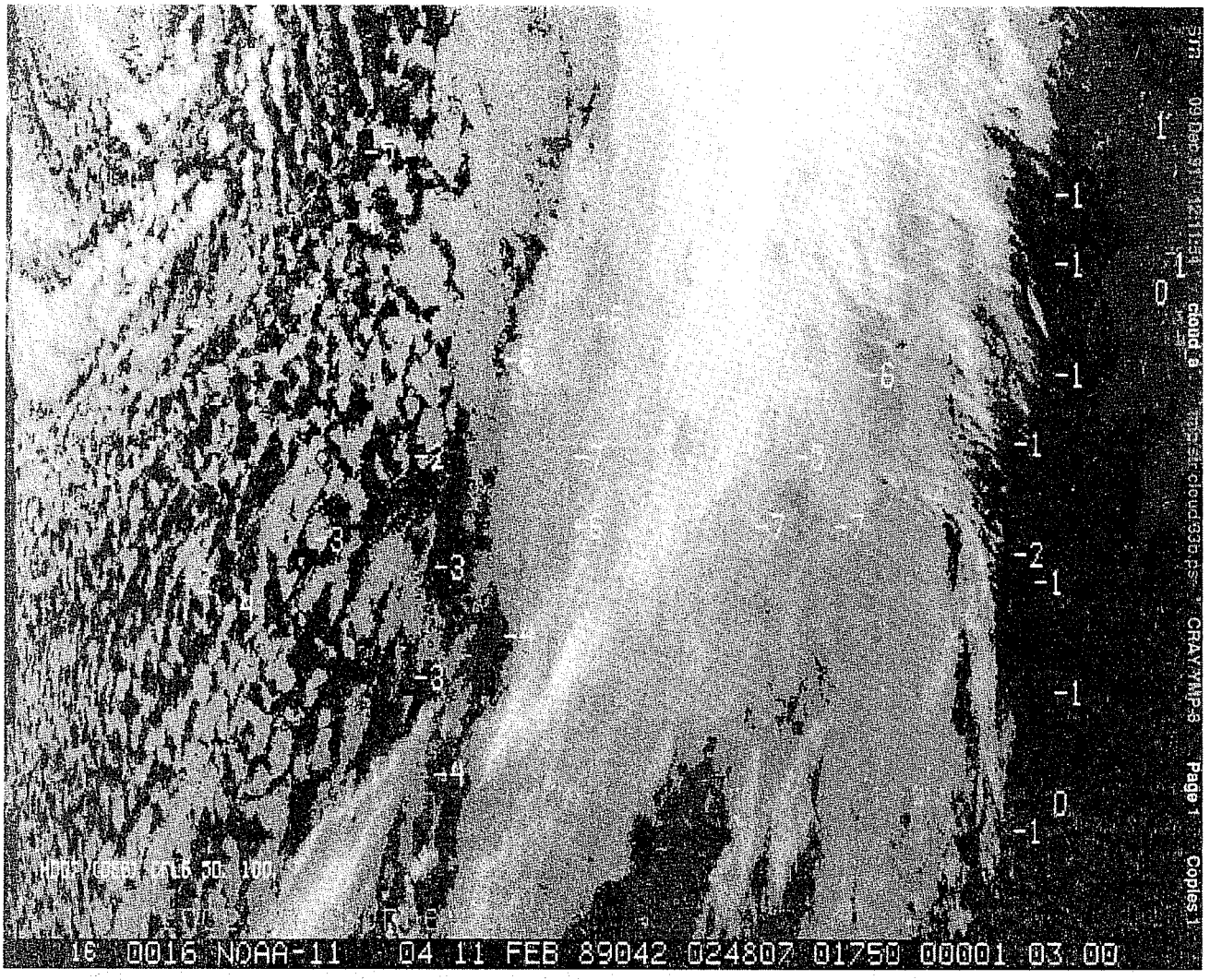

Fig. 19 Difference between NESDIS and simulated BT for HIRS/2 channel 7 superimposed on AVHRR channel 4.

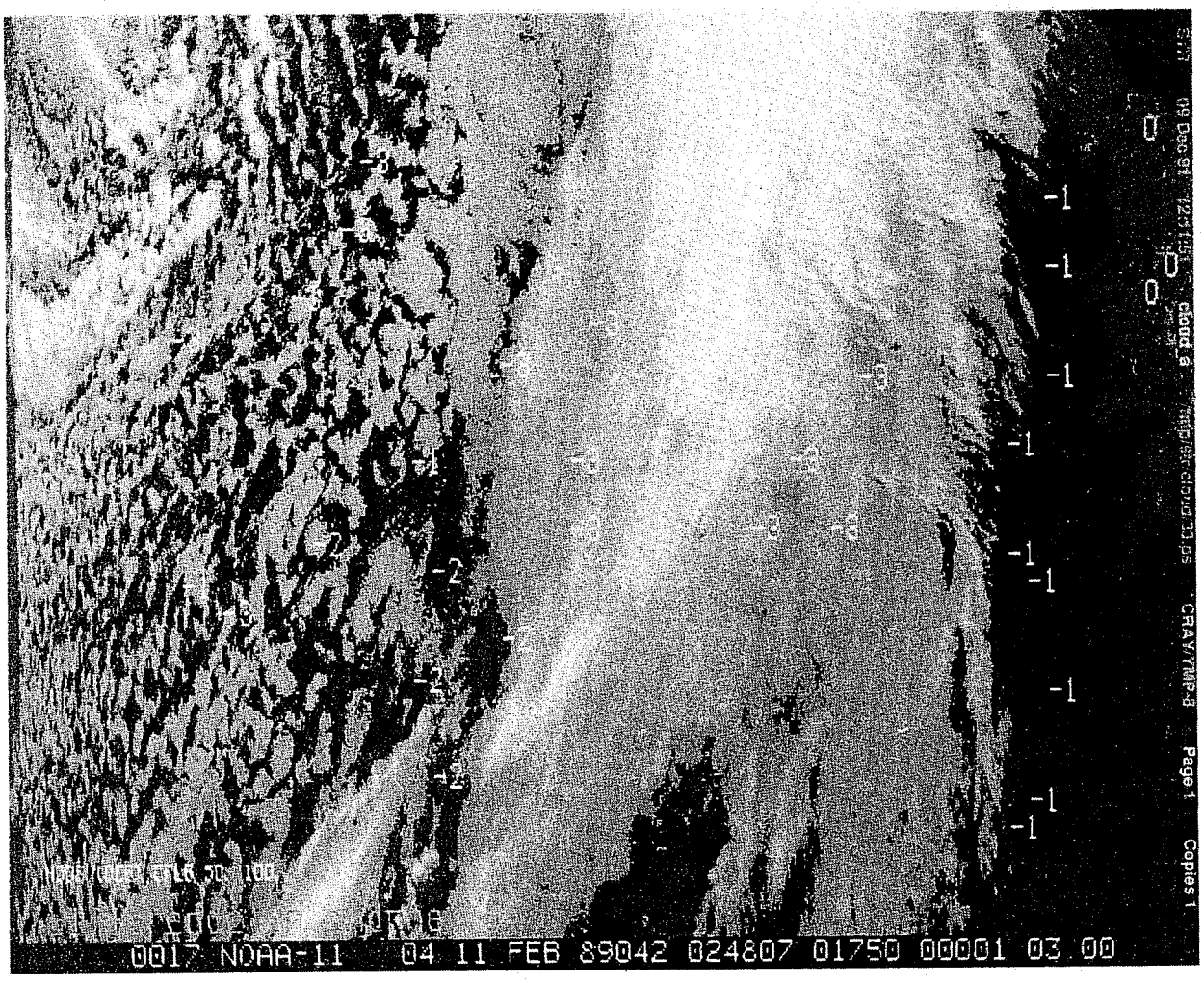

Fig. 20 Difference between NESDIS and simulated BT for HIRS/2 channel 6 superimposed on AVHRR channel 4.